FUNDAMENTAL STUDIES TOWARDS TRANSITION METAL CATALYSIS AND APPLICATION OF CHROMIUM SALEN COMPLEXES FOR THE SYNTHESIS OF POLYMERS

A Dissertation

by

JEREMY REX ANDREATTA

Submitted to the Office of Graduate Studies of
Texas A&M University
in partial fulfillment of the requirements for the degree of

DOCTOR OF PHILOSOPHY

December 2009

Major Subject: Chemistry

FUNDAMENTAL STUDIES TOWARDS TRANSITION METAL CATALYSIS AND APPLICATION OF CHROMIUM SALEN COMPLEXES FOR THE SYNTHESIS OF POLYMERS

A Dissertation

by

JEREMY REX ANDREATTA

Submitted to the Office of Graduate Studies of
Texas A&M University
in partial fulfillment of the requirements for the degree of

DOCTOR OF PHILOSOPHY

Approved by:

Chair of Committee,	Donald J. Darensbourg
Committee Members,	David E. Bergbreiter
	Janet Bluemel
	Daniel F. Shantz
Head of Department,	David H. Russell

December 2009

Major Subject: Chemistry

ABSTRACT

Fundamental Studies towards Transition Metal Catalysis and Application of Chromium Salen Complexes for the Synthesis of Polymers.

(December 2009)

Jeremy Rex Andreatta, B.S., Tarleton State University

Chair of Advisory Committee: Dr. Donald J. Darensbourg

The body of this work spans both fundamental organometallic chemistry and the application of previously studied catalyst systems to produce new polymeric materials. The cone angle of triphenylphosphite was estimated to be 128° by Tolman in the late 70s; however, metal complexes bearing this ligand undergo *cis/trans* isomerization *via* a mechanism indicative of greater steric requirements. X-ray crystallographic studies coupled with data compiled from the Cambridge Crystallographic Database, were used to more accurately calculate the steric demand of this wieldy used ligand to be approximately 140°.

Additionally, in depth kinetic studies of the interaction of furan ligands with electron deficient manganese and chromium metal centers were performed. Data collected from timescales ranging from minutes to microseconds was utilized to calculate the bond dissociation energy of both 2,3-dihydrofuran (DHF) and furan. The aromatic furan ligand was found to bind to the both metals 7-10 kcal mol^{-1} weaker than DHF. Additionally, the more electron rich chromium center was found to bind both ligands

weaker than the manganese center implying a minimization of the M →L π-back bonding interaction. Solution studies coupled with DFT calculations were utilized to estimate the extent that the furan ligand is dearomatized by approximately 50% upon interaction with the metal center.

Application-based studies of the separation of polymer catalyst mixtures were also undertaken. The addition of the 1000 Dalton poly(isobutylene) arms to the salen ligand in (salen)CrCl complexes yielded a catalyst that could be extracted from the reaction mixture containing poly(cyclohexene carbonate) via the addition of heptane. Another approach, not requiring catalyst modification, utilized a secondary amine to facilitate the purification of the polymer product. The reaction of an amine with CO_2 to form an ionic liquid resulted in the precipitation of the polymer while the catalyst and byproducts remained in the liquid carbamate phase. Both approaches provided improvements over the long standing method of precipitating the polymer using methanol and strong acid.

Lastly, the previous work of the Darensbourg group utilizing (salen)CrCl catalyst to produce polycarbonates from CO_2 and epoxides was employed to synthesized sulfur rich poly(thiocarbonate)s. The effects of both CS_2 loading and temperature on the copolymerization of CS_2 and cyclohexene oxide were studied. Optimal conditions of 1 equivalent of CS_2 and 50 °C were found to selectively produce the desired polymeric material. The observation of multiple thiocarbonate as well as carbonate functionalities, led to a detailed study of the reaction byproducts to gain insight into the copolymerization process.

DEDICATION

I dedicate this dissertation to my family. To my parents, my heroes, who always provided me with encouragement and support in all my endeavors. You helped keep me grounded and always reminded me that you love me. Without your love and guidance, I would not be where I am today. To my brother, sister, sister-in-law, and nieces, I love you all and thank you for all the talks we've had over the years. Thank you Zoe for teaching me the consequences of making poor choices and Lexi for proving that dynamite truly does come in small packages! You all were always there to remind me of the true meaning of family. You are all so successful in your own right and I hope I do not let you down. Last but definitely not least, a special nod to my twin brother Jacky. No one will ever know the bond we share. There are no words that can begin to describe how much I love, respect, and look up to you and all your successes.

ACKNOWLEDGEMENTS

Growing up in a small Texas town, I never imagined that I would actually make it to this point. After starting my graduate career, I definitely thought I wouldn't make it. The path was definitely slow and winding and possibly uphill both ways, but I made it. It was not a trek made in singularity by any means, and I would like to give a special thanks to all those who helped me along the way. First and foremost, I would like to thank my research advisor Dr. Donald J. Darensbourg for his patience and guidance throughout my graduate career. He was always on hand to answer my questions or to remind me of my noticeable height disadvantage when needing to get to the top shelf in my lab. Also, I would just like to remind him that my last name is Andreatta and not Adriana, I love my dog, I suck at yo-yo, and I don't even like honey that much! I'd like to thank Drs. David Bergbreiter, Janet Bluemel, Daniel Shantz, and Rodger Morgan for attending my presentations and serving on my committee. I would also like to give a big thanks to Dr. Marcetta Darensbourg for her guidance over the years. Additionally, I would like to express gratitude Dr. Joe Reibenspies and Dr. Nattamai Bhuvanesh (Bhuv) for their patience with the many questions I asked, sometimes more than once, regarding the crystal structures presented in this work. Without question, a monumental thank you goes out to Susan Winters. Our start was rocky with her thinking I was an undergraduate summer research student instead of a new graduate student, but she was infinitely patient with my many inquiries. Without her, none of us would ever get out of this place.

Now to the many friends that have been there through thick and thin. Firstly, to my fellow DJDers past and present, Shawn, Ross, Pop, Adriana, Sunshine, Stephanie (Hank), Wonsook, Polomi, Ryan, Damon, Andrea, Paolo (my Italian brethren), Carla and Adolfo for all the conversations, help with proofreading, and mulling over presentation slides for hours on end. We are a family, and you all have made my time here enjoyable and interesting to say the least. I would like to give a special thanks to Ryan for being my mentor and showing me the ropes, especially how to get back from the EZ mart super incognito. Also, Shawn, I value your friendship and all appreciate your help over the years. Water gun fights were always fun as long as you played by the rules and did not use your assault rifle super soaker. I would also definitely like to give a big shout out to the rest of my hallway family, The MYD group: Steve, Marylyn, Kayla, Elky, Mike, Jen, Scott, William, Jason, Ben, Leo, Tiffany and Ryan, thank you so very much for all the laughs, advice, and times that we shared over the years. I only hope that I was able to be as good a friend to you as you were to me. I would also like to thank Dr. Christine Thomas for all her help and guidance, both while she was here and after she left. I would like to conclude by thanking all those not specifically named here, you know who you are. Your friendship is and will always be an integral part of my life.

There are a few people that I would like to mention separately. First, Scott, my friend and adopted family member, you were always there to listen or pour me a drink when I needed one. Thanksgiving will just not be the same without you there. Jenny, thank you so much for being there whenever I needed someone to talk to and for serving as a role model to me.

Additionally, I would like to thank several people outside of the chemistry department. Randi, you were there for me in some of my darkest and brightest hours both personally and professionally. You are truly one of my closest friends and I will value our friendship all my life. To all of my friends in BV QueSt, you provided me with a purpose outside of science and helped me to grow as a person in so many ways. I miss you all and wish you the best. Finally, and certainly not least, to Mrs. Rita Tallant who provided the initial spark for my love of chemistry so many years ago, thank you so very much. Without knowing it, you are the reason for my passion for chemistry. It was you that started me on the path and your enthusiasm that led me through to the end.

TABLE OF CONTENTS

CHAPTER Page

LIST OF FIGURES

FIGURE Page

FIGURE Page

LIST OF TABLES

TABLE Page

CHAPTER I

INTRODUCTION

A quick search using SciFinder® reveals over 1.6 million hits that contain either the word or concept "catalyst". Catalysts are vital to many of the processes that we have come to rely on. The materials that make up food and beverage containers and the medicines that we take to maintain a healthy body all require the use of catalysts at some point during their production. It is no surprise that there is a significant portion of scientific research, especially in the chemical sciences, devoted to the design, study, and application of catalysts. Important to this dissertation is the study and use of metal based catalysts as a tool for the production of useful materials such as plastics. An extensive source of inspiration for the use of metals in catalysis can be found in nature as approximately one third of the currently known enzymes that catalyze the vital biological process necessary for life contain metals in their active sites.[1]

An understanding of the fundamental steps of the overall reaction under study is crucial for the design and development of new metal based catalyst systems. Chemists utilize knowledge of basic processes to aid in the quest for new and more efficient catalysts. Therefore, it is equally important to investigate both the fundamental concepts and applications of catalysis.

_____

This dissertation follows the style of the *Journal of the American Chemical Society.*

There are two basic elements that make up a catalyst as it pertains to this work: the catalytic metal and the ligand(s) that surround it. The ligand(s) that surround the central metal atom have a large influence on the overall reactivity of the active site of the catalyst. The ligand contributes both sterically and electronically to influence the reactivity and selectivity of the metal catalyst. These elements work in conjunction to lower the activation barrier of the reaction allowing for a path of least resistance towards product formation.

The choice of ligand and metal combination is vital to producing catalysts that can perform complicated reactions efficiently. As a result of this, it is of great importance that scientists intricately understand the effects of various ligands and metals within the catalyst scaffold. They must perform fundamental studies and acquire precise and accurate measurements of the metal and ligand properties using the most up to date techniques to gain insight into the details of the catalyst system.

More specifically, the steric impact of a ligand while bonded to a metal center is very important to the overall efficacy of a catalyst. A ligand with a large spatial requirement can limit access of substrates to the active site, which can enhance both the reactivity and selectivity of the catalyst to form highly stereo- and regioselective products. For example, phosphine ligands are widely used for their relatively predictable spatial properties. Several methods for the estimation of the spatial requirement or "cone angle" of phosphines have been implemented over the years.

In the late 70s, Tolman used scale models of metal phosphines to estimate the spatial requirement or "cone angle" of a wide variety of phosphines.[2] A drawing of the

device utilized by Tolman can be seen in Figure 1-1. He standardized the metal-phosphorous bond length to 2.28Å for M = Ni and measured the angle from the M-P

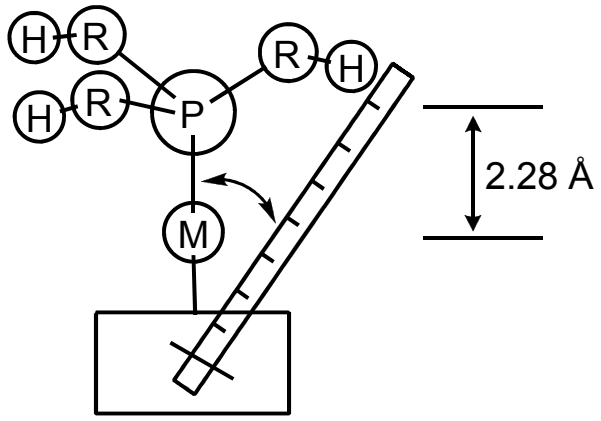

Figure 1-1. Drawing of apparatus utilized by Tolman to measure the steric impact of phosphine ligands.

bond to the outermost van der Waals surface of the ligand. The measured angle was used to quantify the steric requirement of a variety of both alkyl, aryl, and alkoxy and aryloxy phosphines to provide a comprehensive list of steric parameters to aid in the determination of the optimal phosphine ligand for a particular application. A sampling of the cone angles measured by Tolman is provided in Table 1-1. However, when considering the measurements by Tolman, it is necessary to take into account the orientation of the substituents attached to the phosphorous center. When substituent fluxionality was encountered, Tolman oriented all three substituent in the least sterically demanding conformation. For instance, the cone angle for PMe_3 is most likely a very good representation of the actual steric requirement because rotation of the methyl

groups changes the spatial requirement of the ligand very little. However, for P(*n*-Bu)$_3$ (Bu = C_4H_9) the substituents are able to flex about the phosphorous and each carbon center resulting in a conformation what all the Bu groups are not oriented upwards as

Table 1-1. Tolman cone angles for phosphine ligands.

Phosphine	**Tolman Cone Angle (°)**
PMe_3	118
P(*n*-Bu)$_3$	132
PPh_3	145
$P(OMe)_3$	107
$P(OPh)_3$	128

Tolman adjusted them. As such, the Tolman cone angle of 132° is mostly likely an under estimation of the spatial influence of the Bu ligand when bound to a metal center.

Due to the nature of Tolman's measurements, the cone angles must be applied with discretion and methods for more accurate measurements must be sought out. With the advent of modern X-ray diffraction and molecular modeling techniques, more accurate measurements of the spatial requirements of phosphine ligands with flexible substituents can be obtained relatively easily. The more accurate steric parameters obtained by such techniques will allow for better predictions of experimental outcomes and inevitably lead to more efficient catalyst development.

In addition to ligand selection, another important fundamental aspect of catalysis is the nature of the interaction of the metal center with the substrate. It is paramount that as much as possible is understood regarding the interaction of the reactive site of a catalyst with the molecule or molecules that it is to transform. With a greater understanding of the effects of the ligands that surround the active site of the catalyst, scientists will be able to design and develop new, more efficient catalyst tailored towards a specific process.

One particularly interesting interaction that is found in many functional catalysts arises when a metal binds across two carbons of an aromatic system. This interaction is involved in the activation of organic ligands towards several chemical transformations such as hydrogenation, cycloaddition, and electrophilic addition.[3,4] Although several well characterized examples of stable metal-η^2-aromatic complexes exist, their formation usually results in a complete dearomatization of the ligand by the strongly π-basic metal center.[5] A more rare and difficult case to study is the interaction of electron poor metal fragments with aromatic systems. The interaction of metal fragments such as $CpMn(CO)_2$ ($Cp = \eta^5\text{-}C_5H_5$) and $BzCr(CO)_2$ ($Bz = \eta^6\text{-}C_6H_6$) with aromatic ligands such as arenes, furans, pyrols, and thiophenes are much weaker in nature and more labile towards incoming basic ligands.

Even though several examples of metal-η^2-aromatic complexes have been isolated and characterized, there is very little quantitative data regarding the strength of this interaction and especially the extent to which the aromaticity of the ligand is disrupted when coordinated to the metal center. However, qualitatively much is

understood concerning the bonding of the aromatic molecule to the metal center. In order to interact with the metal center, electron density must be localized between two adjacent carbon atoms thus interrupting the aromaticity of the molecule. The bonding interaction the metal and ligand involves a σ-donation of the filled π-orbital of the isolated double bond of the ligand into an empty metal d-orbital as illustrated in Figure 1-2. In addition to the σ-bonding interaction, the metal can back donate electron density

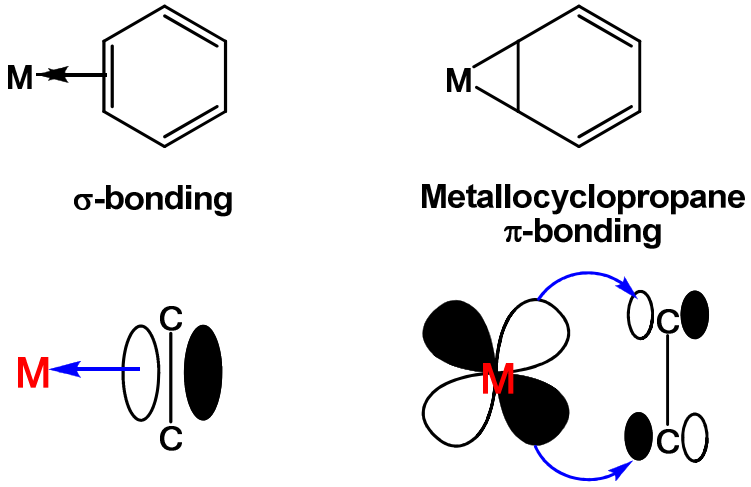

Figure 1-2. Illustration of the bonding interaction of metals and aromatic ligands.

into the empty π^*-orbital of the localized aromatic double bond (Figure 1-2). The π-back bonding interaction in the CpMn and BzCr examples mentioned previously are much weaker due to the reduced electron density at the metal which results in a greater instability of these complexes.

The study of the transition metal complexes bearing ligands with only partially interrupted aromaticity could provide further insight into the nature of this interaction

and lead to more efficient catalyst design. Presented in this dissertation is a comparative study of the bonding of 2,3-dihydrofuan (DHF) and furan to the electron poor $CpMn(CO)_2$ and $BzCr(CO)_2$ fragments. Both heteroatom cyclic ligands have the potential to initially bind through the either oxygen or the olefin bond and studies have been performed to investigate such interactions (Scheme 1-1). Bengali and coworkers

Scheme 1-1.

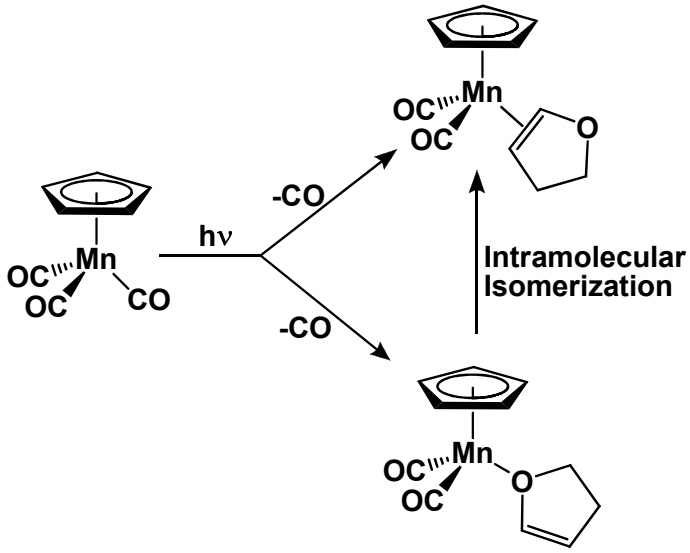

studied the formation and subsequent isomerization of metal complexes of DHF using step-scan FTIR spectroscopy (FTIR = Fourier Transform Infrared) in cyclohexane solution.[6] They found that both the η^1-O and η^2-olefin isomers are present immediately following photolysis of the parent tricarbonyl. The η^1-O complex then isomerizes to the η^2-olefin bound isomer on the millisecond timescale. For all the metals studied, the oxygen bound DHF complex was found to be the kinetically favored product

presumably due to the availability of the lone electrons on the oxygen atom of the DHF molecule. Additionally, the isomerization was found to occur about 70 times faster for the $BzCr(CO)_2(\eta^1$-O-furan) complex than for the Mn or Re complexes. In other words, the rhenium and manganese metal centers bind the DHF ligand considerably stronger when compared to chromium. Additionally, the Re-DHF bond is about 5 kcal mol^{-1} stronger than the Mn-DHF bond as evidenced by the isomerization rate observed for the rhenium complex (Table 1-2).

Table 1-2. Isomerization rate constants and associated activation parameters.[a]

Metal	k_1 **(s^{-1})**	$\Delta H^{\ddagger}$ **(kcal mol^{-1})**	$\Delta S^{\ddagger}$ **(e.u.)**
Mn	163 ± 10	15.4 ± 0.6	+ 4.0 ± 2.0
Cr	12300 ± 200	12.2 ± 0.4	+ 2.0 ± 0.4
Re	24.0 ± 2.0	17.0 ± 0.7	+ 6.0 ± 2.0

[a] all rate constants obtained at 295 K

With a thorough understanding of the formation of the η^2-metal complex, it is possible to undertake a study of the strength of the metal-olefin bond in these systems by investigating the dissociation of the ligand using a base such as pyridine. This can help to elucidate the extent of the disruption of the aromaticity of the furan ligand when bound to an electron deficient metal center. A comparison of the rates of dissociation of

the anti-aromatic DHF and the aromatic furan ligands will provide some insight into the role the aromaticity plays in metal-ligand bonding interaction.

While fundamental studies involving metal-ligand interactions and catalyst design are necessary, it is also important to apply what has been learned from these studies to real world situations. The copolymerization of carbon dioxide and epoxides has been intensively studied since it was first discovered by Inoue and coworkers in 1969.[7] Although the development of more efficient and selective catalyst has progressed over the past 40 years, the method by which the polymer and catalyst are separated has not. Traditionally, the polymer/catalyst mixture obtained at the end of the reaction is dissolved in a minimum amount of dichloromethane (DCM) and excess 1M hydrochloric acid (HCl) and in methanol (MeOH) is added to precipitate the polymeric product. This separation technique creates large volumes of non-recyclable solvent waste. In order to maintain a low environmental impact of the production of polycarbonates from CO_2 and epoxides, it is vital to investigate more benign separation schemes. An approach to the separation of the polymer/catalyst mixture can be envisioned by simply changing one or more components of the system. For example, Darensbourg and coworkers utilized a CO_2 miscible monomer, 2-(3,4-epoxycyclohexyl)-ethyltrimethoxysilane (TMSO), to study the kinetics and mechanism of the CO_2/epoxide copolymerization process which produced a polymer that was also soluble in liquid CO_2.[8] Upon completion of the reaction, the reactor was filled with liquid CO_2 and thepolymer product transferred under

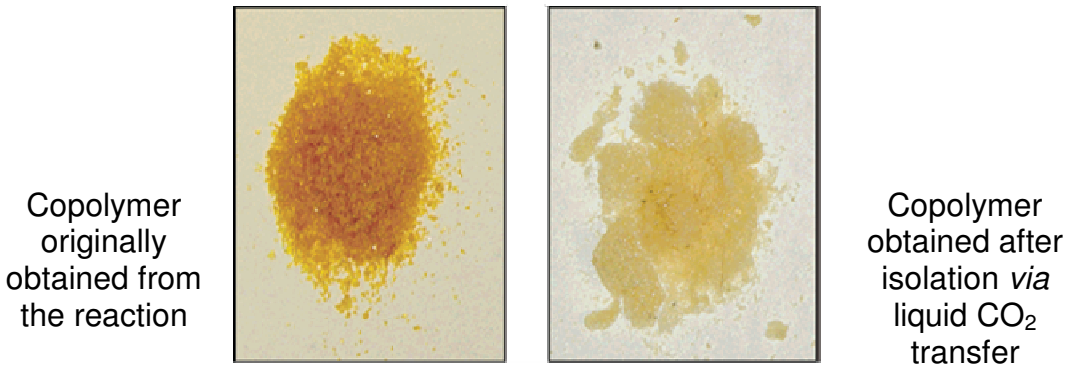

Figure 1-3. Poly(TMSO carbonate) before and after liquid CO_2 isolation.

high pressure via cannula to another high pressure vessel. After the excess CO_2 was vented, the pure polymeric product was obtained (Figure 1-3). There is; however, one significant drawback to the utilization of this monomer with the siloxy group. Although the trimethoxy silyl group facilitates CO_2 solubility, it is also susceptible to hydrolysis. If the polymer is exposed to water and/or a damp atmosphere, the methoxy groups are hydrolyzed resulting in a crosslinked polymeric product that is insoluble in common organic solvents.

Another potential separation route would be to modify the catalyst structure such that the activity and selectivity are not affected, but separation from the polymer would be possible under more green conditions. Several groups have made great strides in this area. The first example was presented by Mang and Holmes in 2000.[9] They utilized a chromium porphyrin catalyst, **1-1**, with four pentafluorophenyl groups attached to the prophyrin ring (Figure 1-4). This ligand afforded a metal complex that was soluble in

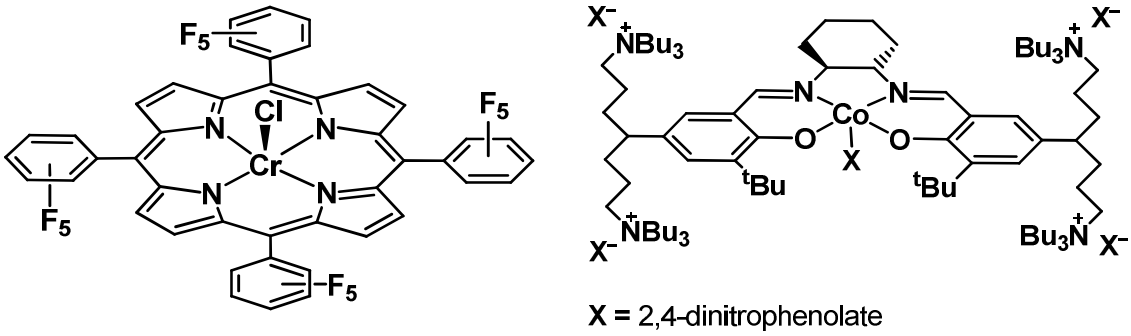

1-1 **1-2**

Figure 1-4. Examples (ftppp)CrCl, **1-1**, and (salen)CoX, **1-2**, of catalysts modified to aid in polymer catalyst separation.

supercritical CO_2. Much like the poly(TMSO carbonate) example, the catalyst could be separated via high pressure transfer to yield purified polymeric product. Unfortunately, the catalyst is not the most active for polymer production; however, it serves as an excellent model for the modification of other active catalysts in the future. Similarly, Lee and coworkers synthesized a series of highly active cobalt salen complexes, **1-2**, with pendant ammonium moieties that allowed for catalyst removal by filtration through a silica column (Figure 1-4).[10] This technique still requires the utilization of large volumes of solvent to accomplish separation; however, the recovered catalyst retains almost full activity over several cycles and there is potential for solvent recycling with this approach. Due to the small number of examples of efficient green polymer/catalyst separation methods , it is necessary to seek out and study the combination of advanced catalyst design with green separation techniques.

Greatly inspired by the copolymerization of CO_2 and epoxides, the copolymerization of CS_2 and cyclic ethers and thioethers has also been explored. Much

like polycarbonates, polythiocarbonates exhibit potential for use in multiple applications due their superior properties of chemical and heat resistance, toughness, and high refractive index. Additionally, the intercalation of sulfur atoms within the polymeric structure could render a material with potential to be used as a heavy metal scavenger.

Similar to the industrial production of polycarbonates, most of the literature for the synthesis of polythiocarbonates utilizes phosgene or thiophosgene and alcohols or thiols. Additionally, attempts to produce polythiocarbonates from CS_2 and epoxides has resulted in polymeric materials with low molecular weights and relatively broad molecular weight distributions. Interestingly, in all cases of the copolymerization of CS_2 and epoxides, the exchange of sulfur and oxygen are observed (Scheme 1-2).

Scheme 1- 2

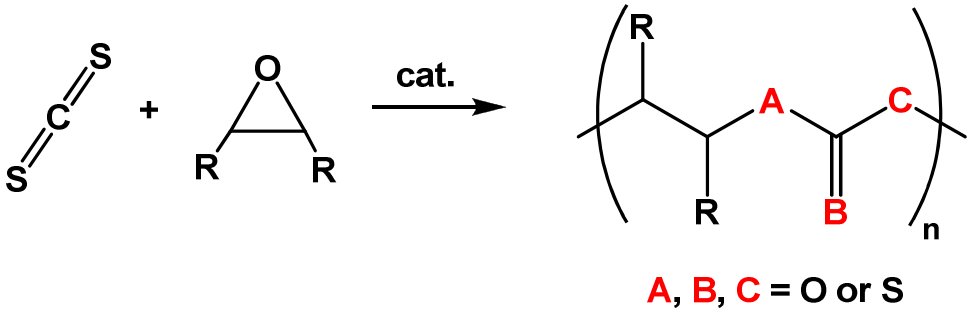

Two recent papers have revitalized interest in the production of polythiocarbonateds from CS_2 and cyclic ethers and thioethers. First, Nozaki and coworkers synthesized poly(propylene trithiocarbonate) utilizing (salphen)CrCl (salphen = N,N'-bis(3,5-di-*tert*-butylsalicylidine)-1,2-phenylenediimine) and PPNCl (PPNCl =

bis(triphenylphosphoranylidene)ammonium chloride) from CS_2 and propylene sulfide with high polymer selectivity at room temperature (Figure 1-5a).[11] Following that report, the copolymerization of propylene oxide and CS_2 was investigated using a zinc cobalt double-metal cyanide complex (Figure 1-5b).[12] This ill-defined catalyst was able to produce polymer with relatively low molecular weight and broad molecular weight distributions. These studies serve as a basis for the current investigation in which (salen)CrCl (salen = N,N'-bis(3,5-di-*tert*-butylsalicylidine)-1,2-ethylenediimine) is investigated as a catalyst for the copolymerization of CS_2 and cyclohexene oxide. Much is known regarding the activity of the (salen)CrCl/PPNCl catalyst system for the

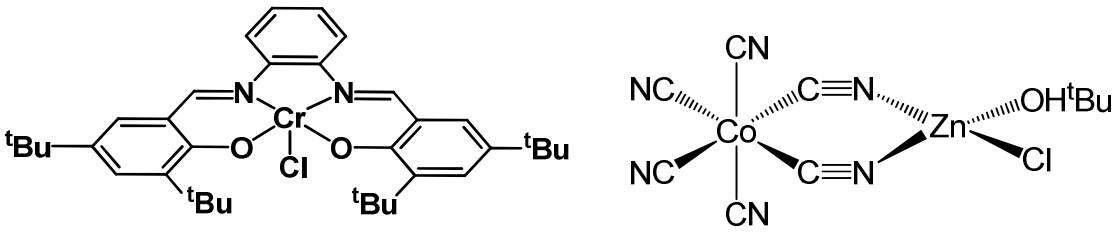

a **b**

Figure 1- 5. Drawing of a) (salphen)CrCl utilized for the copolymerization of CS_2 and propylene sulfide and b) the proposed structure of Zn-Co DMC used in the copolymerization of CS_2 and propylene oxide.

copolymerization of CO_2 and epoxides which has produced a wealth of knowledge that can be applied to the copolymerization of CS_2 and epoxides.[13] Additionally, with a well defined catalyst system it might be possible to quench, control, or at least predict the extent of the sulfur/oxygen exchange that takes place during the reaction.

This dissertation will cover a wide spectrum of both fundamental and application based studies with the central them of catalysis. The topics covered will range from a deeper understanding of the true steric impact of triphenylphosphite and the implications this has in predicting reaction mechanisms. Additionally, an investigation into the nature of the bonding of heteroatom aromatic systems to transition metal centers will be addressed, correlating a more general understanding of transition metal-aromatic bonding schemes. More from an application standpoint, two approaches to the separation of polymer/catalyst mixtures will be discussed with the goal of making the purification portion of a well developed polymerization catalyst system more green. Lastly, studies towards the synthesis of polythiocarbonate materials and their thermal properties will be presented. It will be demonstrated that through the efforts of myself and others that much insight has been gained into several different areas of catalysis that can be applied to a broad spectrum of potential applications.

CHAPTER II

WHAT IS THE REAL STERIC IMPACT OF TRIPHENYLPHOSPHITE?*

Introduction

In order for chemist to overcome present and future challenges, they must first study the fundamental principles that will serve as the foundation for future discoveries. Tolman's studies of the cone angles of phosphine and phosphite ligands have been instrumental in the development of metal based catalysts in a variety of applications. In his investigation, Toleman utilized space filling CPK models to define the angle of the cone formed having the metal at its apex and the periphery composed of the van der Waals spheres of the outermost hydrogen atoms of the tertiary phosphine ligand (Figure 2-1).[2] He fixed the M-P distance at 2.28Å (M = Ni), and then measured the angle from the M-P bond to the outer edge of the van der Waals radius of the outer most hydrogen atoms. Since that time, several methods have been utilized to refine these steric parameters for phosphine ligands, including X-ray structural studies and molecular mechanics models.[14-18]

From the beginning, it has been acknowledged that Tolman's measurements must be applied with some discretion, especially in the case of phosphines or phosphites with non-spherical substituents and/or asymmetry about the phosphorous center. In such cases, Tolman decided to fold the alkyl or aryl groups upward in order to minimize the

---

*Reproduced with permission from Darensbourg, Donald J.; Andreatta, Jeremy R.; Stranahan, Sarah M.; Reibenspies, Joseph H., *Organometallics* **2007**, *26*, 6832 - 6838. Copyright 2007 American Chemical Society.

cone angle. For PPh_3, Tolman realized that restricting the phenyl groups to an angle of less than 145° could cause a serious steric strain on the ligand. However, in the case

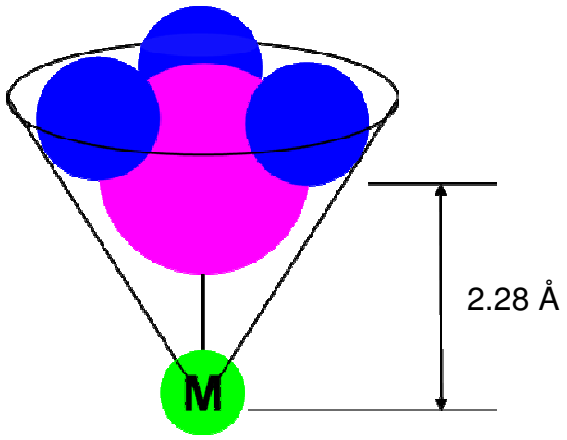

Figure 2-1. Drawing of the cone angle of a phosphine ligand described by Tolman.

of $P(OPh)_3$, there would be no significant barrier to the 'all up' arrangement of the phenoxide moieties to minimize the steric impact of the ligand.[19] Because of this restriction, many of the cone angles measured by Tolman can be considered as an estimation of the minimum steric requirement of a phosphine ligand.

The difference in the steric requirements between PPh_3 and $P(OPh)_3$ makes comparison of the *inter-* and *intramolecular cis-trans* isomerization of metal complexes of alkyl/aryl versus alkoxy/aryloxy phosphines interesting. Earlier solution studies of $Mo(CO)_4(PR_3)$, revealed that the *cis* to *trans* (or *cis* to *cis-trans* mixture) isomerization followed an *intramolecular* pathway for small phosphines such as Me_3P or *n*-Bu_3P. On the other hand, for larger phosphines like PPh_3, the isomerization underwent an

intermolecular rearrangement to the *trans* isomer.[20-23] From these studies, one would predict that the thermal isomerization of *cis*-$Mo(CO)_4[P(OPh)_3]_2$ would follow an *intramolecular* pathway since the cone angle of $P(OPh)_3$ was estimated to be 128° by Tolman which is less than the 132° for *n*-Bu_3P. However, when a solution of *cis*-$Mo(CO)_4[P(OPh)_3]_2$ is heated the isomerization is found to take place *via* a dissociative *intermolecular* pathway *vide infra*. In addition to this discrepancy in the isomerization of the triphenyl phosphite complex, there are a relatively small number of structurally characterized triarylphosphite complexes when compared to triarylphosphine complexes. As of May 2007, there were 10,687 structures of metal complexes with at least one transition metal-PPh_3 bond compared to only 257 structures with at least one transition metal-$P(OPh)_3$ bond. Therefore, it is of interest to synthesize, structurally characterize, and study the isomerization of $M(CO)_4[P(OPh)_3]_2$ complexes in order to gain some insight into the reversal from the predicted *cis/trans* isomerization pathway.

Experimental

Methods and Materials. Unless otherwise stated all synthesis and manipulations were carried out on a double-manifold Schlenk vacuum line under an argon atmosphere or in an argon filled glove box. Molybdenum hexacarbonyl, tungsten hexacarbonyl, and triphenylphosphite were purchased from ACROS. Trimethylolpropanephosphite was obtained from TCI. All solvents were freshly purified using a MBraun Solvent Purification System packed with Alcoa F200 activated alumina desiccant. Infrared spectra were recorded on a Mattson 6021 Galaxy series FTIR, and ^{31}P NMR spectra were collected on an Inova 300 MHz spectrometer. *cis*-

$M(CO)_4[NHC_5H_{10}]_2$ (M = Mo and W) were prepared in 90% yield by the method previously described in the literature.[15]

Synthesis of *cis*-$Mo(CO)_4L_2$ (L = $P(OPh)_3$ (2-1) and $P(OCH_2)_3CEt$ (2-5). Derivatives were prepared from *cis*-$Mo(CO)_4[NHC_5H_{10}]_2$ and excess ligand (L) in refluxing dichloromethane as previously reported.[24] White crystals of complex **2-1** suitable for X-ray analysis were obtained from chloroform and cold methanol in 66.3% yield. The ν_{CO} values of **2-1** in hexane were observed at 2047, 1965, and 1947 cm^{-1}, with the ^{31}P NMR resonance found at 152.1 ppm. White crystals of complex **2-5** were obtained from dichloromethane/methanol in 57.2% yield. The ν_{CO} frequencies of **2-5** in toluene were observed at 2046, 1957, and 1937 cm^{-1}, with the ^{31}P NMR signal found at 139.7 ppm.

Synthesis of (*cis*-$W(CO)_4[NHC_5H_{10}]P(OPh)_3$ (2-2). To 2.57 g (5.51 mmol) of *cis*-$W(CO)_4[NHC_5H_{10}]_2$ suspended in 50 mL of dichloromethane was added 1.47 mL (5.60 mmol) of $P(OPh)_3$ and the solution was refluxed overnight. The resultant reaction solution was filtered through Celite and the solvent was removed under vacuum. Small yellow crystals suitable for X-ray analysis were isolated upon recrystallization of the product from chloroform and cold methanol. The purified product was obtained in a 44.2% yield or 1.68 g. The ν_{CO} infrared bands of **2-2** in hexane appeared at 2029, 1911, 1906 and 1895 cm^{-1}. The ^{31}P NMR chemical shift was observed at 136.4 ppm, with J_{PW} = 419 Hz. Elemental analysis: Found. C, 46.48; H, 3.54. Calcd. C, 46.91%; H, 3.79%.

Synthesis of *cis*-$W(CO)_4[P(OPh)_3]_2$ (2-3). To 0.174 g (0.250 mmol) of **2-2** in 12 mL of toluene was added 0.066 mL (0.250 mmol) of $P(OPh)_3$ and the solution was

heated at 60ºC for 24 hrs. The product which consisted mostly of **2-3** with a small quantity of **2-2** remaining was isolated following removal of solvent under vacuum. The ν_{CO} infrared vibrations of **3** were observed at 2043, 1953, and 1933 cm^{-1}.

Isomerization Reactions. (a) Complete rearrangement of *cis*-$Mo(CO)_4[P(OPh)_3]_2$ (**2-1**) to *trans*-$Mo(CO)_4[P(OPh)_3]_2$ (**2-6**) occurred in toluene at 85ºC over a 48 hr period. The ν_{CO} infrared absorption of **2-6** was observed at 1939 cm^{-1} in toluene, with a ^{31}P NMR signal appearing at 160.5 ppm. Crystals suitable for X-ray analysis were obtained from chloroform and cold methanol. When this process was similarly carried out under an atmosphere of carbon monoxide the sole reaction product was $Mo(CO)_5P(OPh)_3$ (**2-7**).**(b)** Isomerization of *cis*-$W(CO)_4[P(OPh)_3]_2$ (**2-3**) in toluene was performed as described above leading to *trans*-$W(CO)_4[P(OPh)_3]_2$ (**2-4**). The ν_{CO} infrared absorption of **2-4** in toluene appeared at 1932 cm^{-1}, with the ^{31}P NMR signal observed at 135.4 ppm (J_{PW} = 564 Hz). Single crystals of complex **2-4** suitable for X-ray analysis were obtained from a chloroform solution of the complex layered with cold methanol. This isomerization reaction was unaffected when carried out under an atmosphere of carbon monoxide. **(c)** Complex (**2-5**), *cis*-$Mo(CO)_4[P(OCH_2)_3CEt]_2$, was heated in toluene solution for 48 hrs at 80ºC, followed by further heating at 95ºC for 24 hrs with *no* change occurring in its infrared spectrum.

X-ray Crystallography Data Collection and Refinement. X-Ray data for compounds **2-1**, **2-3**, **2-4**, **2-5**, **2-6**, and **2-7** were collected on a Bruker Smart 1000 CCD

Table 2-1. Crystal and refinement data for complexes **2-1**, **2-2**, **2-4**, **2-5**, **2-6**, and **2-7**.

Compound	2-1	2-2	2-4	2-5	2-6	2-7
Empirical formula	$C_{40}H_{30}MoO_{10}P_2$	$C_{54}H_{52}N_2W_2O_{14}P_2$	$C_{40}H_{30}WO_{10}P_2 \bullet CHCl_3$	$C_{16}H_{22}MoO_{10}P_2$	$C_{40}H_{30}MoO_{10}P_2$	$C_{23}H_{15}MoO_8P$
Fw	828.52	1382.62	1035.80	532.22	828.52	546.26
Temp (K)	110(2)	110(2)	110(2)	110(2)	110(2)	110(2)
Cryst system	Monoclinic	Orthorhombic	Triclinic	Monoclinic	Triclinic	Triclinic
Space group	P2(1)	Pbca	P-1	P2(1)/n	P-1	P1
a (Å)	11.197(3)	18.3660(18)	9.170(1)	13.017(4)	8.483(7)	9.505(4)
b (Å)	16.033(3)	14.5829(15)	11.151(1)	19.538(6)	9.623(4)	11.103(4)
c (Å)	11.737(3)	19.565(2)	11.375(1)	16.406(5)	12.110(5)	11.161(4)
α (deg)	90	90	69.755(1)	90	74.843(5)	105.927(6)
β (deg)	118.030(4)	90	89.766(1)	99.544(5)	75.001(2)	94.806(6)
γ (deg)	90	90	68.296(1)	90	76.930(5)	98.846(6)
V (Å^3)	1860(1)	5240.0(9)	1003.7(3)	4115(2)	1818(2)	1109.3(7)
D_c (Mg/m^3)	1.479	1.747	1.714	1.718	1.515	1.635
Z	2	4	2	8	2	2
μ (mm^{-1})	0.497	4.516	3.125	0.844	0.509	0.711
Reflcns colled	17547	47056	7889	38363	8549	7624
Indpndt reflcns	8191	5987	3453	9318	3966	3464
Params	478	337	277	527	241	299
Goodness-of-fit	1.137	1.084	1.069	1.039	1.131	1.073
Final *R* indicies [$I > 2\sigma(I)$]	$R_1 = 0.0457$[a] $R_w = 0.1120$[b]	$R_1 = 0.0504$ $R_w = 0.1237$	$R_1 = 0.0200$ $R_w = 0.0491$	$R_1 = 0.0772$ $R_w = 0.1656$	$R_1 = 0.0475$ $R_w = 0.1160$	$R_1 = 0.0488$ $R_w = 0.1230$

[a] $R_1 = \Sigma||F_o|-|F_c||/\Sigma F_o$. [b] $R_w = \{[\Sigma w(F_o^2-F_c^2)^2]/[\Sigma w(F_o^2)^2]\}^{201/2}$

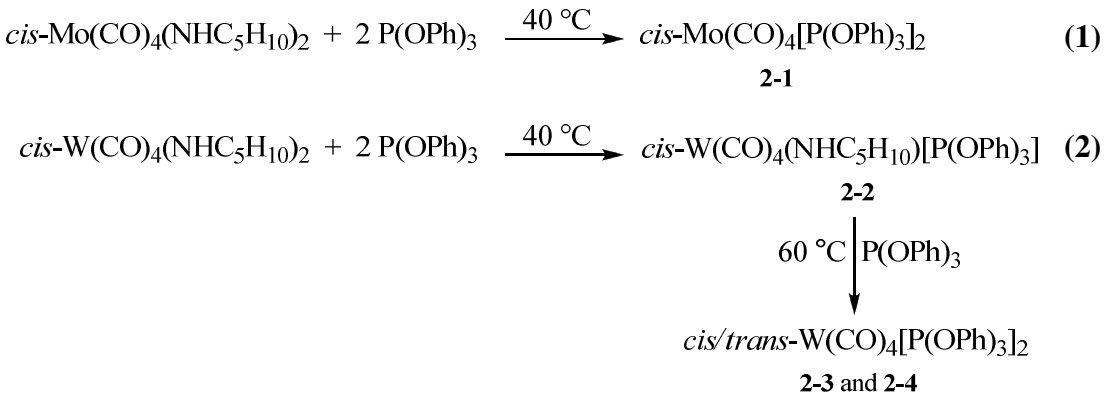

diffractometer and covered more than a hemisphere of reciprocal space by a combination of four sets of exposures. The structures were solved by direct methods utilizing SAINT,[25]SHELEX,[26-28] and WinGX[29] suite programs; graphics and publication materials, X-Seed version 1.5[30]. Crystal details and details of data collection are provided in Table 2-1.

Results and Discussion

The synthesis of the *cis*-$Mo(CO)_4[P(OPh)_3]_2$ was achieved in essentially quantitative yield from *cis*-$Mo(CO)_4(NHC_5H_{10})_2$ and triphenylphosphite in refluxingCH_2Cl_2 (~ 40 °C) (see eq 1).[24] The *cis*-Mo tetracarbonyl phosphite was the only product isolated from the reaction mixture which is not the case if the metal is changed from Mo to W. Even after prolonged heating of 24 h (eq 2), only one piperidine is displaced by the incoming phosphite ligand. An increase in the reaction to 60 °C for 24 h was required to displace the second equivalent of piperidine, which led to mostly *cis* mixture a *cis*- and *trans*-$W(CO)_4[P(OPh)_3]_2$.

Crystals suitable for X-ray diffraction studies of **2-1**, **2-2**, and **2-4** were obtained from chloroform solutions of the metal complexes layered with cold methanol. The room temperature structure of complex **2-1** has been previously reported.[31] For consistency, the structure has been repeated at the same temperature as the other structures reported herein. Figure 2-2 depicts complex **2-1** with the molybdenum in a

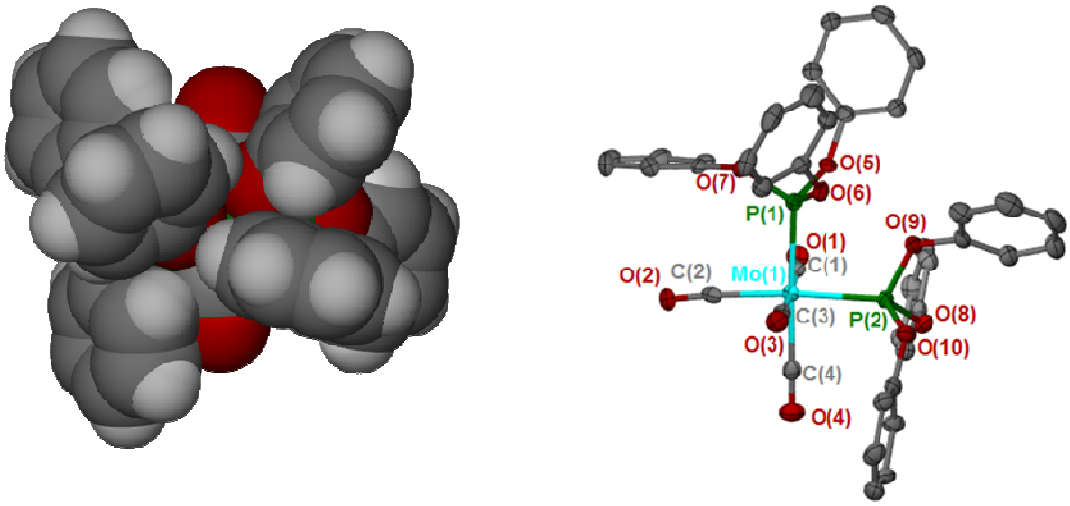

Figure 2-2. Thermal ellipsoid representation of complex **2-1** at 50% probability with atomic numbering scheme and space-filling model illustrating the intertwining of the two triphenylphosphite ligands.

pseudo-octahedral coordination environment. A study of the bond distances and bond angles show only a slight deviation from those measured by Alyea and coworkers.[31] The average Mo-P distance is 2.447(10) Å and the P-Mo-P angle is 89.05(3)° which is close to the average Mo-P distance of 2.442(1) Å and P-Mo-P angle of 89.55(5)° reported for

the room temperature structure. The *cis*-$Mo(CO)_4[P(OPh)_3]_2$ fully converts to the *trans*-isomer in solution upon heating in toluene solution (*vide infra*).

In addition to the similarities in bond distance, the orientation of the phenoxy groups of the triphenylphosphite ligands in *cis*-$Mo(CO)_4[P(OPh)_3]_2$ are in the same orientation in both the ambient and low temperature structures. That is, for P(1) two phenyl groups are *up* and one is *down* (Figure 2-2). On the other hand, the other $P(OPh)_3$ ligand adopts the complementary two *down* and one *up* conformation. One way to more precisely determine the *up* and *down* state of the different conformers of the triphenylphosphite ligand is to measure the angle that determines whether the phosphite ligand is *gauche (down)* or *anti (up)* to the metal phosphorous bond using the torsion angel about the P-O bond of the phosphite ligand denoted as τ (Figure 2-3).[32] From Figure 2-2, it is apparent that the conformation of the triphenylphosphite ligands readily allow for the *cis* arrangement about the octahedral molybdenum center. This is

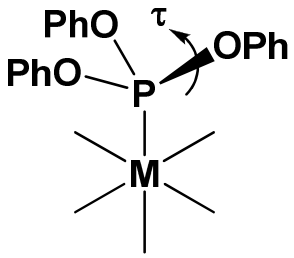

Figure 2-3. τ defines the angle which indicates whether the aryl substituent is gauche (τ ~60º) or anti (τ ~180º) to the metal bonded to the phosphite ligand.

especially visible when in the space filling model also illustrated in Figure 2-2. The second phosphite ligand adopts the mirror image conformation with two phenoxy groups *up* and one *down* in order to reduce steric interactions between the two ligands. In

Table 2-2. Selected bond distances (Å) and angles (º) for cis-$Mo(CO)_4$[phosphite]$_2$.

Phosphite =	**$P(OPh)_3$**	**$P(OCH_2)_3CC_2H_5$**
Mo(1)–C(1)	2.060(4)	2.044(5)
Mo(1)–C(3)	2.025(4)	2.051(5)
Mo(1)–C(2)	2.035(4)	2.032(5)
Mo(1)–C(4)	2.034(4)	2.026(5)
Mo(1)–P(1)	2.4318(10)	2.4247(14)
Mo(1)–P(2)	2.4360(10)	2.4218(13)
C–O_{ave}	1.134(5)	1.137(6)
P(1)–Mo(1)–P(2)	89.05(3)	93.76(4)
P(1)–Mo(1)–C(1)	89.36(10)	87.10(13)
P(1)–Mo(1)–C(3)	87.83(11)	89.40(12)
P(1)–Mo(1)–C(2)	94.44(11)	87.97(13)
P(2)–Mo(1)–C(1)	95.90(10)	89.40(13)
P(2)–Mo(1)–C(3)	86.59(11)	85.93(12)
P(2)–Mo(1)–C(4)	88.62(11)	88.51(12)
P(1)–Mo(1)–C(4)	177.65(11)	174.93(12)
P(2)–Mo(1)–C(2)	174.01(11)	177.40(13)
Mo(1)–P(1)–O_{ave}	116.8(11)	116.5(12)
Mo(1)–P(2)–O_{ave}	117.9(11)	116.7(13)
O–P(1)–O	(96.97 – 103.61)	(100.96 - 102.20)
O–P(2)–O	(97.30 - 104.05)	(100.77 – 101.81)

addition to the sterically encumbering $P(OPh)_3$ ligand, the structure of the smaller sterically less demanding $[P(OCH_2)_3CEt]_2$ metal complex, *cis*-$Mo(CO)_3[P(OCH_2)_3CEt]_2$

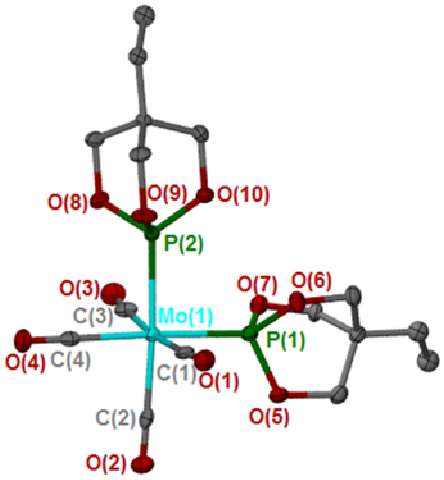

Figure 2-4. Thermal ellipsoid plot of **2-5** at 50% probability level.

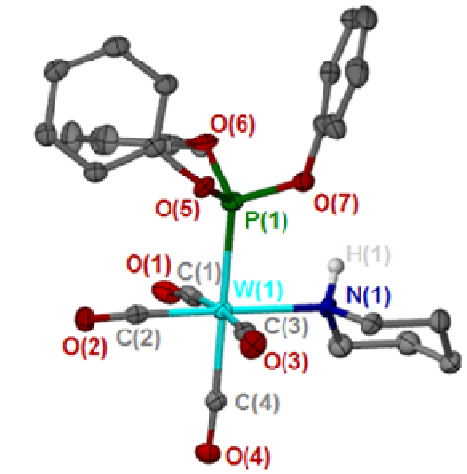

Figure 2-5. Thermal ellipsoid drawing of complex **2-2** at 50% probability level.

(**2-5**) was also studied. A thermal ellipsoid drawing of **2-5** can be viewed in Figure 2-4 and the structural parameters are listed in Table 2-2 along with those of the *cis*-$Mo(CO)_4[P(OPh)_3]_2$ for comparison. From the data in Table 2-2, the metal-ligand distances are quite similar; however, the P-Mo-P angle in **2-5** is somewhat opened up to 93.76(3)° compared to the 89.05(3)° in **2-1**. The cone angle of $[P(OCH_2)_3CEt]$ from the crystal structure of **2-5** (*vide infra*) was calculated to be between 68 and 72° implying the *cis*-isomer to be more thermodynamically stable than the *cis*-$Mo[P(OPh)_3]_2$ complex. Indeed, this is the case when **5** is heated under same conditions of 80-95° in toluene, no

Table 2-3. Selected bond distances (Å) and angles (º) in cis-$W(CO)_4[P(OPh)_3][NHC_5H_{10}]$ (**2-2**).

C(2)–O(2)	1.171(7)	C(2)–W(1)–P(1)	91.88(14)
C(4)–O(4)	1.157(6)	C(4)–W(1)–P(1)	176.23(14)
C(1)–O(1)	1.159(7)	C(3)–W(1)–P(1)	85.90(14)
C(3)–O(3)	1.155(6)	C(1)–W(1)–P(1)	98.23(15)
W(1)–C(1)	2.039(5)	C(2)–W(1)–C(4)	87.2(2)
W(1)–C(2)	1.947(6)	C(2)–W(1)–C(3)	86.1(2)
W(1)–C(3)	2.027(5)	C(4)–W(1)–C(3)	90.4(2)
W(1)–C(4)	1.995(5)	C(2)–W(1)–C(1)	87.8(2)
W(1)–N(1)	2.332(5)	C(4)–W(1)–C(1)	85.4(2)
W(1)–P(1)	2.4465(12)	C(3)–W(1)–C(1)	172.7(2)
N(1)–W(1)–P(1)	88.23(10)	W(1)–P(1)–O_{ave}	117.08(13)
C(2)–W(1)–N(1)	178.00(17)	O–P(1)–O_{ave}	100.7(2)
C(4)–W(1)–N(1)	92.58(18)		
C(3)–W(1)–N(1)	91.96(19)		
C(1)–W(1)–N(1)	94.16(18)		

isomerization to the *trans*-isomer is observed providing further evidence of the stability of the *cis*-isomer as a result steric requirements of the smaller $P(OCH_2)CEt$ ligand. Parenthetically, it is of interest to note that the phosphite ligands in **2-1** and **2-5** exhibit similar electronic properties as revealed by infrared spectroscopy in the carbonyl region of the spectrun. Complex **2-1** exhibits ν_{co} values of 2047, 1965, and 1947 cm^{-1} while ν_{co} values of 2046, 1957, and 1937 cm^{-1} are observed for complex **2-5**.

In addition the *cis*-Mo phosphite complexes, the tungsten analogues were also studied. Due to the greater stability of the tungsten-amine bond, the reaction of $W(CO)_4(pip)_2$ and triphenyphosphite did not proceed directly to the *cis*-tungsten diphosphite product allowing for the isolation of *cis*-$W(CO)_4[P(OPh)_3](NHC_5H_{10})$ (**2-2**).

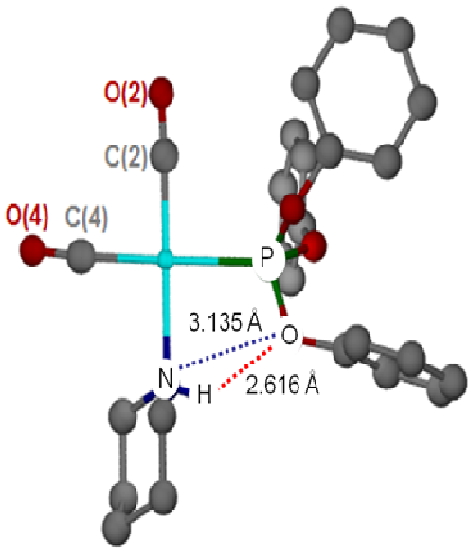

Figure 2-6. Ball-and-stick view of complex **2-2** shown down the *trans*-$W(CO)_2$ axis.

Crystals suitable for study by X-ray diffraction were obtained and a thermal ellipsoid drawing is depicted in Figure 2-5. Additionally, Table 2-3 contains a compilation of selected bond distances and bond angles. From this data, several interesting observations can be made. As seen in Figure 2-6, the phosphite and piperidine ligands orient in order to minimize steric interference with concomitant H-bonding capability.[33,34] A comparison of the M-C distances reveals that the W-C(2) bond *trans* to the piperidine is shorter (1.947(6) Å) than the W-C(4) bond distance *trans* to the triphenylphosphite ligand (1.995(5) Å), and both are shorter than the W-C distances of the two *trans* carbonyl ligands (2.033(5) Å). This is a textbook example of the effect of the stronger donation of the amine ligand to the metal center when compared to the phosphite resulting in more π-back bonding of the tungsten to the CO ligand trans to the amine. In order to achieve the synthesis of *cis*-$W(CO)_4[P(OPh)_3]_2$, the isolated piperidine complex was heated to 60 °C with 1 equivilent of $P(OPh)_3$ for 24 hours. The reaction resulted in the production of the *cis*-tungsten complex as the major product with some of the *trans* complex present in solution as determined by infrared spectroscopy.

The thermal isomerization of the *cis*-isomers was then studied. A toluene solution of *cis*-$Mo(CO)_4[P(OPh)_3]_2$ was heated to 85 °C over a 48 hour period by infrared spectroscopy to ensure the conversion to *trans*-$Mo(CO)_4[P(OPh)_3]_2$ (**2-6**). In the case of molybdenum, a 100 % conversion is observed as evidenced by the growth of a band at 1939 cm^{-1} and a total disappearance of the IR peaks attributed to the *cis*-isomer. Further evidence for the complete conversion can be observed *via* ^{31}P NMR.

The *cis*- Mo complex has a ^{31}P resonance at 152.1 ppm which is not observed in the NMR of the product solution after heating. The only signal observed after the 48 hours of heating is that of the *trans*-$Mo(CO)_4[P(OPh)_3]_2$ at 160.5 ppm. Crystals of **2-6** suitable for X-ray diffraction studies were obtained from a chloroform solution of the product layered with cold methanol and allowed to mix slowly. The thermal ellipsoid representation of **2-6** can been seen in Figure 2-7 and selected bond distances and bond angles can are can be found in Table 2-4.

The thermal isomerization of the *cis/trans*-$W(CO)_4[P(OPh)_2]_2$ product mixture also leads to the exclusive formation of the *trans*-isomer. Again, disappearance of the

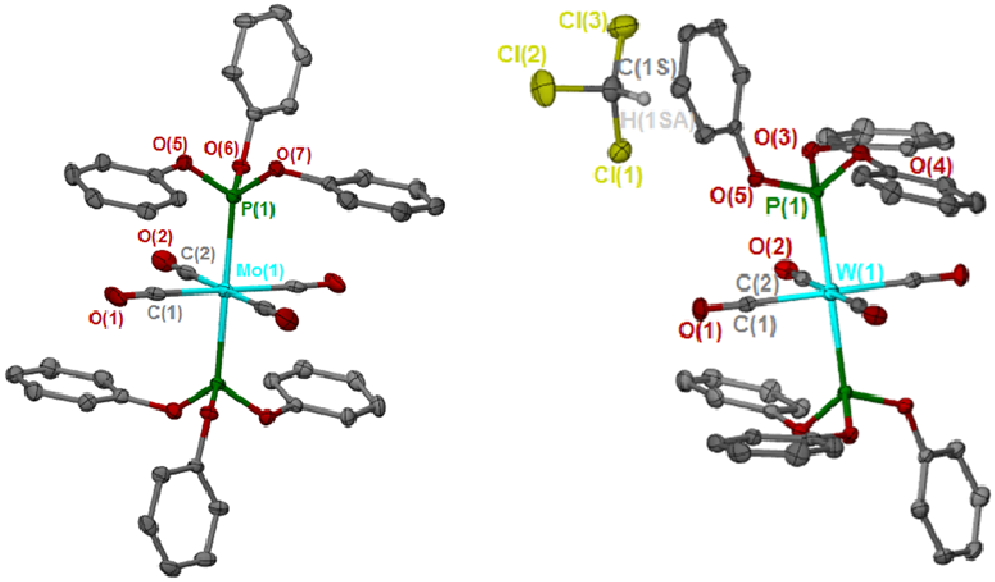

2-6 **2-4**

Figure 2-7. Thermal ellipsoid drawing of complex **2-6** and **2-4** at 50% probably. Hydrogen atoms have been omitted for clarity.

bands attributed to the *cis*-phosphite isomer accompanied by the growth of a single band at 1932 cm^{-1} and observance of a single ^{31}P NMR signal at 135.4 ppm are evidence of the complete conversion. Interestingly, tungsten satellites were observed in the ^{31}P NMR of **2-4** due to W-P coupling with a J_{PW} of 564 Hz. Crystals of *trans*-$W(CO)_4[P(OPh)_3]_2$ (**2-4**) were obtained in the same manner as the Mo complex and submitted to analysis by X-ray diffraction. A thermal ellipsoid drawing of **2-4** can be seen in Figure 2-7 and selected bond distances and bond angles can be found in Table 2--4.

A comparison of the *trans*-isomers reveals several interesting similarities in the two complexes. Both phosphite ligands in both the Mo and W complexes exhibit the

Table 2-4. Selected bond distances (Å) and bond angles (º) for trans-$M(CO)_4[P(OPh)_3]_2$, M = Mo and W.

	Mo	**W**
$C–O_{ave}$	1.143(4)	1.144(3)
M(1)–C(1)	2.045(3)	2.036(3)
M(1)–C(2)	2.040(3)	2.047(3)
M(1)–P(1)	2.4063(7)	2.4017(7)
P(1)–M(1)–C(1)	92.74(8)	87.86(8)
P(1)–M(1)–C(2)	86.35(8)	86.50(8)
$M(1)–P(1)–O_{ave}$	118.42(8)	118.23(7)
O–P(1)–O	95.79 - 103.8	96.32 – 103.4

two *up* and one *down* confomation in the solid state structures. Interestingly, the *up* groups are situated on opposite sides of the molecule to further reduce the steric interaction of the *trans*-phosphite ligands. The other bond distances and bond angles are practically identical except for the M-C(1) angles with differ by about 5°.

A relationship between the Tolman cone angle and the thermal stability of the *cis/trans*-isomers has be previously established (eq 3).[20,21] The K_{eq} for the isomerization defined in eq 3 for R = *n*-Bu (Tolman cone angle = 132°) was determined to be 5.3 at 60-70 °C. On the other hand, for the less sterically hindering PMe_3 complex (Toleman cone angle = 118°) the *cis*-isomer is slightly more favored as evidenced by a positive ΔG of 0.32 kcal/mol at 65 °C for the thermal isomerization outlined in eq 3. For both the

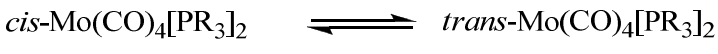

(3)

n-Bu_3P and PMe_3 cases, the rearrangement to the *trans*-isomer was established as being *intramolecular* in nature. That is, the isomerizaiton took place through a trigional prismatic intermediate via a Bailar twist mechanism (Scheme 2-1a). By contrast, the *cis*-to-*trans* isomerization for R = Ph, where PPh_3 is more sterically demanding (Tolman cone angle = 145°), follows an *intermolecular* isomerization pathway to the highly thermodynamically favored *trans*-isomer. That is to say that the isomerization takes place *via* the dissociation of one of the phosphine ligands followed by a Barry pseudo rotation and re-association of the phosphine ligand to reform the *trans*-bisphosphine

complex (Scheme 2-1b). As seen in Scheme 2-1b, one experiment to determine the isomerization mechanism would be to perform the thermal isomerization in the presence

Scheme 2-1

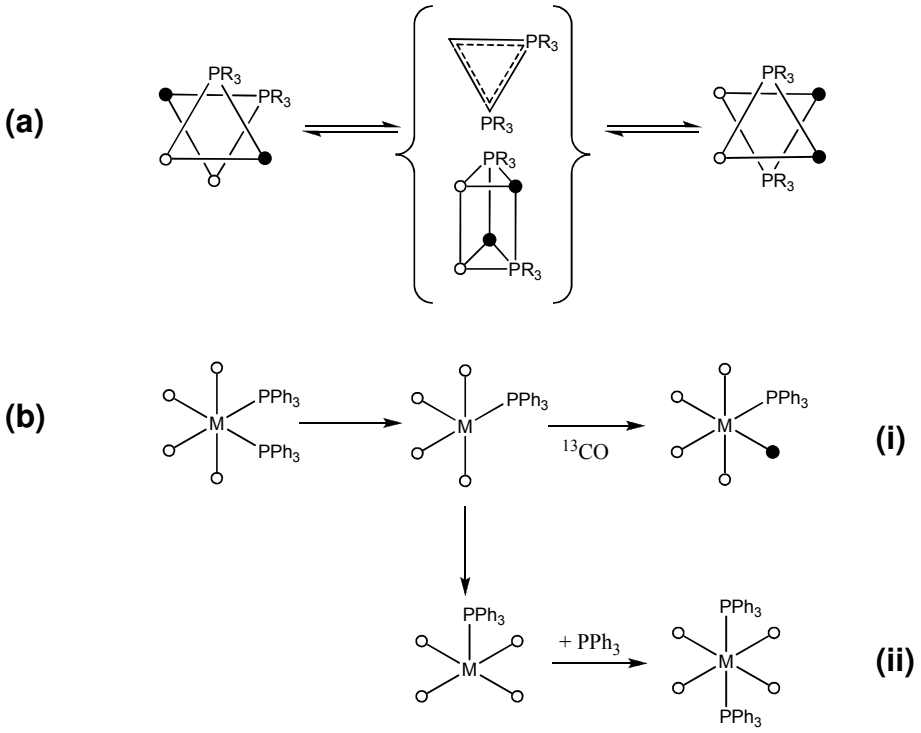

of CO. In the case of the Bailar twist mechanism, no change in the product would be expected; however, if ligand dissociation were required for isomerization, $Mo(CO)_5[P(OPh)_3]$ would be present at the conclusion of the reaction. With this in mind, the thermal isomerization of *cis*-$Mo(CO)_4[P(OPh)_3]_2$ would be expected to follow the intramolecular pathway since the Toleman cone angle is estimated to be 128°; less than that of the *n*-Bu_3P which follows the *intramolecular* mechanism (*vide supra*). Interestingly, when the isomerization reaction is performed under an atmosphere of CO,

the major product isolated from the reaction solution is the pentacarbonyl complex, $Mo(CO)_5[P(OPh)_3]$ (**2-7**), that can only result from the dissociative *intermolecular*

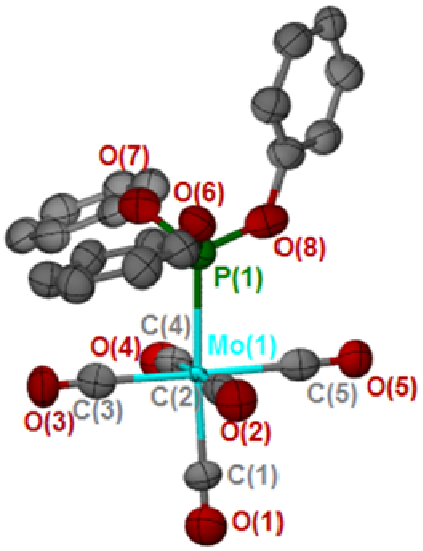

Figure 2-8. Thermal ellipsoid view of complex **2-7** at 50% probability level. Selected bond distances and bond angles: Mo–C_{eq}(ave) = 2.061(9) Å, Mo–C_{ax} = 2.066(9) Å, Mo–P = 2.448(2) Å, P–Mo–C_{eq}(ave) = 90.1(2)°.

mechanism. The identity of this product was confirmed by IR, ^{31}P NMR, and X-ray crystallography. A thermal ellipsoid drawing of **2-7** along with selected bond distances and bond angles can be viewed in Figure 2-8. It is worth pointing out the two *down*, one *up* conformation of the triphenylphosphite ligand in **2-7**. The presence of this conformation whenever it is sterically feasible implies a stability over the other possible orientations of the phenoxy groups. In a stark reversal of the Mo complex, the *cis*-W phosphite complex undergoes isomerization by the expected intramolecular pathway. That is, when the isomerization was performed in the presence of CO, the only product

observed via IR and ^{31}P NMR is the *trans*-$W(CO)_4[P(OPh)_3]_2$ complex. This is primarily attributed to the strength and thermal stability of the W-P bond over that of the Mo-P bond.

Tolman realized early on that PPh_3 experienced a large amount of strain when its cone angle was compressed beyond 145°; however, phosphite ligands like $P(OPh)_3$ endured no barrier when the phenoxide moieties were in the all *up* conformation to minimize its spatial requirements. It is worth mentioning here that other researchers have also demonstrated the conformational variability of phosphite ligands. Ernst and co-workers showed that $P(OMe)_3$ generally adopts conformations where all the OMe groups are not bent upwards as Toleman assumed.[35,36] More recently, Coville *et. al.* have investigated several transition metal phosphite complexes and found that many exhibit conformational flexibility.[37,38] Similar to the studies discussed herein, using crystallography they measured cone angles to be significantly larger than those predicted by Tolman. Additionally, they found that the steric requirements of the $P(OR)_3$ ligands had a marked effect on the *cis/trans* isomerization of $Mo(\eta^5\text{-}C_5H_5)(CO)_2[P(OR)_3]I$. Also pertinent to the current study, Yarger and co-workers have established experimentally and confirmed using theoretical calculations that $P(OPh)_3$ exist in two configurations at low temperature, which exhibit either C_3 (all phenoxide subsitutuents bent toward the lone pair of electrons on the phosphorous center) or C_s (two toward the lone pair and one away) symmetry.[39]

In order to more accurately estimate the steric impact of $P(OPh)_3$, we have calculated the *minimum* and *maximum* cone angles using the crystal structures of each of

the complexes utilizing the method employed by Müller and Mingos.[40] Although Tolman's original models of the most compact conformer of the phosphine and phosphite ligands have served chemists well when discussing spatial requirements, the values fail to take into account variations in the cone angle that result from the different ligand conformations. As depicted in Figure 2-9, triphenylphosphite can adopt several conformers. In the crystallographically characterized complexes in this study, two of the

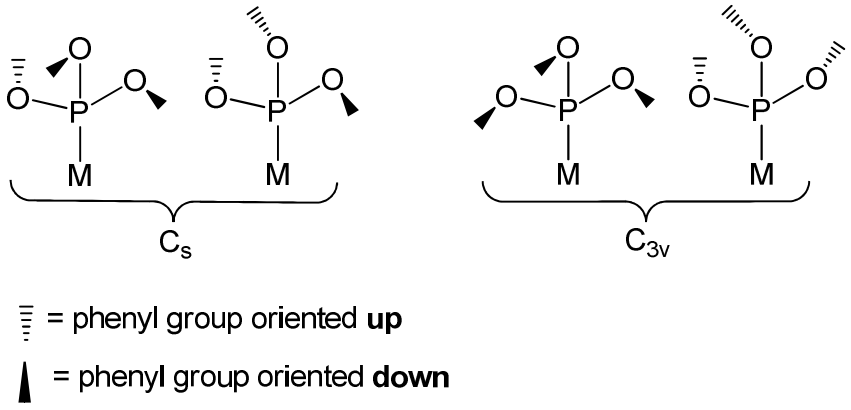

Figure 2-9. Conformers of $P(OPh)_3$.

four possible conformers were observed, i.e. those of C_s symmetry with either two *up* (*anti*) and one *down* (*gauche*) or two *down* and one *up*. The later conformer, C_{3v}, has been observed via low temperature ^{31}P NMR and X-ray crystallography in the free triphenylphosphite.[41] Indeed, of the 362 transition metal-triphenylphosphite structures in the Cambridge Crystallographic Database as of May 2007, only 1.7% (6) displayed the Tolman's all *up* (*anti*) arrangement[42], whereas 33.7% (122) and 62.4% (226) display the two *up* (*anti*) and one *down* (*gauche*) or one *up* (*anti*) and two *down* (*gauche*)

configurations respectively. The remaining 2.2 % (8) of the transition metal complexes exhibit structures with all three phenoxy substituents in the *gauche* (*down*) orientation that would give rise to the maximum cone angle and thus represents the most sterically demanding conformation of $P(OPh)_3$.

Table 2-5 contains the calculated phosphite cone angles for all the phosphite ligands in the crystallographically characterized complexes **2-1**, **2-4**, **2-6**, and **2-7** along with the three τ angles as described in Figure 2-3. The Müller and Mingos[40] method (eq 4) for calculating cone angles uses the center of the outermost hydrogen atom of the

$$\theta_i = \alpha + {}^{180}/_{\pi} \times sin^{-1}({}^{r_H}/_{d}) \qquad \textbf{(4)}$$

Table 2-5. Calculated cone angles of triphenylphosphite in group 6 metal carbonyl derivatives.[a]

Complex	Phenyl Orientations (τ values, deg)	Cone Angle (deg)°	
		Average	Maximum
cis-$Mo(CO)_4[P(OPh)_3]_2$ (**2-1**)	two down (160, 55, 44)	140	162
	one down (165, 125, 48)	125	152
trans-$Mo(CO)_4[P(OPh)_3]_2$ (**2-6**)	two down (179, 52, 40)	139	154
trans-$W(CO)_4[P(OPh)_3]_2$ (**2-4**)	two down (168, 53, 37)	143	166
$Mo(CO)_5P(OPh)_3$ (**2-7**)	two down (160, 55, 44)	143	162

[a] θ_i values calculated from crystallographic data using the method of Müller and Mingos.

substituent in question as defined by the crystallographic data, , where θ_i is the half angle to the van der Waals radius of the outermost hydrogen atom. The angle α is defined as the angle between the phosphorous and metal centers and the center othe outer most hydrogen atom on the phenyl substituent. The distance *d* is the crystallographic distance between the metal center and the outermost hydrogen atom, and r_H is the van der Waals radius of hydrogen. The *average* cone angle is defined as $\frac{2}{3}\Sigma_i\theta_{i.}$ Additionally, the *maximum* cone angle was calculated by taking twice the largest half angle, θ_i. From this data, the most commonly observed conformer, i.e. the two *down* and one *up* arrangement, has a *average* cone angle of 141±2° and a *maximum* cone angle of 161±5°. On both accounts, the calculated steric impact of $P(OPh)_3$ is much greater than that measured by Tolman and accounts for the difference in the isomerization pathway from the expected *intramolecular* pathway for complex **2-1**. The other phosphite ligand in complex **2-1**, adopts the two *up*, one *down* conformation to reduce the steric interaction of the two phosphite ligands. In this case, the *average* cone angle is somewhat closer to the Tolman conne angle at 125° with a *maximum* cone angle of 152°. It is also interesting that upon isomerization to the thermodynamically more stable *trans*-$Mo(CO)_4[P(OPh)_3]_2$ complex, both phosphite ligands adopt the more common two phenyl substituents *down* conformation. This behavior is also observed in the *trans*-tungsten complex. Further evidence for the stability of the two *down* conformation is exhibited in the structure of the monosubitituted $Mo(CO)_5P(OPh)_3$ complex where the phosphite ligand is not sterically influenced by any other nearby ligands . The C_s

symmetry conformation was also observed in the crystal structure of the free $P(OPh)_3$ ligand discussed previously.[39]

Conclusions

Tolman's cone angles have played in integral role both the study and application of organometallic chemistry ever since they were first published in the late 70; however, there are instances where the exact values of the cone angle is necessary for a full understanding of the subject matter. Therefore, the spatial requirements estimated by Toleman for various phosphine and phosphite ligands must be applied with a certain level of skepticism. In particular, discretion must be used when different conformers of the ligand are possible which result in significant differences in the actual steric demands of the ligand. The complexes discussed herein serve as a prime example of an instance when the experimental data is in disagreement with the predicted experimental outcome. Triphenylphosphite has the potential of 4 different conformations (Figure 2-9), two of which are more prevalent than others. Additioanlly, the conformer predicted by Tolman is actually the least prevalent among crystallographically described metal phosphite complexes and the free ligand itself. As shown *via* X-ray crystallography, the estimated steric demands of $P(OPh)_3$ in Group 6 metal carbonyl complexes is much greater than the 128° estimated by Tolman.

Also, the steric requirements of the $P(OPh)_3$ ligand found in the solid state persist in solution as evidenced by the *cis-trans* isomerization studies of both the molybdenum and tungsten complexes. According to previous studies, one would predict the isomerization to involve a prismatic intermediate that does not require ligand

dissociation. This would imply that the *cis*-$M(CO)_4[(OPh)_3]_2$ (M = Mo or W) would be somewhat thermodynamically favored. Therefore, it was unexpected when upon heating both complexes underwent complete rearrnagement to the *trans*-isomer. Additoinally, in the case of *cis*-$Mo(CO)_4[P(OPh)_3]_2$, the isomerization was found to follow an *intermolecular* pathway as proven by the isolation of significant quantities of the pentacarbonyl complex when the isomerization was performed under an atmosphere of CO. Also of interest, in the case of the small, sterically non-demanding $P(OCH_2)CEt$ complexes (*average* cone angle = 69° and *maximum* cone angle = 72°) little to no conversion to the *trans*-$Mo(CO)_4[P(OCH_2)CEt]_2$ is observed by infrared spectroscopy even after extended periods of heating.

Future studies of such complexes are vital to gaining a more thorough understanding of the effects that such widely used ligands can have on the reactivity of metal complexes. In order to design more effective catalysts that utilize sterically demanding ligands, such as phosphines and phosphites, studies of the true steric impact must be undertaken. With the availability of modern X-ray crystallographic techniques, these studies are becoming more common among scientists studying transition metal catalysis.

CHAPTER III

DISPLACEMENT KINETICS OF η^2 FURAN AND 2,3-DIHYDROFURAN FROM MANGANESE AND CHROMIUM CENTERS: EVIDENCE FOR PARTIAL DEAROMATIZATION OF THE FURAN LIGAND*

Introduction

The activation of organic substrates by transition metals serves as the cornerstone for the production of a number of products utilized in our everyday lives. One area of particular interest is the activation and transformation of aromatic compounds through processes such as hydrogenation, cycloaddition reactions, electrophilic addition, and several others.[3-5] In order to synthesize catalysts that can facilitate these types of conversions faster and more efficiently, it is important to study the nature of the interaction of aromatic substrates with transition metal centers. Several examples of η^2 binding of aromatic compounds with metal centers have been reported; however, in most cases the strong π basic nature of the metal involved results in complete dearomatization of the ligand. For instance, the reaction of the TpM(L)(π-acid) fragment (Tp = hydridotris(pyrazolyl)borate, M = rhenium, molybdenum, tungsten, L = variable ligand, π-acid = CO, NO) with a variety of aromatic molecules including arenes, furans, pyrroles, and thiophenes results in total disruption of the aromaticity of the ligand upon binding with the metal center.[5]

---

*Reproduced with permission from Andreatta, J. R.; Cieslinski, G. B.; Batool, M.; Sun, X.; George, M. W.; Brothers, E. N.; Darensbourg, D. J.; Bengali, A. B. *Inorg. Chem.***2009**, *48*, 7787-7793. Copyright 2009 American Chemical Society.

Similarly, aromatic ligands also interact with electron poor metal centers albeit in a much more transient manner. That is to say, the metal aromatic bond is much more labile in nature when compared to complexes with strongly π basic metal centers. The liability of this bond is primarily attributed to a reduction in the π-back bonding interaction between the metal and aromatic substrate. Kinetic studies have estimated the strength of the metal-(η^2-arene) bond to be 11-15 kcal mol^{-1} for electron deficient metal centers such as those in $CpMn(CO)_2$(Cp = η^5 C_5H_5) and $BzCr(CO)_2$ (Bz = η^6-C_6H_6) fragments.[43,44]

While several examples of metal-(η^2-aromatic) complexes have been isolated and structurally characterized, quantitative data regarding the strength of this interaction and the extent of the disruption the aromatic system undergoes when interacting with the metal center is rare.[45] Though qualitatively much is understood regarding the bonding of aromatic ligands to metal centers, *vide supra*, quantitative data for this interaction is necessary to design new catalyst for the transformation of aromatic substrates into more useful products.

Experimental

Experimental and Theoretical Methods. Unless otherwise stated, all synthesis and manipulations were carried out on a double-manifold Schlenk vacuum line under an argon atmosphere or in an argon filled glovebox. Cyclohexane (Acros), cyclopentadienylmanganese tricarbonyl (Strem), and benzene chromium tricarbonly (Strem) were used as received.

Step-scan and Rapid-scan FTIR Studies. A Bruker vertex 80 FTIR spectrometer equipped with both rapid and step-scan capabilities was used. Sample photolysis was conducted using 355 nm light from a Nd:YAG laser (50 mJ/pulse, 1 Hz repetition rate). To ensure a fresh solution was photolyzed by every laser shot, either a syringe or peristaltic pump was used to flow solution through a temperature controlled 0.5 mm pathlength IR cell with CaF_2 windows (Harrick Scientific). The temperature was monitored by a thermocouple located close to the photolysis solution and maintained by a water circulator to within ~ 0.10 °C. All spectra were obtained at 8 cm^{-1} resolution.

The photolysis solution contained ~ 4mM $CpMn(CO)_3$ or $BzCr(CO)_3$ in cyclohexane solvent and was 0.53 M in either furan or DHF. To this solution varying amounts of pyridine was added as the displacing ligand. All kinetic runs were carried out under pseudo-first order conditions with the concentration of pyridine at least ten times greater than that of [M]-(η^2-furan) and [M]-(η^2-DHF). The observed rate constants (k_{obs}) were obtained from single exponential fits to the absorbance *vs.* time dependence of the reactant and product complexes. The reported errors were obtained from least squares fits to the available data.

Solution Phase ATR-FTIR Studies. 100 mg (0.490 mmol) of $CpMn(CO)_3$ was weighed into a vial and sealed with a septum in an argon filled glove box. The vial was then moved into a fume hood and placed under an argon atmosphere where 10 mL of cyclohexane (CyH) was added via syringe. After dissolution, the $CpMn(CO)_3$ solution was cannulated to a jacketed reaction flask. The vial was rinsed with 10 mL of CyH

which was also cannulated into the reaction flask. After the addition of 1.0 mL (13.0 mmol) of DHF, a background scan was obtained. The reaction medium was then photolyzed with a 100 W Hg lamp (Newport) while it was monitored using an ASI ReactIR 1000 in-situ FTIR until the $CpMn(CO)_3$ was consumed (~ 30 min). After heating the resulting $CpMn(CO)^2(\eta^2$-DHF) solution to the desired temperature, the appropriate amount of CyH was added and the temperature allowed to stabilize (± 0.5 °C). Upon addition of pyridine, a background was obtained and the reaction was then monitored until the formation of $CpMn(CO)_2$(pyridine) was no longer observed.

Synthesis of $CpMn(CO)_2(\eta^2$-DHF) and X-ray Crystal Analysis. 100 mg (0.49 mmol) of $CpMn(CO)_3$ was weighed into a 50 mL round bottom flask with a Teflon® coated stir bar in an argon filled glove box and sealed with a septum. The complex was then dissolved in 20 mL of CyH and 1 mL (13.0 mmol) of DHF was added. The solution was photolyzed for approximately 2 hours after which solvent was removed via vacuum. Crystals suitable for X-ray analysis were obtained from slow evaporation of a diethyl ether solution of the complex in the presence of pentane and selected using a Lecia microscope. The representative crystal was coated with cryogenic protectant and affixed to a nylon sample loop. The crystal was then placed in a cold nitrogen stream and maintained at 213 K. Data was collected on a Bruker-AXS ApexII diffractometer and covered more than a hemisphere of reciprocal space. The structure was solved using direct methods utilizing SAINT[25], SHELX[28], XSEED[30] suite of programs. Crystal details and details of data collection can been found in Table 3-1.

Nanosecond IR Studies. The laser based TRIR apparatus at the Nottingham University is based upon the PIRATE facility at the Rutherford Appleton Laboratory and has been described previously.[46] Briefly, a commercial Ti:sapphire oscillator (MaiTai)/regenerative amplifier system (Spitfire Pro, Spectra Physics, 1KHz) is used to

Table 3-1. X-ray crystallographic data for $CpMn(CO)_2(\eta^2\text{-DHF})$

Empirical formula	$C_{11}H_{11}MnO_3$
Fw	246.14
Temp (K)	213(2)
Cryst system	Monoclinic
Space group	C 2/c
a (Å)	11.8494(15)
b (Å)	13.2037(17)
c (Å)	14.3448(18)
α (deg)	90
β (deg)	107.760(7)
γ (deg)	90
V ($Å^3$)	2137.4(5)
D_c (Mg/m^3)	1.530
Z	8
μ (mm^{-1})	1.217
Reflcns colled	21968
Indpndt reflcns	3945
Params	136
Goodness-of-fit	1.050
Final *R* indicies [$I > 2\sigma(I)$]	$R_1 = 0.0362$[a]
	$R_w = 0.0990$[b]
Final *R* Indicies (all data)	$R_1 = 0.0484$[a]
	$R_w = 0.1071$[b]

[a] $R_1 = \Sigma F_o||F_o|-|F_c|| \Sigma F_o$ [b] $R_w = \{[\Sigma w(F_o^2-F_c^2)^2]/[\Sigma w(F_o^2)^2]\}^{471/2}$

generate 800 nm laser pulses which pumps a TOPAS-C OPA (Light Conversion) with a DFG (difference frequency generator) unit to produce a tunable mid-IR pulse with a

spectral bandwidth of *ca.* 180 cm^{-1}. Part of the IR pulse is reflected onto a single-element MCT detector (Kolmar Technology) to serve as a reference, and the other part serves as the probe beam, which is focused and overlaps with the pump beam at the sample position.

In these experiments on the nanosecond/microsecond timescale the excitation pulse a Q-switched Nd:YVO laser (ACE- 25QSPXHP/MOPA, Advanced Optical Technology, UK), which is synchronized to the Spitfire Pro amplifier. The delay between pump and probe pulses can be controlled with a pulse generator (DG535, Stanford Research System) from 0.5 ns to 100 μs. The broadband transmitted probe pulse is detected with a 5 HgCdTe array detector (Infrared Associates), which consists of 128 elements, amplified by a 144-channel amplifier and digitized by a 16-bit analogue-to-digital converter (IR-0144, Infrared Systems Development Corp.). The measurements were performed on flowing solutions (3 mmol) in a CaF_2 IR cell, which was also raster-scanned to prevent localized laser-heating and photochemical decomposition.

DFT Calculations. The aromatic stabilization energy for furan was calculated through an extrapolation of the energy of hydrogenation of DHF and furan. This hydrogenation energy was calculated using the meta-GGA density functional of Tao, Perdew, Staroverov, and Scuseria[48] (TPSS) with the aug-cc-pvTz[49] basis set at the optimum geometries.

For the ligated metal complexes, TPSS was also used as it has been shown to perform well for transition metal systems. In order to keep computational costs low, geometry optimization and frequency calculations were done using the Couty-Hall[50]

basis set as in the previous work on this type of system.[6] All enthalpies of binding were thus calculated as the differences of the TPSS/aug-cc-pvTz energies plus frequency corrections from TPSS/Couty-Hall.

All calculations were performed by Edward Brothers in the development version of the GAUSSIAN suite of programs[51] using the high performance computing facilities available at Texas A&M University at Qatar.

Results and Discussion

Kinetic Studies Using 2,3-DHF. As previously reported, photolysis of a cyclohexane solution of either $CpMn(CO)_3$ or $BzCr(CO)_3$ in the presence of DHF results in the formation the linkage isomers M-(η^1-O-DHF) and M-(η^2-C,C-DHF).[6] Over time, the kinetically stable η^1 oxygen bound isomer transforms to the thermodynamically preferred η^2-olefin isomer on the millisecond and microsecond timescale for the Mn and Cr complexes, respectively. Subsequent displacement of the η^2-DHF from the metal center by pyridine can provide vital quantitative information concerning the strength of the metal-ligand bond (Figure 3-1). Due to the difference in the reactivity of the Cr-DHF and Mn-DHF, both rapid-scan FTIR and ATR-FTIR techniques (ATR = attenuated total reflectance) were utilized. For example, the reaction of $CpMn(CO)_2(\eta^2$-DHF) with pyridine occurs on the minute and even hour timescale, even at 60°C ,where the BzCr-(η^2-DHF) reaction goes to completion at room temperature in a matter of seconds.

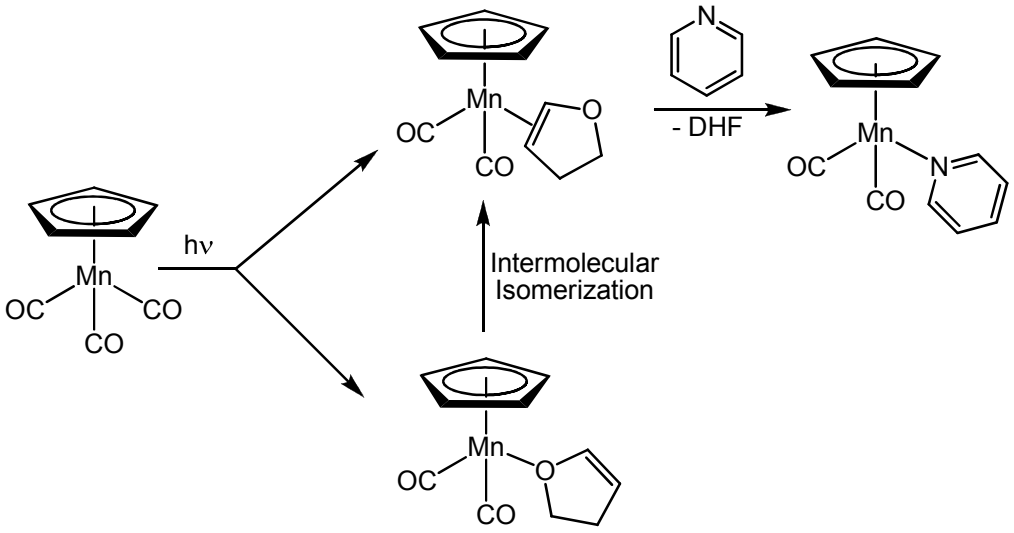

Figure 3- 1. Synthesis and isomerization of $CpMn(CO)_2(DHF)$ and reaction with pyridine.

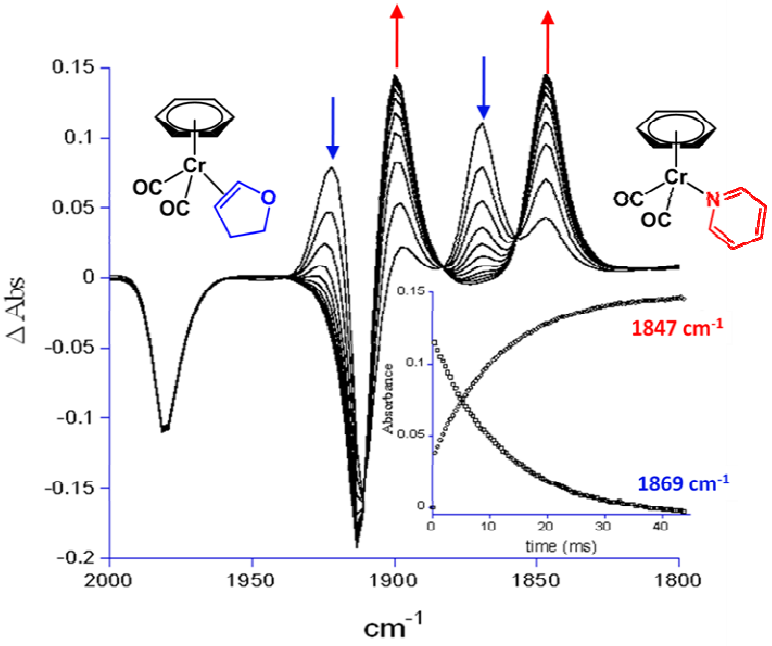

Figure 3- 2. Difference absorbance spectra showing the photolytically generated $BzCr(\eta^2\text{-DHF})$ complex with 0.06 M pyridine at 293K. The inset displays the growth and decay of the reactant and product complexes.

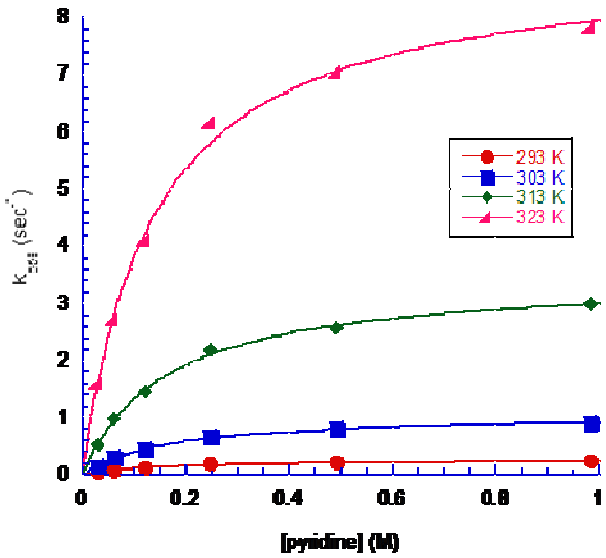

Figure 3-3. A plot of k_{obs} vs [pyridine] at several temperatures for the reaction of BzCr(η^2-DHF) with pyridine.

As shown in Figure 3-2, Cr(η^2-DHF), ν_{co} bands at 1924 and 1869 cm^{-1}, undergoes first order exponential decay at the same rate as the formation of $BzCr(CO)_2(py)$ (py = pyridine) (IR bands at 1897 and 1847 cm^{-1}) in the presence of 0.06 M pyridine.[52] The $CpMn(CO)_2(\eta^2$-DHF) shows similar spectral behavior with the DHF complex displaying CO bands at 1968 and 1906 cm^{-1} and the resulting pyridine complex absorbing at 1932 and 1866 cm^{-1}. Although the complexes are spectroscopically very similar, their reactivity towards the incoming pyridine ligand is markedly different. The Cr(η^2-DHF) complex reacts with pyridine approximately 50,000 times faster than the analogous Mn complex. This difference in reactivity is related to a stronger interaction between the DHF ligand and the Mn center, *vide infra*.

As shown in Figure 3-3, k_{obs} exhibits a nonlinear dependence on the pyridine concentration at all temperatures studied and approaches saturation kinetics at high concentrations of pyridine for both metals. The observance of this saturation behavior implies that the substitution reaction follows a dissociative mechanism (Figure 3-4).

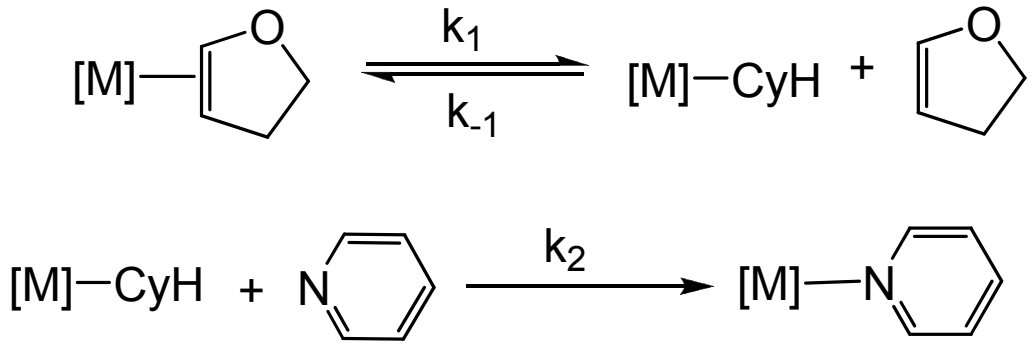

Figure 3- 4. Dissociative reaction mechanism proposed for the displacement of DHF by pyridine.

Adding to the support of a dissociative mechanism, displacement of other weekly coordinating ligands, such as tetrahydrofuran, arenes, alkenes, and silanes, from both $CpMn(CO)_2$ and $BzCr(CO)_2$ have been found to proceed through a dissociative mechanism.[43,44,47,53,54] Additionally, others have observed the formation of the [M]-CyH intermediate on the microsecond timescale; therefore, it is presumed that the reaction pathway for the displacement of DHF from the metal center also proceeds *via* this intermediate.[55,56] Assuming a steady state concentration of the [M]-CyH complex, the dependence of k_{obs} on the [pyridine] can be derived as

$$k_{obs} = \frac{k_1 k_2 [pyridine]}{k_{-1}[DHF] + k_2[pyridine]} \quad (\mathbf{5})$$

A fit of the data according to eq 1 is shown in Figure 3-3 and yields values of both k_1 and k_2/k_{-1} for the displacement of DHF by pyridine (Table 3-2). A comparison of the k_1 values at 323K reveals the rate associated with the bond breaking step of the

Table 3-2. Rate constants and activation parameters obtained from the plot of k_1 vs. [pyridine] according to eq 1 for the reaction of [M]-(η^2-DHF) with pyridine.

[M] = $CpMn(CO)_2$			M = $BzCr(CO)_2$		
T (K)	$k_1 \times 10^4$ (s^{-1})	k_2/k_{-1}	T (K)	k_1 (s^{-1})	k_2/k_{-1}
323	1.9 ± 0.2	3.0 ± 1.2	293	0.29 ± 0.01	3.7 ± 0.5
333	7.0 ± 0.5	4.8 ± 1.4	303	1.1 ± 0.1	3.3 ± 0.2
343	22 ± 1	5.7 ± 1.0	313	3.5 ± 0.1	3.3 ± 0.2
353	93 ± 5	4.2 ± 1.0	323	9.0 ± 0.3	3.9 ± 0.4
$\Delta H^‡$ = 28 ± 1 kcal mol^{-}			$\Delta H^‡$ = 21 ± 1 kcal mol^{-}		
$\Delta S^‡$ = +12 ± 4 e.u.			$\Delta S^‡$ = +11 ± 2 e.u.		

reaction is nearly 50,000 times larger for the Cr(η^2-DHF) complex over the Mn analogue. An Eyring analysis indicates that this difference can be attributed to a ~7 kcal mol^{-1} larger activation enthalpy in the case of the Mn complex. Additionally, the relatively large positive entropy term (+11-12 e.u.) associated with k_1 are consistent with the transition state being more of a bond breaking event, thus supporting the conclusion of the dissociation of DHF prior to the binding of the pyridine. Assuming that the CyH solvent binds to the metal after dissociation of DHF in the transition state, the calculated

activation enthalpies of 21 and 28 kcal mol^{-1} (± 1 kcal mol^{-1}) for the Cr and Mn complexes respectively, are expected to serve as reliable estimates of the [M]-(η^2-DHF) bond.

Good agreement between the experimentally obtained enthalpy values and the bond dissociation enthalpies calculated by Edwards *vide infra*, also suggest the metal DHF bond is mostly broken in the transition state. Additionally, the weaker binding of the DHF to the Cr center is consistent with previous studies that also showed weaker binding of ligands such as tetrahydrofuran and η^2-arenes to the $BzCr(CO)_2$ fragment relative to the $CpMn(CO)_2$ complexes.[44,47,53,54] The lower ν_{co} band positions in $BzCr(CO)_2$ implies that the Cr center is more electron rich than the Mn in $CpMn(CO)_2$ and the difference in binding strength is mostly due to a reduction in the ligand-to-metal σ donation. Additionally, if the π-back-bonding were to play major role in the metal DHF interaction, the rate of the Cr-DHF dissociation would be expected to be slower due to the increased electron density at the metal, which is not experimentally observed.

The virtually constant values of k_2/k_{-1} with respect to both temperature and [pyridine] suggest that the [M]-CyH intermediate is not very selective in it reaction with either DHF to reform the starting complex or pyridine to form the product. This observation is consistent with previous results that focused on the reactivity of [M]-CyH solvate complexes. For example, $CpMn(CO)_2(CyH)$ was observed to react 3-4 times faster with pyrrolidine than with cyclopentene with only a 1.4 kcal mol^{-1} difference in the activation enthalpies.[56]

Due to the relative stability of the $CpMn(CO)_2(\eta^2$-DHF) complex, the complex was successfully isolated and structurally characterized via single crystal X-ray diffraction. A thermal ellipsoid representation of the complex can be viewed in Figure 3-5. The metal is bound almost symmetrically between the π face of the C-C double

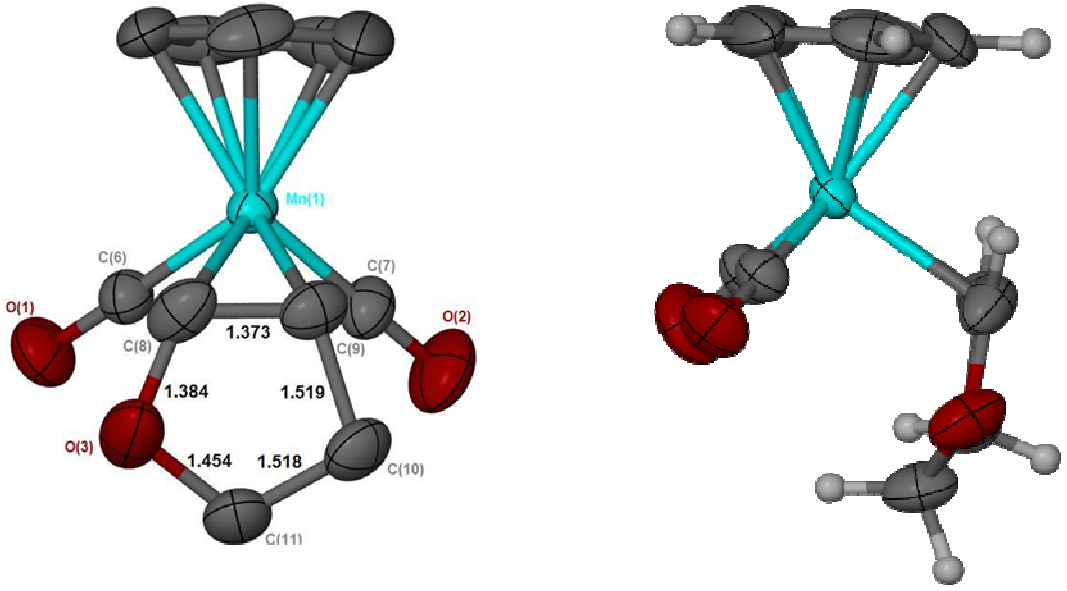

Figure 3- 5. Thermal ellipsoid drawings of $CpMn(CO)_2(\eta^2$-DHF).

bond of DHF as evidenced by the Mn(1)-C(8) and Mn(1)-C(9) distances of 2.203(2) and 2.171(2) Å respectively. Importantly, the C-C bond distance is slightly elongated, 1.373 Å compared to the typical bond length of 1.33 Å for an uncoordinated double bond, indicating some metal-to-ligand π-back bonding. Although some lengthening is to be expected due to conjugation of the olefin bond with the oxygen of the DHF heterocycle,

DFT calculations support the π-back bonding interaction with the Mn center which serves to weaken the C=C bond.

Kinetic Studies Using Furan. Photolysis of either parent carbonyl in the presence of furan also results in the formation of a single species with CO absorptions at 1869, 1925 cm^{-1} and 1906, 1965 cm^{-1} for the Cr and Mn complexes respectively. By correlation with the ν_{co} bands of the [M]-(η^2-DHF) complexes and those for $CpMn(CO)_2(\eta^2$-cyclopentene), these bands are aassigned to the [M]-(η^2-furan) complexes.[56] Interestingly, the formation of the η^1-O-furan complex was not observed on the millisecond timescale, unlike the DHF experiments. Experiments performed by George and coworkers on the submicrosecond timescale in neat furan do provide evidence for the existence of the oxygen bound isomer, $CpMn(CO)_2(\eta^1$-O-furan), with an absorbance at 1869 cm^{-1}.

At room temperature, this species has a half life of about 2 μs before fully converting to the more thermodynamically stable $CpMn(\eta^2$-C,C-furan) complex. The conversion from the oxygen bound to the η^2-(C,C) isomer is almost 3000 times faster in the case of furan relative to DHF implying a lower (~2-3 kcal mol^{-1}) activation barrier to isomerization. The weaker η^1-O binding of furan suggests that the lone electron pairs on the oxygen are much less accessible for bonding due to delocalization within the aromatic ring system. Alternatively, the lone electron pair on the oxygen might also be held tighter do to the increased *s* character also attributing to the weaker donor characteristics of this ligand.

When exposed to pyridine, [M]-(η^2-furan) converts to [M]-pyridine almost 20,000 times faster than the [M]-(η^2-DHF) under similar reactions conditions. Again,

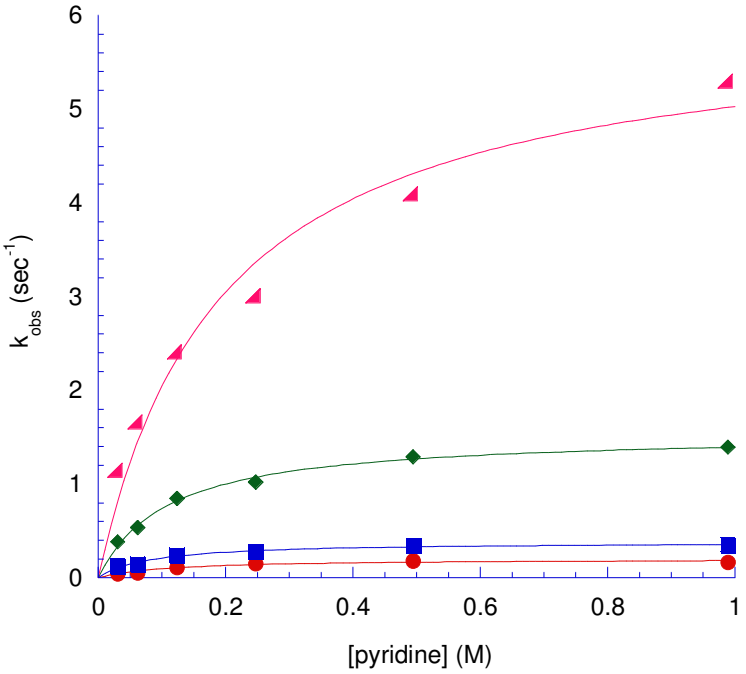

Figure 3- 6. Plot of k_{obs} vs. [pyridine] at several temperatures for the reaction of $CpMn(CO)_2(\eta^2$-furan) with pyridine.

saturation kinetics are observed for k_{obs} indicative of a dissociative mechanism similar to the DHF complexes (Figure 3-6). The displacement of the furan ligand from the Cr center is also 10,000 times faster than the same reaction for the Mn complex. Values of k_1 and k_2/k_{-1} obtained from the fit of the data in Figure 3-6 using eq 1 can be found in Table 3-3. From the temperature dependence of k_1, activation enthalpies of 22 ± 1 and ~11 kcal mol^{-1} were obtained for dissociation of the Mn(η^2-furan) and Cr(η^2-furan)

bonds respectively. Because of the significantly faster displacement rates for the BzCr(η^2-furan) complex, step-scan FTIR was utilized to study the substitution kinetics. In order to achieve these measurements, a continuous flow of reaction solution was

Table 3- 3. Rate constants and activation parameters obtained from the plot of k_1 vs. [pyridine] according to eq 1 for the reaction of [M]-(η^2-furan) with pyridine.

[M] = $CpMn(CO)_2$			M = $BzCr(CO)_2$		
T (K)	k_1 (sec^{-1})	k_2/k_{-1}	T (K)	k_1 (sec^{-1}) x 10^{-3}	k_2/k_{-1}
288	0.25 ± 0.01	3.5 ± 0.4	293	5.8 ± 0.6	2.0 ± 0.3
293	0.41 ± 0.01	5.3 ± 0.5	305	12 ± 1	3.2 ± 0.3
303	1.7 ± 0.1	3.8 ± 0.3			
313	5.4 ± 0.2	3.7 ± 0.5			
$\Delta H^{\ddagger}$ = 22 ± 1 kcal mol^{-}			$\Delta H^{\ddagger} \approx$ 11 kcal mol^{-}		
$\Delta S^{\ddagger}$ = +15 ± 3 e.u.			$\Delta S^{\ddagger} \approx$ +0 e.u.		

required. Due to the boiling point of furan, thermal loss in the circulation apparatus, and a buildup of moisture on the cell windows, measurement temperature was limited to below 40 and above 20 °C. Therefore, it is important to note that the both the $\Delta H^{\ddagger}$ and $\Delta S^{\ddagger}$ values are expected to be estimates since k_1 was determined at two temperatures over a narrow temperature range (ΔT = 12 K).

As shown in Table 3-4, estimates of the bond dissociation enthalpies of the [M]-(η^2-DHF) and [M]-(η^2-furan) complexes show that both the furan and DHF bind to Cr 7-10 kcal mol^{-1} weaker than when binding to the Mn center. Also interesting, is the 7-10

kcal mol^{-1} difference between the binding of furan and DHF to either the Cr or Mn center. Since the major difference between furan and DHF is that the former ligand is

Table 3- 4. Experimental and theoretical estimates for the bond dissociation enthalpies of the [M]-(η^2-L) interactions.[a]

Complex	ΔH_1 (kcal mol^{-1})
[Mn]-(η^2-DHF)	28 (29.2)
[Mn]-(η^2-furan)	22 (20.6)
[Cr]-(η^2-DHF)	21 (21.3)
[Cr]-(η^2-furan)	~11 (14.1)

[a] Numbers in parentheses were obtained from DFT calculations at the TPSS/aug-cc-pTZ level of theory

aromatic, the 7-10 kcal mol^{-1} difference can be related to the disruption of the resonance stabilization of the furan ligand upon binding to the metal center. Metal to ligand π back bonding would serve to further localize the electron density and result in a partial loss of resonance energy in the case of the aromatic furan ligand. Therefore, the difference in the binding enthalpy can be attributed to the energetic cost of disrupting the aromaticity of the furan ligand upon biding to either the $CpMn(CO)_2$ or $BzCr(CO)_2$ fragment. These results provide important quantitative information regarding the capability of a metal center to dearomatize a η^2-aromatic ligand. In order to further understand and aid in the interpretation of the experimental results, DFT calculations were performed by Prof. Edward Brothers.

Results from DFT Calculations. The calculated structure of [Mn]-(η^2-DHF) can be viewed in Figure 3-7 along with the structure obtained from X-ray diffraction studies of the same complex. Additionally, selected bond distances and calculated bond dissociation enthalpies can be viewed in Table 3-5 and 3-4 respectively. A comparison

Table 3- 5. Calculated and experimental bond distances.[a]

	Bond Distance (Å)		
Compound/Complex	C(8)-C(9)	[M]-C(8)	[M]-C(9)
furan	1.37		
DHF	1.34		
[Mn]-(η^2-DHF)	1.41	2.21	2.16
[Mn]-(η^2-DHF)[b]	1.379	2.203	2.171
[Mn]-(η^2-furan)	1.42	2.19	2.26
[Cr]-(η^2-DHF)	1.40	2.34	2.26
[Cr]-(η^2-furan)	1.41	2.31	2.39

[a] Numbering scheme refers to Figure 3-5. [b] Experimental values.

of the calculated and experimental structures in Figure 3-7 along with those in Table 3-5 demonstrate good agreement between the calculated and experimental values. Additionally, the calculated bond dissociation enthalpies are also in excellent agreement with the experimentally determined values suggesting that the activation enthalpies do in fact serve as good estimates for the M-L bond strengths. The precision in the calculated and experimental values lends support to the conclusion that the substitution reaction proceeds through a dissociative pathway and that the M-L bond is fully dissociated in the transition state.

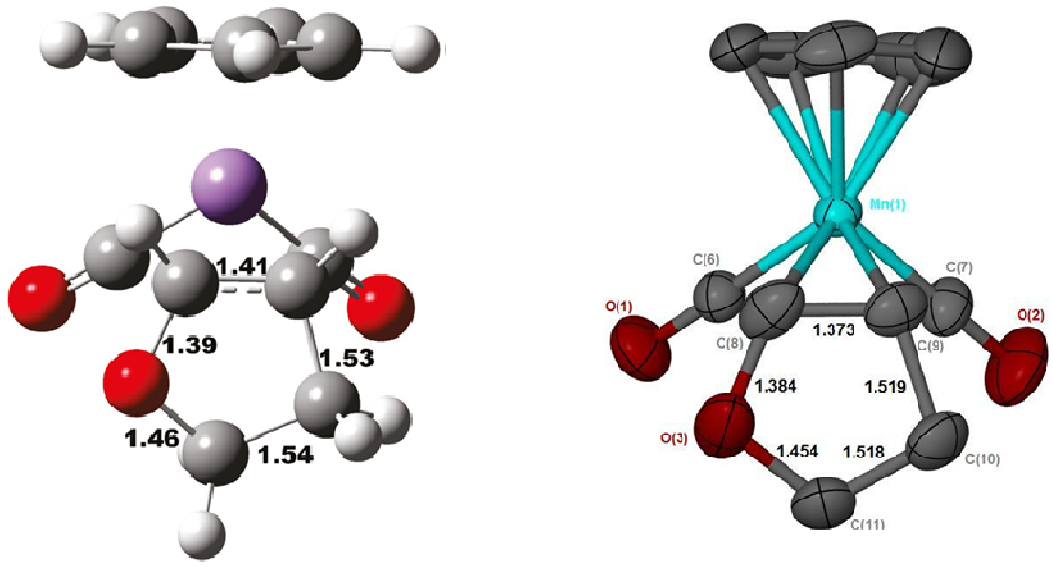

Figure 3- 7. (A) Calculated and thermal ellipsoid drawing (B) of $CpMn(CO)_2(\eta^2$-DHF) with selected bond distances (Å).

A comparison of the calculated bond distances for the [Mn]-(η^2-DHF) and [Mn]-(η^2-furan) complexes reveals a ~ 0.1 Å shorter C=C bond than in the analogous Cr complexes, consistent with the experimentally observed weaker binding of both ligands to the more electron rich Cr center. In agreement with experimental results, the calculated C=C distance upon metal binding is ~ 4-5 % longer suggesting a π-back bonding contribution to the overall metal-η^2 interaction. Also, the calculated C-C bond length of the metal bound olefin is slightly longer for the bound DHF implying a stronger interaction of the DHF over furan when binding to a metal center, which is also observed experimentally.

Among the five membered heterocycles, furan is expected to be the least aromatic due to the higher electronegativity of the oxygen atom when compared to both

sulfur and nitrogen of thiophene and pyrrole. Some estimates of the resonance stabilization energy of furan calculate a range from 11 to 23 kcal mol^{-1}.[57,58] Brothers obtained an approximation for the resonance stabilization energy for furan by calculating the enthalpy for the hydrogenation reactions of both DHF and furan. The calculations revealed a value of 15.8 kcal mol^{-1} that falls in the range previously mentioned. Remembering that furan binds to the metal center 7-10 kcal mol^{-1} weaker than DHF regardless of the identity of the metal center implies an approximately 50% loss of resonance stabilization that the furan ligand must undergo in order to interact with the metal center.

Further evidence for a dearomatization of the furan upon binding to the metal was found using natural bond order analysis (NBO). The bond order of the free ligands and each ligand bound to both Mn and Cr centers were utilized to gain further insight to the effect metal binding has on the ligand. From Figure 3-8, some electron delocalization can be observed in the free furan ligand as evidenced by a C-C bond order of 1.27 and the slightly reduced olefinic bond orders of 1.65. Additionally, in the case of the DHF and furan interacting with both metals, a reduction in both the C-C and C=C bond orders implies a localization of electron density about the metal-η^2 bond and a disruption of the π system of the aromatic furan ligand. A 20-30 % lessening of the bond order of the coordinated π-bond, independent of the metal center, suggest that the weaker binding of the ligands to Cr is primarily due to a weaker ligand $\rightarrow$ M σ donation in the case of the more electron rich $BzCr(CO)_2$ fragment. The NBO analysis also calculates the change in the bond order upon interacting with the metal center of the

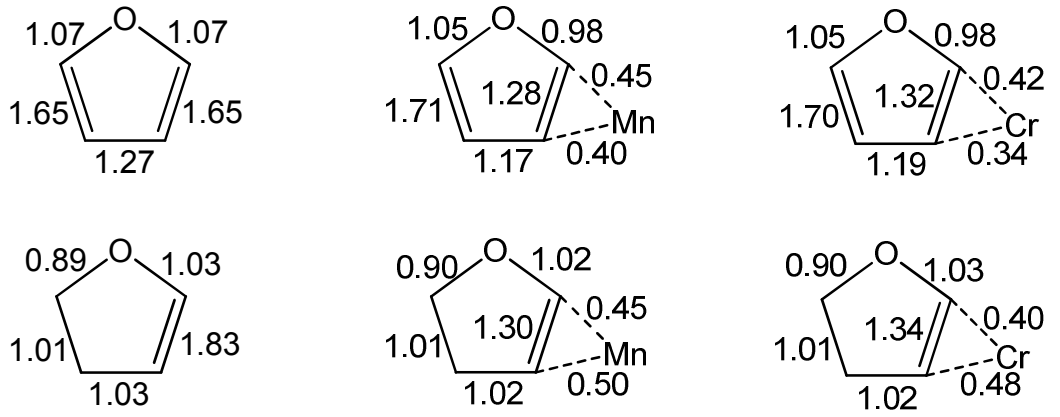

Figure 3- 8. Calculated bond orders for uncoordinated and coordinated furan and DHF ligands.

furan ligand is less than in the case of DHF suggesting a reduced contribution of π-back bonding in the [M]-(η^2-furan) interaction versus the [M]-(η^2-DHF) instance.

Conclusions

The study of the interaction of electron poor metal fragments with unsaturated C-C bonds, especially those of aromatic compounds, is of great interest to catalysis. Until now, very little quantitative information has been reported regarding this very important bonding interaction that has implications in a variety of applications from hydrogenation, electrophilic aromatic substitution, and several other areas. A study of the displacement of photolytically generated $CpMn(CO)_2(\eta^2\text{-L})$ and $BzCr(CO)_2(\eta^2\text{-L})$ where L = DHF or furan, has provided insight into both the interaction of these ligands with electron poor metal centers as well as evidence for a dearomatization of the furan ligand upon interaction with the metal center. The ligand substitution was found to follow a dissociative pathway and the temperature dependence studies of the limiting

rate constant provides an estimate of the strength of the metal-η^2 bond. Results suggest that DHF and furan interact 7-10 kcal mol^{-1} weaker with Cr than with Mn due to a reduced ligand to metal σ donation for the more electron rich $BzCr(CO)_2$ fragment. Interestingly, the metal-DHF interaction is found to be stronger than the metal-furan interaction independent of the identity of the metal. This difference in the binding enthalpy is attributed to a partial loss of resonance energy that occurs upon metal binding of the aromatic furan ligand. DFT calculations performed by Brothers are consistent with the experimental results and support the partial dearomatization of the furan ligand upon metal binding. Whereas most of the work in this area concentrates on strongly π-basic metals that upon interaction with an aromatic ligand, such as benzene, results in a complete dearomatization of the ligand, information regarding the weaker interaction of such ligands with metals can provide much needed information for the development of more active and efficient catalysts.

CHAPTER IV

TECHNIQUES FOR THE SEPARATION OF POLYMER/CATALYST MIXTURES*

Introduction

In recent years, the need for a reduction in the production of greenhouse gases has become an ever present topic in our society. Probably the most discussed among the various pollutants is carbon dioxide. To utilize even a small portion of this gas for the production of consumer products would be of great value. Even though the total impact of CO_2 utilization would be small when compared to the annual production, it is important to make use of a chemical that is otherwise considered nothing more than a byproduct with negative environmental side effects.

Carbon dioxide is cheap, abundant, inert, non-corrosive, and nontoxic. Traditionally, it has been used as a solvent and more recently as a C1 carbon feedstock. One possible chemical use for CO_2 is as a monomer in the production of polycarbonates. Polycarbonates are much sought after for their strength, clarity, heat capacity, potential use in biological applications, and several other attributes that make them useful for a wide variety of applications. One route to these materials is represented in Scheme 4-1.

---

*Reprinted in part with permission from Hongfa, C.; Tian, J.; Andreatta, J., Darensbourg, D. J.; Bergbreiter, D. E. *Chem. Commun*, **2008**¸ 975-977. Copyright 2008 The Royal Chemical Society. and Phan L.; Andreatta, J. R.; Horvey, L. K.; Edie, C. F.; Luco, A.-L.; Mirchandani, A. Darensbourg, D. J.; Jessop, P. J. *J. Org. Chem.* **2008**, *73*, 127-132. Copyright 2009American Chemical Society.

The copolymerization of CO_2 and epoxides has been studied in great detail over the past 40 years. It began with the discovery by Inoue and coworkers utilizing a heterogeneous catalyst derived from an Et_2Zn/H_2O mixture that was able to couple CO_2

Scheme 4- 1. The reaction of CO_2 and epoxides to afford polycarbonate, polyether, and cyclic carbonate.

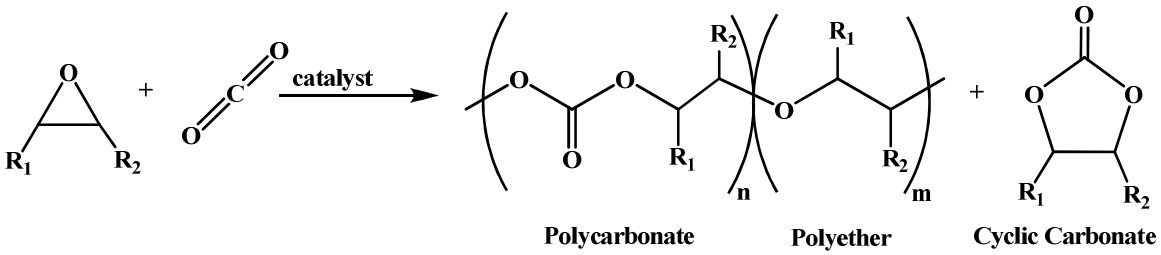

and propylene oxide to form poly(popylene carbonate) (PPC) (Scheme 4-1, R_1 = Me, R_2 = H).[59] As depicted in Scheme 4-1, the desired polycarbonate product can be formed in conjunction with other undesired byproducts. Consecutive ring opening of epoxides leads to polyether linkages which have a detrimental effect on the thermal properties of the product. Additionally, the copolymerization is accompanied by the production of cyclic carbonates that serve to shorten the polymer chain length by one unit.

The first homogeneous zinc based catalysts for the copolymerization of epoxides and CO_2 were synthesized by Darensbourg and coworkers in 1995.[60] Zinc bisphenoxides were found to be highly active and selective for the formation of poly(cyclohexene carbonate) (PCHC) with turnover frequencies (TOF) (TOF = (mol epoxides consumed)(mol catalyst $\cdot$ h)$^{-1}$) of up to 16.5 h^{-1}(Figure 4-1).[61] The next major

advancement came with the utilization of zinc betadiiminates that were able to selectively form PCHC with TOF of up to 2300 h^{-1}(Figure 4-1).[62] The first example of a

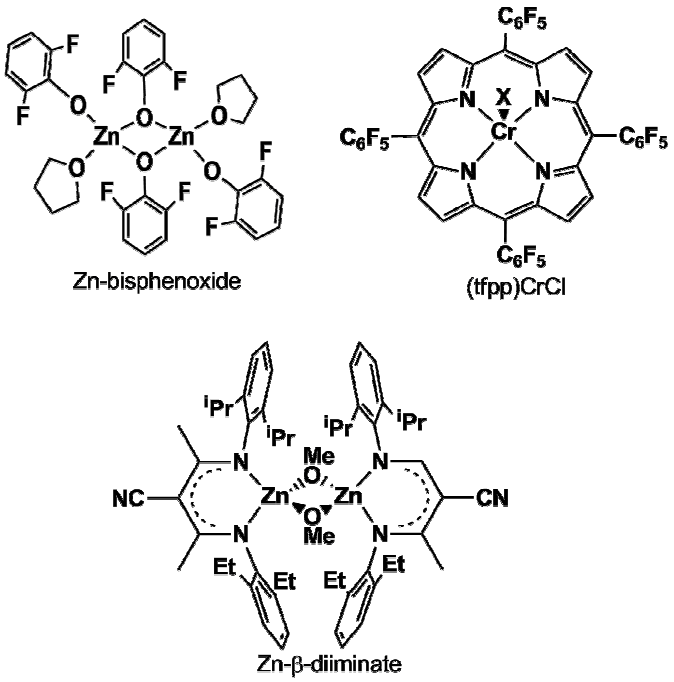

Figure 4- 1. Active catalysts for the copolymerization of CO_2 and epoxides.

CO_2 soluble catalyst was synthesized by Mang and (Figure 4-1) and was able to achieve TOFs of up to 173 h^{-1}.[9] This highly fluorinated chromium-porphyrin catalyst (tfppCrCl) was active for the copolymerization, and also exhibited solubility in super critical CO_2.

Since that time, the Darensbourg group has concentrated on the utilization of transition metal salen (salen = *N,N´-bis*(3,5-di-*tert*-butylsalicylidene)-1,2-ethylenediimene) complexes. The most active catalyst displayed in Figure 4-2

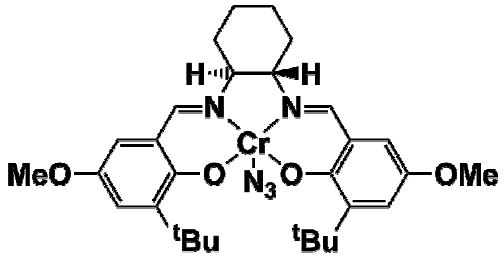

Figure 4- 2. (Salcy)CrN_3 catalyst utilized for the copolymerization of CO_2 and epoxides.

achieved TOFs of 1153 h^{-1} with > 99% CO_2 inclusion and minimal cyclic production.[63] Other groups have utilized the salen architecture with Co(III) to facilitate the copolymerization of propylene oxide and CO_2 to form the industrially useful PPC. Cobalt salen complexes were able to selectively form PPC at room temperature and CO_2 pressures as low as 1 atmosphere.[64-66] The next major advance was the addition of pendant ammonium moieties attached *para* to the metal bound oxygen of the salen ligand (Figure 4-3).[10,67] These complexes facilitated the copolymerization of propylene oxide and CO_2 with high selectivity and TOF of up to 26,000 per hour. In addition to high activity, these catalysts were able to produce high molecular weight polymers at high monomer to initiator ratios compared to the Cr(salen)Cl/PPNCl catalytic system.

Catalytic activity has made great strides since the initial discovery of the copolymerization of CO_2 and PO; however, the manner in which the polymer is isolated has not. One of the attractive and green attributes of polymerization process is that it

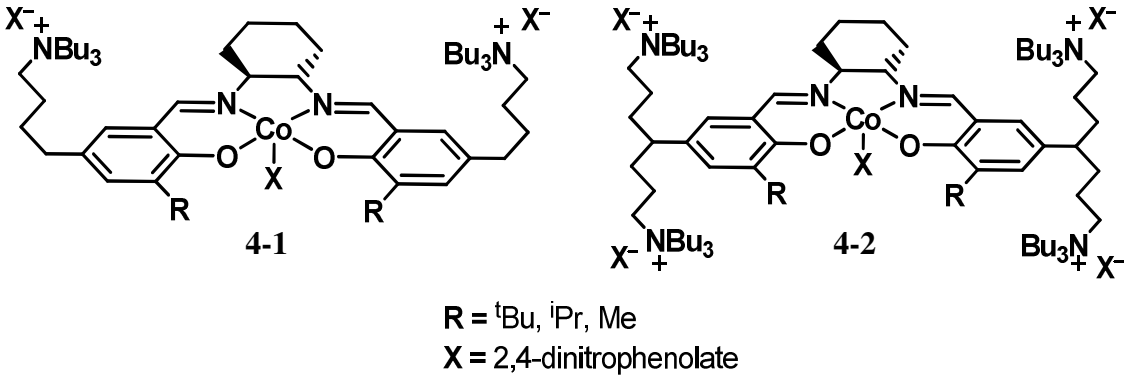

Figure 4- 3. Cobalt salen complexes synthesized by Lee and coworkers.

does not require extraneous solvents. The traditional method for polymer isolation requires the utilization of organic solvents and strong acid. As new, highly active catalysts are developed, methods for green separations must be developed to keep the overall impact of polycarbonate production as environmentally benign as possible.

There are several approaches that could be taken to achieve the green polymer/catalyst separation. One approach would to be the utilization of CO_2 as a solvent. This would require either the polymer or the catalyst to be CO_2 soluble. The only example of a CO_2 soluble catalyst for the copolymerization of CO_2 and epoxides is the Cr(tfpp)Cl synthesized by Mang and Holmes (Figure 4-1) which was soluble in supercritical CO_2.[9] The fluorination of ligands has been utilized in the past to impart CO_2 solubility and usually requires multistep synthesis and lengthy work ups. If this process is to be used in an industrial setting, separation must be cost effective; therefore, this option was not explored do the cost of both time and money required for fluorination.

The other option for the utilization of CO_2 as a solvent is to synthesize a CO_2 soluble polymer. Darensbourg and coworkers performed experiments using a carbon dioxide soluble epoxide for kinetic studies and also explored its isolation via liquid CO_2 transfer (Figure 4-4).[8] The silated epoxide, 2-(3,4-epoxycyclohexyl)-ethyltrimethoxysilane (TMSO), has a structure very similar to the well studied cyclohexene oxide (CHO) monomer. When utilizing Cr(salen)Cl and PPN salts

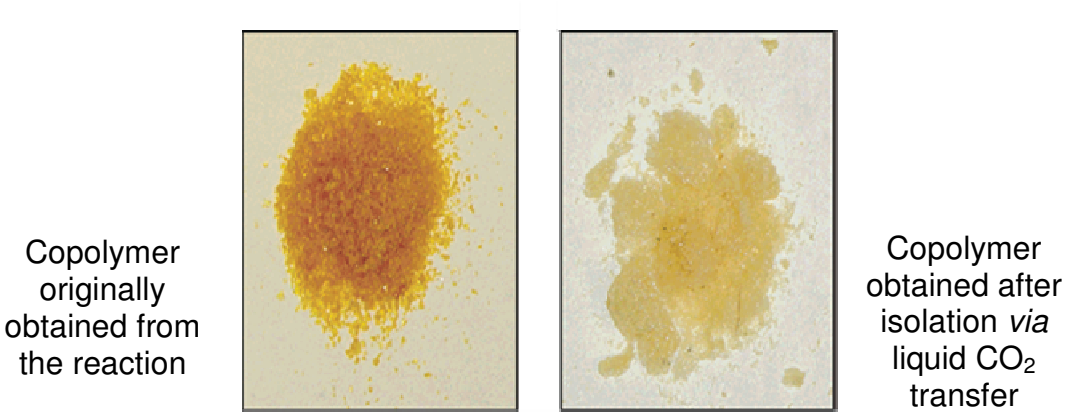

Figure 4- 4. Poly(TMSO carbonate) before and after liquid CO_2 extraction.

(PPN = bis(triphenylphosphoranylidene)ammonium cation) as the catalyst system, the rate of polymer formation was almost identical for the formation of poly(TMSO carbonate) versus that of PCHC. This system was not without drawbacks. The siloxy group of the polymer was found to be prone to hydrolysis, and the subsequent crosslinking which leads to insoluble materials.

The only example of a catalyst that is both highly active and easily separated from the polymer/catalyst mixture is complex **4-2** (Figure 4-3). The pendent ammonium groups allow this catalyst to be removed via filtration through a of silica gel column.[10] In addition to easy separation of the catalyst, the researchers were able to recycle, recover, and reuse the catalyst several times with very little loss in activity.

Experimental

Methods and Materials. Unless otherwise stated, all synthesis and manipulations were carried out on a double-manifold Schlenk vacuum line under an argon atmosphere or in an argon filled glove box. Methylene chloride, diethyl ether, acetonitrile were freshly purified via MBraun Manual Solvent Purification System packed with Alcoa F200 activated alumina desiccant. Cyclohexene oxide and N-butyl-N-ethyl amine were purchased from VWR International. Cyclohexene oxide was freshly distilled from CaH_2 before use. N-ethyl butyl amine (HNEtBu) was used degassed by bubbling nitrogen through the solution for approximately 10 minutes prior to use. Bone dry carbon dioxide was supplied in a high pressure cylinder equipped with a dip tube by Scott Specialty Gases. PPNCl was purchased from Aldrich Chemical Company, recrystallized from dichloromethane and diethyl ether, and stored in a controlled atmosphere glove box. $PPNN_3$ was prepared via literature method and stored in an argon filled glove box.[68] Cr(salen)Cl was synthesized via literature methods.[69] Cr(PIBsalen)Cl (H_2PIBsalen = *N*,*N'*-bis(3-*tert*-butyl-5-poly(isobutylene))-1,2-ethylenediimene) was synthesized by Chayanant Hongfa and stored in an controlled atmosphere glove box.[70] All infrared spectra were obtained using a Mattson 6021 FT-IR

spectrometer with DGTS and MCT detectors. *In situ* infrared measurements were performed using an ASI ReactIR 1000 as previously described.[71] All ^{1}H and ^{13}C NMR spectra were obtained using either an INOVA Unity+ 300 MHz or INOVA 500 MHz superconducting NMR spectrometers. Molecular weights were measured using a Viscotek Gel Permeation Chromatograph equipped with refractive index, right-angle and low-angle light scattering detectors and THF as the eluent.

General Polymerization Procedure. 50 mg of Cr(salen)Cl (or 210 mg of Cr(PIBsalen)Cl, 0.104 mmol) and 1 equivalent (0.0104 mmol) of PPNX (X = Cl or N_3) were weighed into a glass vial containing a Teflon® coated stir bar and sealed using a septum in an argon filled glove box. The vial was moved to a hood and placed under an atmosphere of argon and approximately 15 mL of CH_2Cl_2 was added. The solution was stirred for 30 minutes and solvent was then removed *in vacuo*. The "activated catalyst" was dissolved in 10 mL of cyclohexene oxide and loaded via cannula into a 300 mL Parr reactor at 80 °C. The vial was rinsed with 10 mL of cyclohexene oxide which was subsequently added to the reactor. The reaction vessel was pressurized to 35 bar CO_2 pressure and heated to 80 °C for 4 hours. Upon completion of the reaction, the reactor was cooled and the CO_2 vented. The remaining viscous liquid was treated according to the prescribed polymer/catalyst separation procedure.

Procedure of Polymer/Catalyst Separation Using Switchable Polarity Solvent. Upon completion of the aforementioned polymerization reaction, the CO_2 was vented and the reactor placed under vacuum for 20 minutes to remove all traces of CO_2 rapidly. Degassed HNEtBu (20 mL) was loaded into the reactor via cannula and the

reaction mixture stirred for 1 hour. The reactor was opened and the contents emptied into a 125 mL Erlenmeyer flask and rinsed with an additional 10 mL of degassed HNEtBu and added to the flask. CO_2 was bubbled through the reaction mixture for 30 minutes resulting in the precipitation of the polymer. The resultant polymer/catalyst/ionic liquid slurry was mechanically stirred to ensure maximum catalyst removal and then filtered using a Buchner funnel. The amine was recovered and recycled via the distillation of the ionic liquid/catalyst solution. Further polymer purification was achieved via the addition 20 mL of HNEtBu. The solution was mechanically stirred for 20 minutes at which time CO_2 was bubbled through the solution to access the high polarity ionic liquid. After filtration, the polymer was dried in a vacuum oven at 60 °C overnight.

Results and Discussion

Catalyst design and efficiency for the copolymerization of CO_2 and epoxides has made vast improvements since 1969; however, the manner in which the polymer and catalyst are separated has remained relatively unchanged. In the case of chromium, cobalt, and manganese based catalysts, the polymer product requires several washings to remove the undesired color due to catalyst contamination. Zinc metal catalysts do not impart color to the catalyst, but, like all the metal complexes, catalyst remnants could potentially cause polymer degradation during the late steps of the production process, in addition to any potential health risks that might result from exposure to metal contamination during the consumer use of products. With such advances in catalyst design, the day that this technology will be adapted and scaled to the industrial level is

nearing. In order to reduce the production of massive amounts of organic and acidic waste, new techniques must be explored to streamline the separation of the polymer/catalyst mixtures in an equally efficient and environmentally benign manner.

One approach to this problem would be to modify a highly active catalyst, such as Cr(salen)Cl (**4-3**), to assist in the separation process. The ideal complex would require the modification be both synthetically non-intense while retaining or even enhancing the overall activity and selectivity of the catalyst. Bergbreiter and coworkers have presented several examples of attaching polymeric moieties to known catalysts to

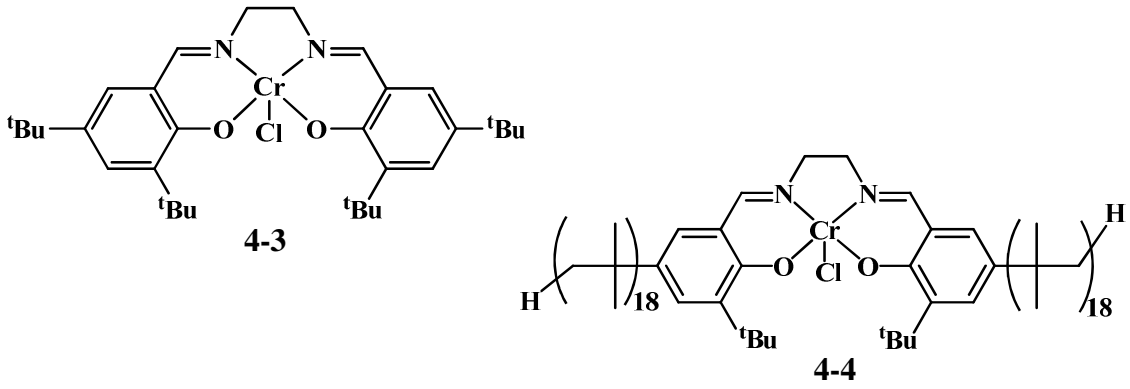

Figure 4- 5. Catalysts **4-3** and **4-4** for the copolymerization of $CO_2$and epoxides.

aid in the separation of the catalyst from the reaction mixture.[72-76] In the same spirit, Chayanant Hongfa synthesized a salen ligand that replaced the *t*-butyl group in the five position of the phenolates with 1,000 Dalton poly(isobutylene) chains (Figure 4-5). The Cr(PIBsalen)Cl (**4-4**) complex was synthesized in good yields from commercially available starting materials and isolated in high purity.[70]

We next set out to determine if the addition of the polymer groups to the salen architecture would have any detrimental effects on the activity of the catalyst. The rate of reaction of each catalyst for the coupling of CHO and CO_2 was measured using *in situ* ATR-FTIR. A comparison of the rates of reaction can be observed in Figure 4-6. As observed in the plot, the activity of the Cr(PIBsalen)Cl complex is almost identical to the rate of the Cr(salen)Cl. In addition to activity, both catalyst produced polymers with very similar molecular weights and polydispersity indices (PDI). Analysis of the polymeric products obtained using **4-3** revealed a M_n of 33,269 Daltons (PDI = 1.53) while complex **4-4** produced polymer with a M_n of 28, 829 (PDI = 1.66).

Though the addition of the poly(isobutylene) (PIB) groups to the salen have very little effect on the activity of the catalyst, they do have a large effect on the solubility. Complex **4-3** is readily soluble in a variety of organic solvents such as dichloromethane (DCM), tetrahydrofuran (THF), acetonitrile, methanol (MeOH) and several others, but it is not soluble in non polar organic solvents. The addition of the PIB moieties imparts solubility of **4-4** in solvents such as hexane and heptane which are immiscible with the somewhat polar solvents that are traditionally used to dissolve **4-3**. Therefore a scheme was developed to take advantage of this added solubility. The conventional method for polymer purification is to dissolve the reaction mixture in a minimal amount of DCM and then add a large excess of 1M HCl in MeOH resulting in the precipitation of the polymeric product. This process is usually repeated several times to ensure that most of the chromium catalyst is removed from the desired product. This creates a large amount of acidic organic waste which is one of the major drawbacks of the current industrial

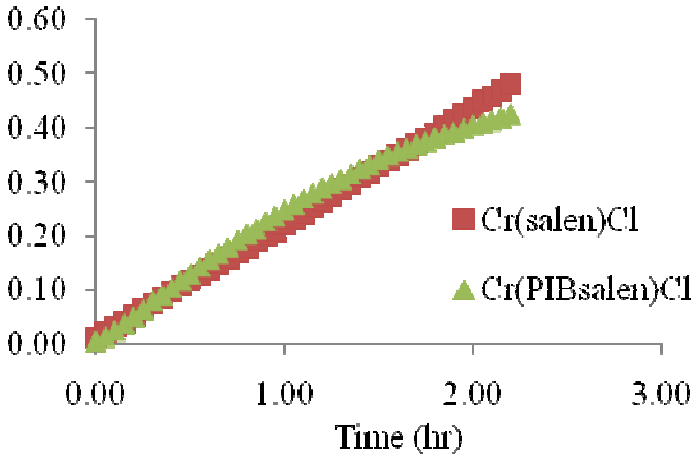

Figure 4- 6. Plot of reaction profile of polymer peak at 1750 cm^{-1} for the copolymerization of CHO and CO_2 using (salen)CrCl and (PIBsalen)CrCl.

process. In addition to the production of large amounts of solvent waste, this process also renders the catalyst inactive, thus requiring fresh catalyst be used each time a polymerization is performed.

Utilization of **4-4** allows for less harsh and more green conditions. In this scheme the polymer/catalyst mixture is dissolved in minimal amount acetonitrile.[70] To this, a few drops of concentrated HCl are added followed by extraction of **4-4** using heptane. A comparison of the polymeric products obtained after one round of purification can be seen in Figure 4-7. It is clear from the picture that the polymer obtained using **4-4** and the acetonitrile/heptane isolation scheme (Figure 4-7b) is much more pure than the polymer isolated via the traditional route(Figure 4-7a). In order to quantify the efficiency of the respective methods for metal removal, samples of each polymer were subjected to Inductively Coupled Plasma-Mass Spectrometry (ICP-MS) to

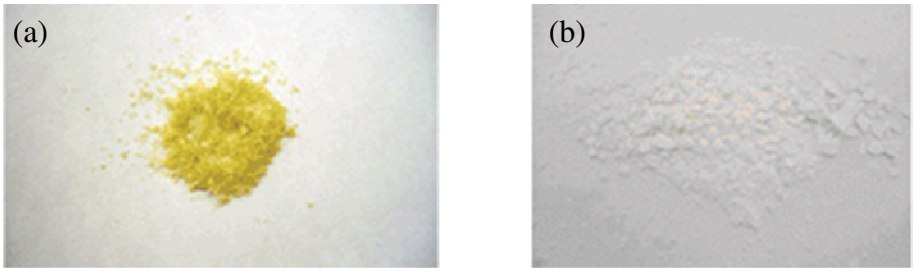

Figure 4- 7. Colorimetric comparison of (a) the polycarbonate formed using **4-3** and isolated after 1 acidified MeOH precipitation and (b) the polycarbonate isolated after using **4-4** after one heptane extraction.

measure chromium content. The DCM/acidified MeOH isolated product had a Cr content of 151.5 ppb while the Cr(PIBsalen)Cl/acetonitrile/heptane separation resulted in a polymer with only 39.9 ppb Cr. This represents a fourfold improvement in purity in the resulting polymeric material. In addition to facilitating a more efficient polymer/catalyst separation, recovered complex **4-4** exhibited only a 20-30% loss in activity of the recovered catalyst. This deactivation is most likely due to the degradation of the catalyst upon addition of acid. Overall, this proof-in-principle study represents a simple approach towards rendering the polymer purification more green in nature.

The Cr(PIBsalen) catalyst system is not without its pitfalls. The process still requires the use of relatively large amounts of multiple solvents and strong acids to isolate highly pure polymeric product, even though the solvents utilized in this process are considered to be much more green than the dichloromethane and acidified methanol that it replaces. Since the use of solvents cannot, at this point, be avoided, it is of interest to explore any system that would reduce the number of components involved in the separation process.

One particularly interesting area is the application of switchable polarity solvents (SPS). These systems are a unique in that they are able to change their polarity upon the addition of a trigger. In most cases it involves the combination of two low polarity component solvents that react to form a high polarity mixture, usually an ionic liquid, upon the addition of a third component.[77] The group of Phillip Jessop at Queen's University has been influential to this field in recent years. They have developed a wide variety of SPSs that have properties which potentially lead to use in the separation of product/catalyst mixtures in a variety of applications. Additionally, many of the SPSs utilize CO_2 as the trigger to form the high polarity solvent. In many cases this transformation from low to high polarity is at least partially reversible upon the addition argon or nitrogen and/or heating.

One especially attractive option is the utilization of relatively simple secondary amines and carbon dioxide as a SPS system. The reaction of 2° amines with CO_2 to produce ionic liquids is not new. One of the first examples utilized dimethyl aimine and carbon dioxide to form dimethylammonium dimethylcarbamate (DIMCARB) and has been studied extensively for various applications.[78-84] The major drawbacks of DIMCARB is that the starting amine is a gas and the system is not reversible. That is to say, once the ionic liquid has been formed it cannot be returned to its low polarity state easily. It is more desirable to utilize a liquid amine with a relatively high boiling point and low vapor pressure to facilitate a reversible transformation in order to keep exposure to potentially harmful vapors to a minimum. The use of relatively high boiling secondary amines allows for both of these requirements to be met.

Jessop and coworkers investigated the utilization of several secondary amines of varying initial polarity that were both readily available in high purity and at a low cost for their ability to form SPS.[85] Upon exposure to CO_2, the amine reacts to first form the carbamic acid followed by a successive reaction with an additional equivalent of the amine to form the carbamate salt ionic liquid (Scheme 4-2).

Scheme 4- 2. Reaction of secondary amine with CO_2.

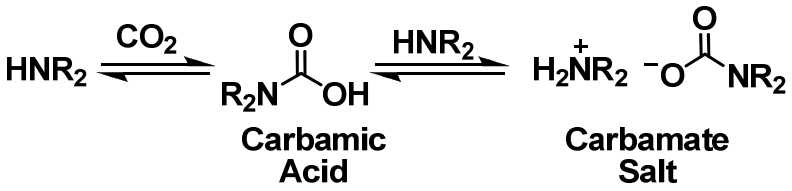

In the case of N-ethylbutylamine, the process is completely reversible upon the addition of argon or nitrogen or by simply heating the high polarity ionic liquid to drive off the CO_2.[85] The polarity of the high and low polarity states of the SPS can be measured using the solvatochromatic probe Nile Red. The results indicate that the low polarity state of the parent amine is comparable to ethyl acetate and upon addition of CO_2 the resultant ionic liquid is akin to the polarity of acetone. Additionally, after the same solution is heated to 60 °C for 2.5 hours with N_2 bubbling, the λ_{max} returned to within 2 nm of the original parent amine providing the necessary proof that the SPS transition from low to high polarity is completely reversible. In addition to reversibility, the carbamate ionic liquid derived from HNEtBu does not solidify even when stored at

-80 °C for 12 hours and is less sensitive to degradation by water than the other amines studied.

Due to its interesting properties and low cost, HNEtBu was chosen as the model amine for application to polymer/catalyst separation. Initial studies were undertaken to test the solubility of the catalyst, monomer, and polymeric product in the parent amine and ionic liquid phases. The results indicated that the catalyst and monomer were

Scheme 4- 3. Recycling of catalyst and SPS during the copolymerization of CO_2 and CHO. Colors indicate species in the low polarity SPS (green), high polarity SPS (red), solid state (yellow), and without solvent (colorless). The carbamate ligand on the complex is speculative.

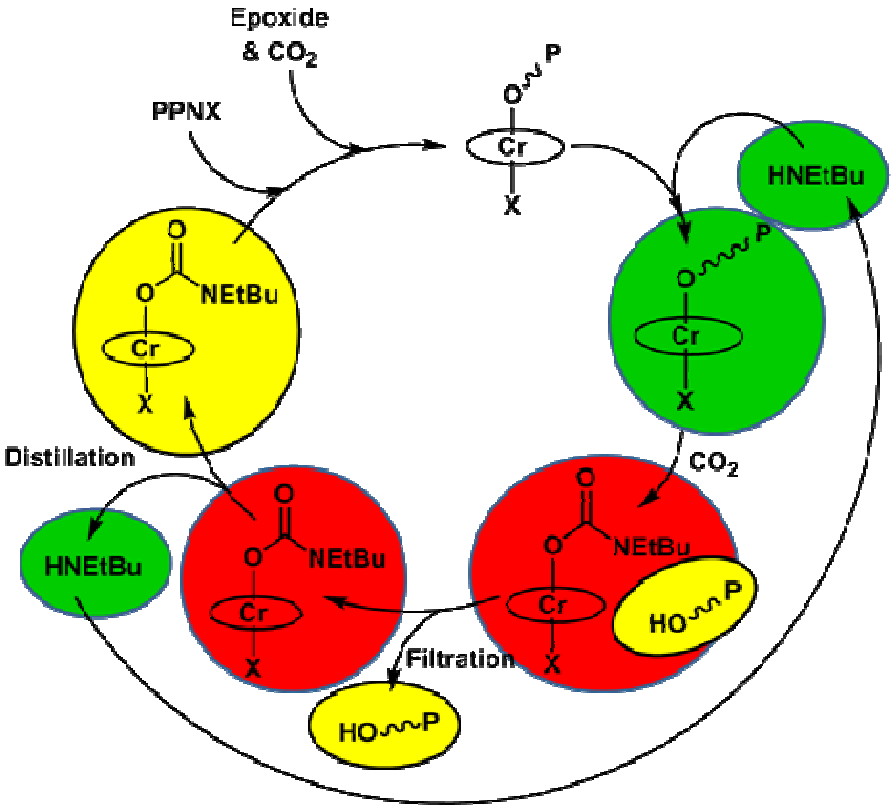

completely soluble in both the low and high polarity states of the SPS, while the polymer exhibited no initial solubility in either phase. However, upon application of HNEtBu actual reaction conditions, the catalyst/polymer/monomer mixture was found to be completely soluble. After the contents of the reactor were emptied into a flask, the addition of CO_2 resulted in a precipitation of the poly(cyclohexene carbonate). Subsequent attempts to redissolve this mixture in the parent amine were unsuccessful. Therefore, any further purification steps are to be considered as washings rather than re-precipitation as in the DCM/acidified MeOH or Cr(PIBsalen)Cl/MeCN/heptane systems.

Utilizing the initial solubility results, a search for a methodology for the utilization of HNEtBu/CO_2 as a system for the isolation and purification of PCHC was undertaken (Scheme 4-3). Upon completion of the copolymerization of CHO and CO_2 utilizing Cr(salen)Cl and PPNCl at 80 °C and 500 psi CO_2 pressure, the CO_2 was vented and placed under vacuum for approximately 20 minutes. The solid residue was then dissolved in HNEtBu and transferred to a flask where CO_2 was bubbled through the solution to trigger the transformation of the low polarity amine to the high polarity ionic liquid carbamate solution. The polymer precipitated as a white to off-white viscous solid which was mechanically stirred to facilitate easier filtration and a more complete initial Cr(salen) extraction in the next step of the separation procedure. The remaining carbamate SPS had a dark brown color and the dried polymer was nearly white (M_n = 23,000 Daltons, PDI = 1.13) indicating colormetrically that most of the catalyst remained in the SPS solution. The slight brown tinge to the purified polymer was indicative of catalyst contamination. Attempts to redissolve the polymer in HNEtBu

were unsuccessful; however, subsequent washings with the amine/carbamate SPS resulted in further purification of the PCHC. Samples taken after the second SPS treatment of the polymer were subjected to GPC analysis to ascertain any effects the washings might have on the products. A comparison of the data obtained implies that the repetitive exposure to the SPS does not degrade the polymer in any way.

When samples from the same polymerization run were purified by the two different methods, the traditional CH_2Cl_2/acid/MeOH or HNEtBu/CO_2, and analyzed by GPC, they exhibited almost identical molecular weights and PDIs. The polymer obtained after several cycles of the traditional method had a M_n values of 40, 300 Daltons (PDI = 1.06) compared to the M_n of 39,600 Daltons (PDI = 1.06) obtained from the SPS extraction process. This implies that the SPS separation has no detrimental effects on the product when compared to the traditional methods. In contrast to the traditional separation methodology, the catalyst from the SPS separation was isolated via distillation of the amine and CO_2 and recycled in another copolymerization of fresh CHO and CO_2 under identical reaction conditions as the first polymerization.[86] The copolymer yield (17 g versus 21 g in the first run) and M_n both decreased (15,300 Daltons) but the PDI of the resultant polymer remained low (1.10). An attempt to utilize the HNEtBu SPS system as a cocatalyst for the copolymerization of CO_2 and CHO was unsuccessful for the production of PCHC from CHO and CO_2.

There are several advantages of to the SPS separation process over both the traditional CH_2Cl_2/acid/MeOH system and Cr(PIBsalen)Cl/acid/MeCN/heptane systems. The SPS based on HNEtBu as only one liquid component that must be handled. It does

not require the addition of any other solvents to facilitate the isolation of a high purity product. Since it also utilizes CO_2, it represents a greener route for polymer catalyst separation even when compared to the Cr(PIBsalen) system. The Cr(PIBsalen) system forgoes the use of toxic halogenated solvents; however, it still requires the use of relatively large amounts of two different solvents and strong acid. Solvent recovery would require a careful distillation whereas the SPS system only requires a simple distillation to separate the CO_2, amine, and the catalyst that all could potentially be recycled. Even if the solvents were reclaimed from the Cr(PIBsalen) isolation system, there is still the problem of the acid utilized to cleave the polymer chain from the metal center of the catalyst. The addition of a strong acid is not required by the SPS system as the carbamic acid intermediate is presumably strong enough to cleave the polymer chain and not decompose the catalyst as with the other two isolation techniques.

Conclusions

Even though the green production of polycarbonates from epoxides and CO_2 has progressed steadily over the years, the workup of the resultant reaction mixture has remained relatively unchanged. Catalyst research has progressed to the point of industrial production of poly(propylene carbonate) with the promise of growth in the future. If the production of poly(carbonates) from CO_2 and epoxides is to remain truly green, it is of great importance that methods for environmentally friendly separation of the polymer/catalyst mixtures be sought out. The ammonium salt catalysts, **4-2**, of Lee and coworkers are one example of a modified catalyst structure that provides high activity, easy separation from reaction mixtures, and catalyst recyclability. Previously,

very few studies deviated from the traditional method of polymer catalyst separation utilizing halogenated solvents, alcohols, and strong acid to precipitate the polymer and were mainly concerned with the catalyst activity. Due to the availability of highly active and selective catalyst, it is now important to pursue methodologies in green separation processes.

Two approaches have been presented here. Catalyst modification, much like the Lee system, allowed for the use nonhalogenated solvents; however, large volumes of multiple solvents were still required. Additionally the use of strong acids was not avoided. Contrastingly, a process was devised using the simpler Cr(salen) catalyst system but utilizing a switchable polarity solvent system to facilitate the separation of the polymer and catalyst. The single liquid component SPS circumvented the need for multiple solvents and strong acid to provide a highly purified polymeric product. Utilizing CO_2 as the trigger to facilitate the precipitation also served to green the process further. Both of the above proof-of-concept experiments will hopefully spur further research in this area.

CHAPTER V

INVESTIGATIONS INTO THE COUPLING OF CYCLOHEXENE OXIDE AND CARBON DISULFIDE CATALYZED BY (SALEN)CrCl. SELECTIVITY FOR THE PRODUCTION OF COPOLYMERS VERSUS CYCLIC THIOCARBONATES*

Introduction

The intercalation of sulfur into polymeric materials is an area that has been gaining interest recently.[87,88] These materials are desired for their optical and thermal properties, chemical resistance, and potential application as heavy metal scavengers.[89,90] Several approaches to the production of such materials have appeared in the literature. The most prevalent are the ring opening of cyclic thiocarbonates or by the reaction of thiols and phosgene (or thiophosgene).[91-94] The cationic ring opening of cyclic thiocarbonates is often plagued by low selectivity for polymer, low molecular weights, and broad molecular weight distributions.[91,95] Recent reports of the synthesis of poly(trithiocarbonate) from propylene sulfide and carbon disulfide, and the copolymerization of epoxides and carbon dioxide have shown a greater propensity towards polymer formation. Nozaki and coworkers utilized Cr(salen) complexes to produce poly(thiocarbonates) with high selectivity.[11] The polymerization was thought to

---

*Reproduced with permission from Darensbourg, Donald J.; Andreatta, Jeremy R.; Jungman, Matthew J.; Reibenspies, Joseph H., *Dalton Transactions,*DOI:10.1039/b911061e. Copyright 2009, The Royal Chemical Society.

proceed through a mechanism similar to the copolymerization of epoxides and carbon dioxide and not through the initial formation of the cyclic trithiocarbonate, with subsequent ring opening to form the desired copolymer product. Another example of the production of sulfur rich polymers is the copolymerization of epoxides and carbon disulfide. Recently, zinc cobalt double metal cyanides (DMCs) were utilized to facilitate the coupling of carbon disulfide and propylene oxide at high temperatures with limited success.[12] One interesting aspect of this coupling process was the observation of a high degree of sulfur/oxygen exchange that occurred under the reaction conditions. Multiple S_nO_{3-n} combinations were observed in both the copolymer and cyclic byproducts.

It is of interest to study this process in detail to attempt to gain control of the S/O exchange reaction and to increase the selectivity for polymer. Utilization of the well-defined (salen)CrCl/[PPN]Cl (salen = *N,N´-bis*(3,5-*di*-tert-butylsalicylidene)-1,2-ethylenediimene, [PPN]Cl = *bis*(triphenylphosphoranylidene)ammonium chloride) catalyst system towards this coupling reaction could provide insight into this process. Much is understood about this catalyst system regarding the copolymerization of carbon dioxide and cyclohexene oxide which should be transferable towards an understanding of the copolymerization of carbon disulfide and cyclohexene oxide (CHO).[13]

Herein we report studies of the coupling of CHO and carbon disulfide using (salen)CrCl and [PPN]Cl as the catalyst system. Detailed analysis of both the polymer and cyclic products are utilized in an effort to further understand the polymerization process. Density Functional Theory (DFT) calculations of the relative stabilities of the various cyclic products were also performed.

Experimental

All reactions and/or manipulations were carried out using standard Schlenk techniques on a dual manifold vacuum line and under an argon atmosphere. All solvents were dried using an MBraun solvent purification system equipped with dual alumina columns. Carbon disulfide, cyclohexene oxide, and cyclohexene sulfide were obtained from VWR and purified by vacuum distillation over calcium hydride. Care must be taken when working with CS_2 due its toxicity and an autoignition temperature of 100 °C. (Salen)CrCl was synthesized *via* literature procedure.[69] [PPN]Cl was purchased from Aldrich and recrystallized from acetonitrile and ether. All infrared spectra were obtained on a Mattson 6021 FT-IR spectrometer with DTGS and MCT detectors. ^{1}H and ^{13}C NMR spectra were obtained on an Inova Unity+ 300 MHz, Inova 500 MHz, or Inova 400 MHz superconducting NMR spectrometers. Molecular weights were measured using a Viscotek Gel Permeation Chromatograph equipped with refractive index, right-angle and low-angle light scattering detectors, and using THF as the eluent. All mass spectral studies were conducted utilizing either chemical ionization mass spectrometry (CI-MS) performed on a Thermo Fischer DSQ II spectrometer or GCMS using a HP 5970 GCMS by the Laboratory for Mass Spectrometry at Texas A&M University. Thermogravimetric analysis (TGA) measurements were performed using an Instrument Specialists Inc. TGA 1000 Thermogravimetric Analyzer and monitored over a range of 25 to 500°C at 2°C per minute. Glass transition (T_g) and crystallization (T_c) temperatures were measured using a Mettler Toledo polymer DSC equipped with a liquid nitrogen cooling system and 50 mL/min purge of dry nitrogen gas. Samples (~ 6

mg) were weighed into 40 μL aluminum pans and subjected to two heating cycles. The first covered the range from 25 to 140 °C at 5 °C per minute and was cooled back to 25 °C. The second heating cycle covered 25 to 200°C at 2 °C per minute. Elemental analysis was performed by Atlantic Microlab, Inc., Norcross, GA 30071. DFT calculations were performed utilizing B3LYP level of theory as implemented in *Gaussian 03*.[96-98] For each calculation, all atoms were optimized using the 6-311g(d,p) basis set. Concomitant to each of the above calculations, a frequency calculation was performed to ensure the stability of the ground state as determined by the absence of imaginary frequencies. The enthalpy and free energy calculated for cyclic carbonates was converted from values in Hartrees to kcal/mol.

General Procedure for the Copolymerization of CS_2 and CHO. (Salen)CrCl (50 mg, 0.104 mmol) and the [PPN]Cl (50 mg, 0.104 mmol.) were weighed in an argon filled controlled atmosphere glove box into a 20 mL vial containing a Teflon® coated magnetic stir bar and sealed using a rubber septum. The vial was moved to the hood and placed under an argon atmosphere and 15 mL of dry dichloromethane was added. The solution was stirred for 30 minutes and the solvent was removed *in vacuo*. The resulting solid was dissolved in 10 mL of CHO and cannulated to a stainless steel Parr reactor *via* its injection port. The vial was rinsed with the appropriate amount of CS_2 and injected into the reaction vessel. The reactor was then heated to the desired temperature. Upon completion of the reaction, the reactor was vented and the contents dissolved in dichloromethane (DCM) and transferred to a beaker or Erlenmeyer flask. Upon removal of most of the mother solvent, an excess of acidified methanol (1 M HCl

in MeOH) was added to the solution to precipitate the polymeric product. Upon evaporation of the methanol from the remaining solution, the cyclic products were obtained after filtration. The polymer was redissolved in a small amount of DCM and reprecipitated by the addition of acetone. The resulting polymer (8-12 g) was dried in a vacuum oven at 60°C overnight. The solid cyclic material (2-5 g) was dissolved in DCM or acetone and filtered through a pad of silica to remove the catalyst. All elements in one of the purified copolymers (50°C run) were subjected to quantitative analysis. Anal. Found (%): C, 49.82(49.76); H, 5.98(6.11); O, 11.77(11.68); S, 32.11(31.97), where the values in parentheses represent duplicate analysis. From the average values for the elemental analysis, the empirical formula calculated for the copolymer is: $C_7H_{10}S_{1.69}O_{1.24}$, i.e., the copolymer is enriched in oxygen.

General Procedure for the Reaction of CS_2 and CHS. (Salen)CrCl (22.5 mg, 0.039 mmol) and the [PPN]Cl(22.5 mg,0.039 mmol) were weighed into a 20 mL Schlenk tube containing a Teflon® on coated magnetic stir bar, sealed with a rubber septum and transferred to a hood and placed under argon. Dichloromethane (8 mL) was added to the flask and the solution was stirred for 30 minutes. Upon removal of the solvent under vacuum, cyclohexene sulfide (CHS) (1.1g, 9.6 mmol) was added followed by 2 equivalents of CS_2 (19.5 mmol). The reaction was heated or cooled to the desired temperature. Following the completion of the reaction the tube was opened and the contents dissolved in a minimum amount of dichloromethane followed by the addition of acetone to precipitate about 0.4 g of polymeric product.

X-ray Structural Study. Single crystals of compound **5-1** suitable for X-ray diffraction were obtained from the slow evaporation of a dichloromethane solution of the cyclic products. A Licea microscope was utilized to identify suitable crystals of the same

Table 5- 1. Crystallographic data for compound **5-1.**

Empirical formula	$C_{28}H_{40}S_{12}$
Fw	761.32
Temp (K)	110
Cryst system	Orthorhombic
Space group	Pnma
a (Å)	12.6594(14)
b (Å)	10.0870(11)
c (Å)	6.6497(7)
α (deg)	90
β (deg)	90
γ (deg)	90
V ($Å^3$)	851.55
D_c (Mg/m^3)	1.485
Z	2
μ (mm^{-1})	7.302
Reflections collected	6223
Independent reflections	718
Parameters	85
Goodness-of-fit	1.009
Final *R* indicies [$I > 2\sigma(I)$]	$R_1 = 0.0376$[a]
	$R_w = 0.0829$[b]
Final *R* Indicies (all data)	$R_1 = 0.0333$[a]
	$R_w = 0.0811$[b]

[a] $R_1 = \Sigma|F_o| - || F_c|/ \Sigma F_o$. [b] $R_w = \{[(F_o^2 - F_c^2)^2]/[\Sigma(F_o^2)^2]\}^{1/2}$.

habit. The crystal was coated with paratone oil, affixed to a nylon loop, and mounted under streaming nitrogen on a Bruker Apex II CCD diffractometer. Table 5-1 contains crystallographic data for the trithiocarbonate structure obtained. Space group determinations were based on systematic absences and intensity statistics. The structure was solved *via* direct methods and refined on full-matrix least squares on F^2. All hydrogen atoms were placed in idealized positions with fixed isotropic displacement parameters to 1.5 times the equivalent isotropic displacement parameters for of the atoms which they are attached. All non-hydrogen atoms were refined using anisotropic displacement parameters. Programs used: data collection and cell refinement BCP version 2.0.1.9[99], data reduction, SAINT-PLUS version 6.63[25]; absorption correction, SADABS[100]; structural solutions, SHELXS-97[101]; structural refinement, SHELXL-97[102]; graphics and publication materials, X-Seed version 1.5.[30]

Results and Discussion

Copolymerization of Cyclohexene Oxide and CS_2. There are only a few examples of the coupling of epoxides and CS_2 for the purpose of forming copolymers. One report of the copolymerization of CO_2 and propylene sulfide in the late 70s using Et_2Zn and various cocatalysts produced low yields of polymeric material with very little CO_2 inclusion.[103] However, this early example served as a proof of concept for later studies. The most recent example utilized cobalt zinc DMC complexes to copolymerize propylene oxide and CS_2 to produce sulfur rich polymers.[12] This catalyst was able to produce polymers at 80 to 100 °C with molecular weights ranging from 1.2 to 5.4 kg/mol and with various polydispersity indices. An interesting aspect of this process

was the observation of S/O exchange during the polymerization process as determined by analysis of both the polymer and cyclic products. In depth studies of this system are hampered in that the true structure of the active catalytic species was not known. Because of this, it is of interest to study this copolymerization process with a well-defined catalyst system to gain insight and possible control of the polymerization process, as well as the extent of S/O exchange to predictably produce potentially useful polymers *via* this greener route.

The (salen)CrCl/[PPN]Cl catalyst system has been studied extensively for the copolymerization of CO_2 and cyclohexene oxide and propylene oxide.[13,104] There is a vast pool of knowledge regarding the mechanism by which this catalyst produces both polymer and cyclic products that can be applied to the copolymerization of CS_2 and epoxides and other cyclic ether or thioether monomers. There are; however, several differences in the later system. The carbon center of carbon disulfide is much more electrophilic than that of CO_2. Additionally, upon coupling of CS_2 with epoxides, the presence of SCO has been observed leading to a mixture of products during the copolymerization reaction.[12]

Preliminary studies of the coupling of CS_2 and cyclohexene oxide at 50°C proved successful and prompted further investigation. It was initially apparent that the S/O exchange observed by Qi and coworkers was also occurring with the (salen)CrCl catalyst system. From the IR and ^{13}C NMR spectral data, a wide variety of functional "carbonyl" groups are observed in the polymer product even at 50°C. After determining that the (salen)CrCl catalyst system would be effective for the copolymerization of CS_2

and CHO, a study of the effects of temperature and CS_2 loading were undertaken. The effect of temperature on the coupling reaction was first investigated over a 40 degree range, maintaining the CS_2 loading at one equivalent. Since the (salen)CrCl based catalyst system has shown activity at temperatures lower than 80°C for the coupling of CO_2 and epoxides, this implies that the coupling of CS_2 and epoxides should occur at a lower temperature due to the more electrophilic character of the carbon center of CS_2 *versus* that of CO_2. Table 5-2 shows the turnover frequency (TOF) for the overall coupling reaction as a function of reaction temperature. From this data, it was determined that the optimal reaction temperature was 50°C, which is well below the 80 – 130 °C used in the Zn-Co DMC catalyst system using propylene oxide (Figure 5-1).[12]

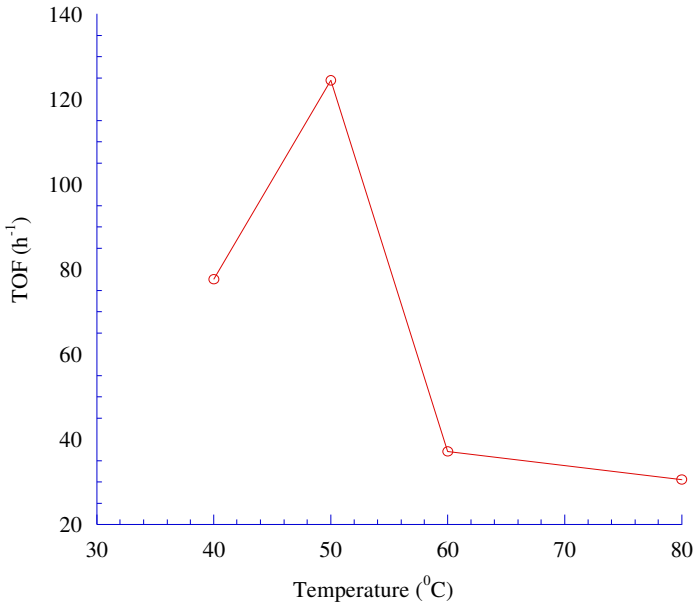

Figure 5- 1. Plot of TOF for copolymer formation vs. temperature for the coupling of CS_2 and cyclohexene oxide.

By comparison, the (salen)CrCl based catalyst system shows little activity for the coupling of CO_2 and CHO at 50 °C. It should be noted as well that [PPN]Cl

Table 5- 2. Copolymerization of cyclohexene oxide with CS_2 utilizing the (salen)CrCl/[PPN]Cl catalyst system. Temperature dependence study.[a]

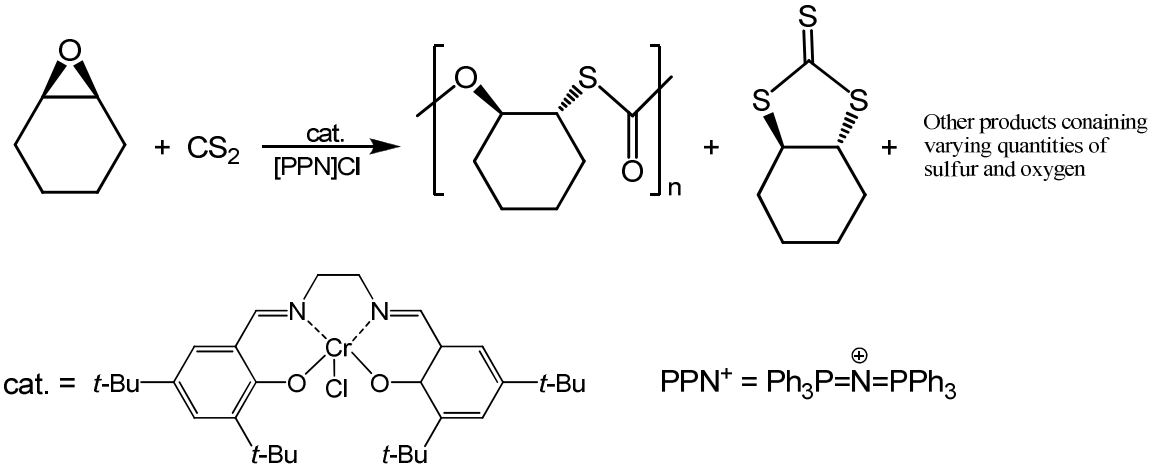

Temperature (°C)	Mass Polymer (g)	Mass Cyclic (g)	% Conversion[b]	TOF[c] (h^{-1})	M_w[d] (kg/mol)	PDI
40	4.68	2.27	40.6	77.6	15.3	1.19
50	7.50	3.01	61.4	124.4	34.8[e]	1.31
60	2.24	9.35	67.7	37.2	15.2	1.48
80	1.85	—	—	30.6	3.03	1.26

[a]50 mg (salen)CrCl, 50 mg [PPN]Cl, 10 mL CHO, 6.1 mL CS_2, 4hr. [b]Determined by isolated combined weights of copolymer and cyclic products. [c](mol epoxide consumed)/(mol Cr · hr)$^{-1}$. [d]Determined by GPC analysis. [e]Theoretical molecular weight equals 83,600.

alone does not catalyze the coupling of CS_2 and cyclohexene oxide under the reaction conditions employed in this study.[105] The copolymer and cyclic products observed from

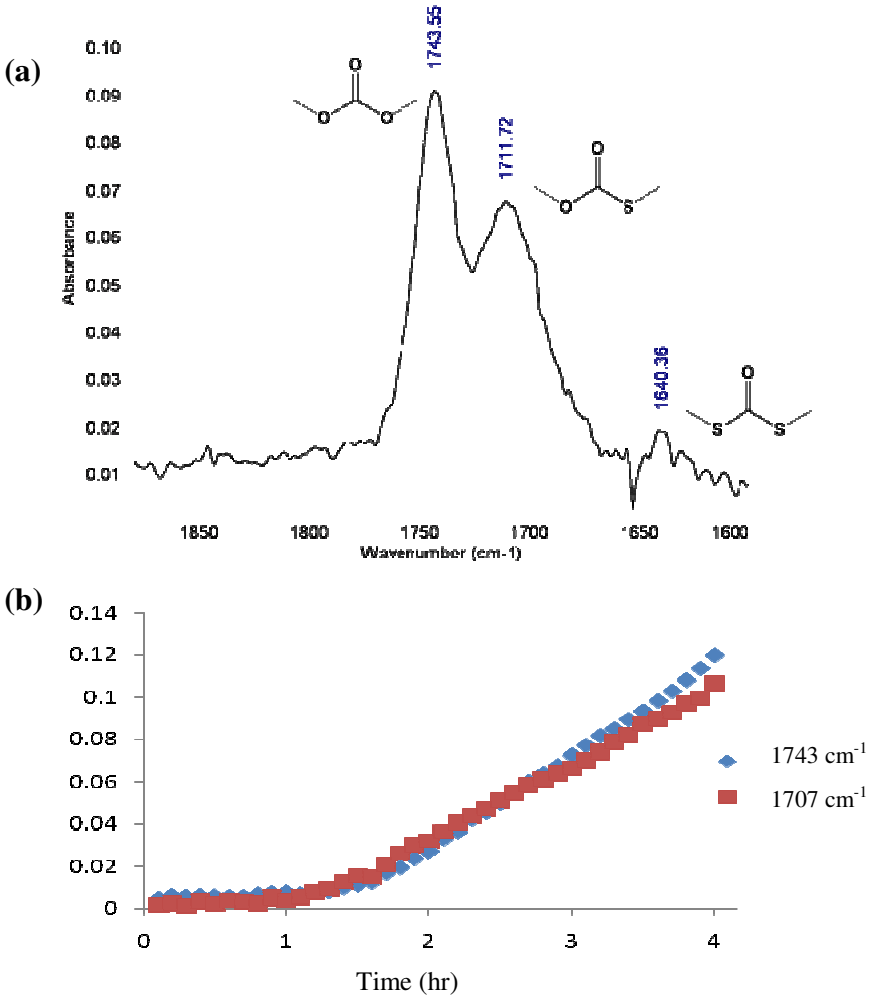

Figure 5- 2. (a) IR spectrum of polymer from the copolymerization of CS_2 and CHO at 50°C and (b) Reaction profile for copolymer formation obtained from *in situ* infrared monitoring.

each of the above reactions exhibited S/O exchange as confirmed by both solution IR and ^{13}C NMR spectroscopy. In the IR spectrum (see Figure 5-2), peaks corresponding to both carbonate (1750 cm^{-1}) and monothiocaarbonate (1706 cm^{-1}) are observed. Because of the numerous overlapping vibrational modes in the trithiocarbonate region of the

infrared spectrum, we were unable to definitively assign a band primarily due to the C=S stretching vibration. The ^{13}C NMR spectrum of copolymers shows resonances for the trithiocarbonate (220 ppm), monothiocarbonate (168 ppm), and carbonate (154 ppm) in all the polymer samples (Figure 5-3). The resonance for the dithiocarbonate seen at 212 ppm is observed in most samples; however, it is usually very weak in intensity.

In addition to temperature effects, the ratio of the two monomers can influence the product distribution and potentially the extent of S/O exchange. Other studies for the coupling of CS_2 and other monomers, both sulfur and oxygen containing, have found a 2 to 1 molar ratio of CS_2 to comonomer to exhibit the best activity, polymer selectivity, higher molecular weights, and narrow PDIs. It was initially thought that this trend

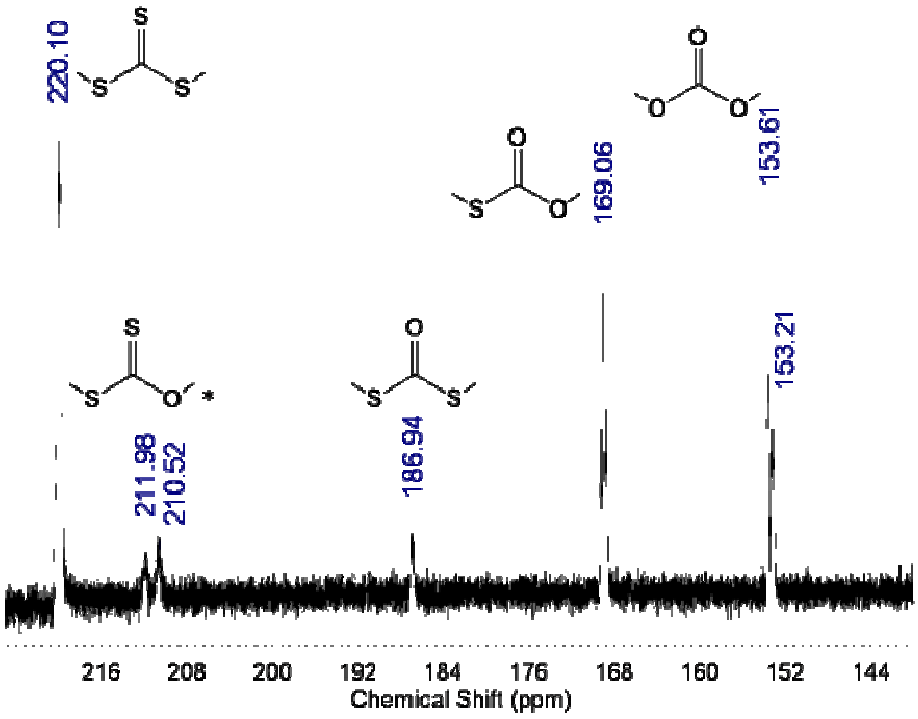

Figure 5- 3. ^{13}C NMR spectrum of the carbonyl region of polymer product from the coupling of CS_2 and CHO at 50°C. Peak marked with asterisk is acetone.

would also hold for the (salen)CrCl system with CHO, especially since it was observed with the same catalyst system utilizing CS_2 and propylene sulfide.[11] Upon varying of the carbon disulfide loading, it was apparent that the optimal loading of CS_2 for catalytic activity was 1 equivalent (Table 5-3). The CS_2 loading study is analogous

Table 5- 3. Copolymerization of carbon disulfide and cyclohexene oxide.[a]

Equiv. CS_2	Mass Polymer (g)	Mass Cyclic (g)	% Conversion[b]	TOF[c]	M_w (kg/mol)[d]	PDI
0.5	2.97	3.02	69.9	78.8	14.7	1.29
1.0	6.11	3.61	56.8	131.8	26.8	1.25
2.0	3.84	1.42	30.7	59.8	17.2	1.19
4.0	3.56	3.69	42.4	35.8	13.3	1.17

[a] 4.3×10^{-3} M (salen)CrCl, 1 eq. [PPN]Cl, 10 mL CHO, 50°C, 4 hr. [b] Determined by isolated combined weights of copolymer and cyclic products. [c] mol epoxides consumed/(mol Cr · h), calculations based on monomer molecular weight of copolymer of 167.9 as determined by elemental analysis. [d] Determined by GPC analysis.

to pressure dependence studies with the CO_2 system. However, as indicated in Figure 5-4, the optimal CS_2 loading for copolymer selectivity was two equivalents. It is also worth noting here that the PDI of all the polymerizations are narrow (1.2 – 1.5) and the polymers produced have relatively predictable molecular weights (Figure 5-5). The average molecular weight for this copolymerization process is around 18,000 Daltons which is about three to five times the average value found for the Zn-Co DMC/propylene oxide/CS_2 copolymerized system. As with the variable temperature studies, all the samples obtained by varying the CS_2 loading show evidence of S/O exchange.

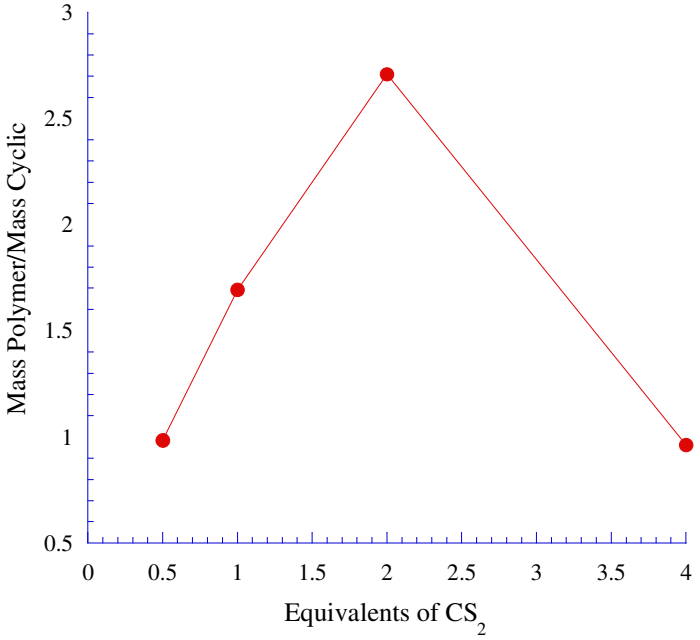

Figure 5- 4. Plot of the ratio of the masses (g) of polymer and cyclic versus equivalents of carbon disulfide.

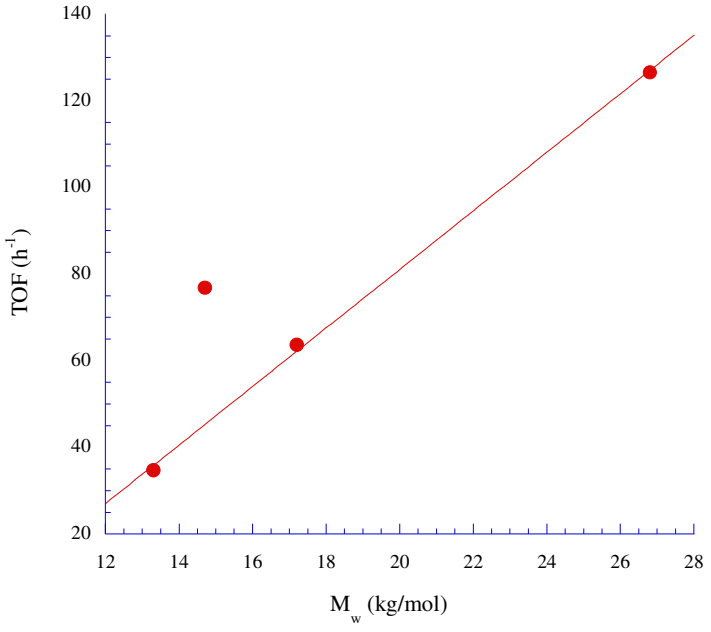

Figure 5- 5. Plot of M_w (kg/mol) versus TOF (h^{-1}) for the copolymerization of CS_2 and CHO. Point off linear relationship was found for the CS_2 deficient run.

A potential pathway for sulfur/oxygen exchange would involve ring-opening of the initially afforded cyclic thiocarbonate accompanied by COS and subsequently CO_2 extrusion (Scheme 5-1). If the reaction is monitored by *in situ* infrared spectroscopy, the formation of both poly(carbonate) (~ 1750 cm^{-1}) and poly(thiocarbonate) (~ 1710 cm^{-1}) are observed from the onset of the reaction, nevertheless there is an initiation period (see Figure 5-2). This implies that the S/O exchange process occurs previous to and during the polymerization process.

Scheme 5- 1

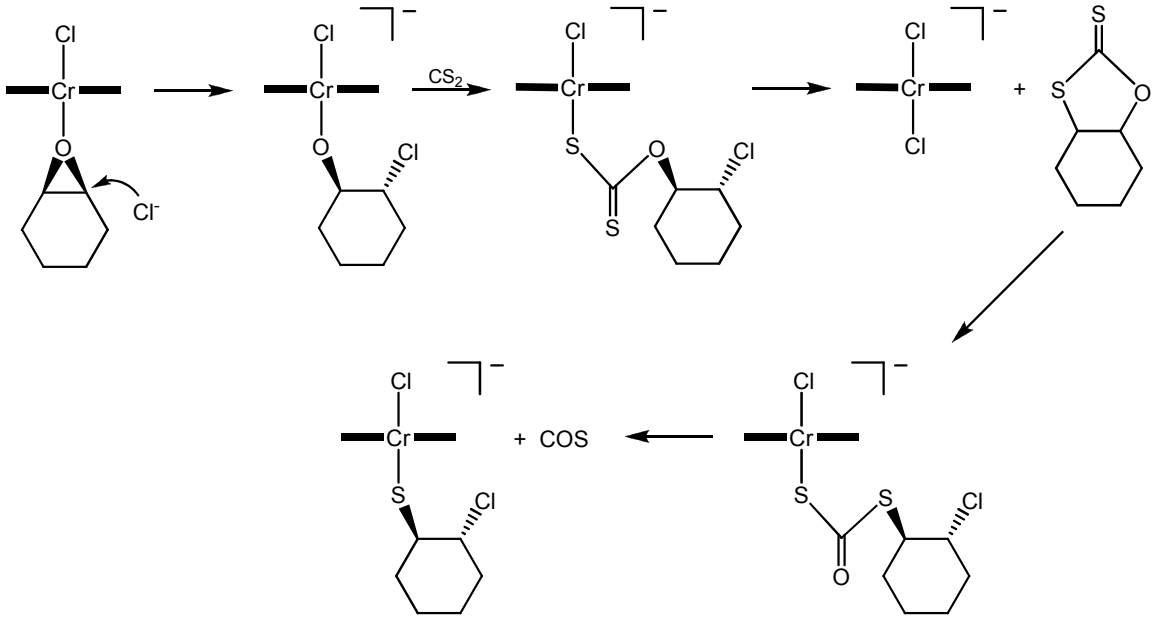

It is well-established that cyclohexene oxide and CO_2 copolymerization reactions catalyzed by the (salen)CrCl/[PPN]Cl system show little propensity for affording the

cyclic product, cyclohexylene carbonate, at 80ºC. However, we note herein that the analogous process between cyclohexene sulfide and CS_2 leads almost exclusively (96%)

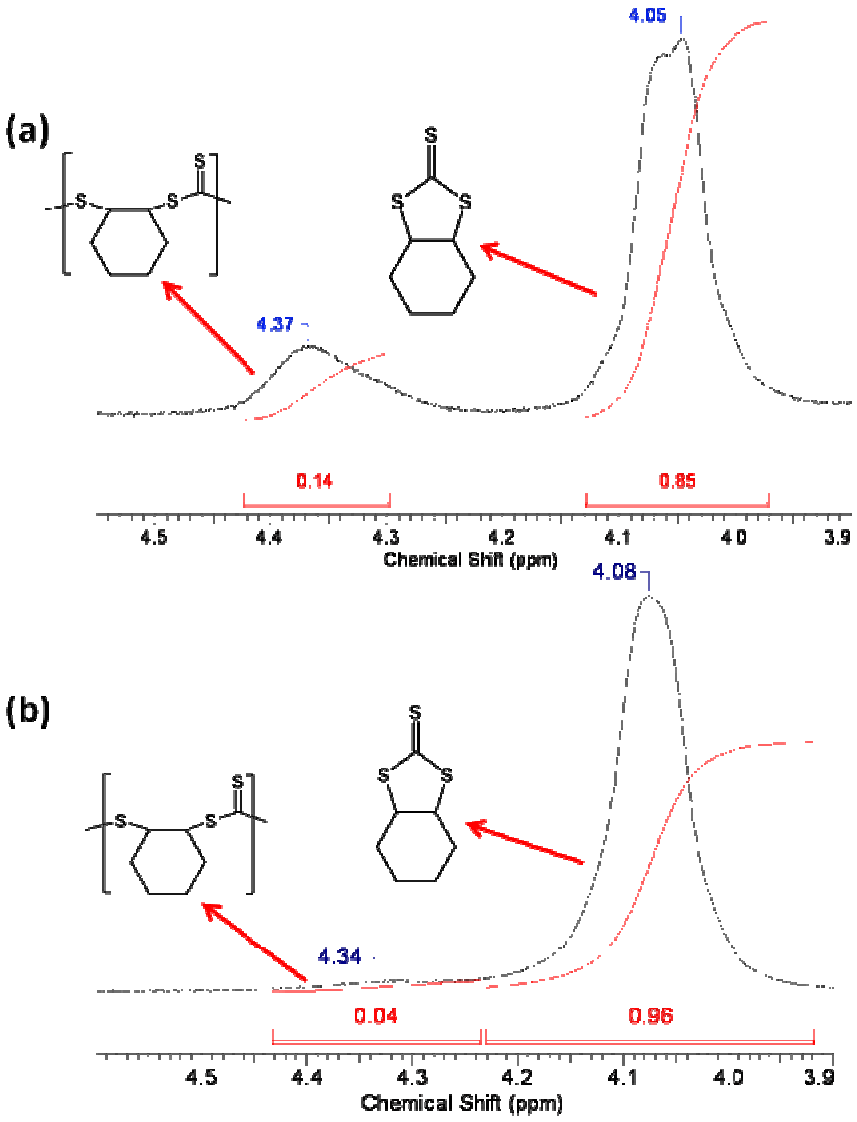

Figure 5- 6. ^{1}H NMR in the methine region of product mixture obtained from the reaction of CHS with two equivalents of CS_2 catalyzed by 0.020 M (salen)CrCl in the presence of one equivalent of [PPN]Cl at (a) 30ºC, and (b) 60ºC.

to the cyclic material at 50-60 ºC. Even at 30ºC, the copolymerization process yields only 15% copolymer of modest molecular weight, M_n = 4,930 with a PDI or 1.19. The copolymer decomposed rapidly at 280 ºC. Figure 5-6 clearly illustrates these findings in the ^{1}H NMR spectra of reactions involving cyclohexene sulfide and two equivalents of carbon disulfide. Our initial thoughts about the much greater tendency for cyclohexene sulfide and CS_2 to provide cyclic product as compared with cyclohexene oxide and carbon dioxide, is that this is due to the better metal binding ability of cyclohexene sulfide which can readily displace the growing polymer chain leading to more facile back-biting and cyclic production. That is, the cyclic product is afforded by an intramolecular back-biting process from the propagating chain end, either attached to the metal center or free. In the latter instance, the rate of back-biting is significantly enhanced. It is also shown by computations *vide infra* that the cyclic trithiocarbonate is thermodynamically more stable than its cyclic carbonate analog.

Cyclic Byproduct Studies. An additional matter worthy of careful investigation is the transition metal catalyzed coupling of carbon disulfide and cyclohexene oxide to provide the cyclic byproducts. Here again, the observation of several different products is expected as a result of S/O exchange pathways during the reaction. Qi and coworkers were able to observe many of the possible cyclic byproducts in their high temperature propylene oxide system.[12] It was expected that the CHO system might also exhibit this same characteristic; therefore, a study of the cyclic byproducts, including DFT calculations,

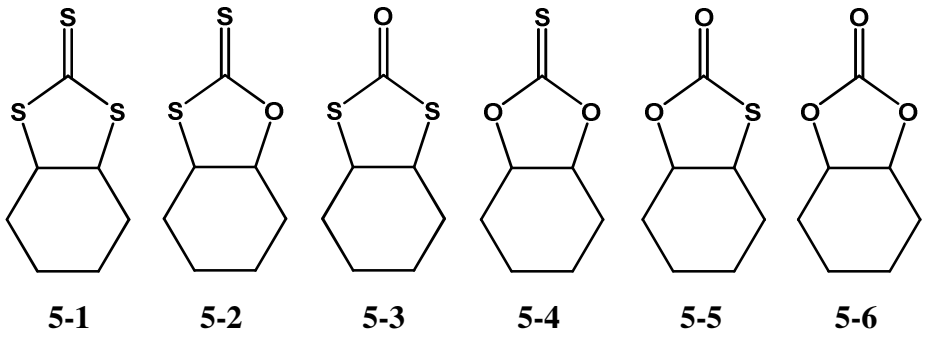

Figure 5- 7. Possible cyclic byproducts from the coupling of CS_2 and CHO.

was undertaken. There are six potential byproducts that can result from the coupling of the various sulfur and oxygen containing monomers that most likely exist in the reaction (Figure 5-7). It would be expected that all of the following would be observed, as in the

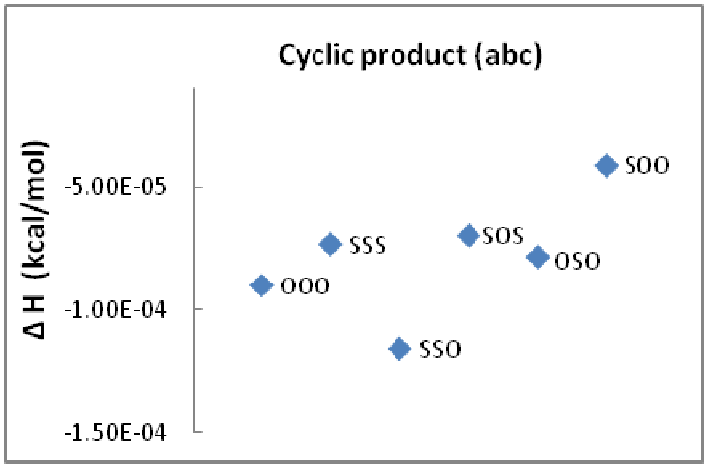

Figure 5- 8. Enthalpy of formation of cyclic thiocarbonate and carbonate.

Zn-Co DMC system. Additionally, during the ring opening polymerization of other five member cyclic dithiocarbonates, similar to **5-2**, the rearranged cyclic product, akin to

5-3, has been observed.[91] For the (salen)CrCl catalyzed reaction, all of the above byproducts were observed by mass spectral analysis except compound **5-6**, the cyclic carbonate.

The calculated enthalpy and free energy values of each of the starting materials (CO_2, CS_2, OCS, CHO, and CHS) and *trans*-cyclic products were utilized to determine the enthalpy and free energy of formation for each of the possible products. From the ΔH_f values for the formation of the various cyclic products (Figure 5-8), it is observed that the most enthalpicly favored cyclic byproduct results from the reaction of CS_2 and CHO, the two most abundant molecules in the reaction. The next cyclic product is cyclohexene carbonate which is observed in the copolymerization of CO_2 and epoxides but not observed here, however, carbonate linkages are observed in the polymer *via* ^{13}C NMR. Additionally, the least enthalpicly favored product is the result of the coupling of CO_2 and CHS. Neither is present at the onset of the reaction and would have to be generated during the reaction via S/O exchange.

Energetically, all the cyclic byproducts are very close in energy; however, the trithiocarbonate (ABC = SSS) byproduct is 8.0×10^{-4} kcal mol^{-1} lower in free energy than the next closest potential byproduct (ABC = SSO) which agrees with experimental results (Figure 5-9). As mentioned before, the trithiocarbonate cyclic product is the most abundant byproduct observed in the coupling of carbon disulfide and cyclohexene oxide. Due to this stability, single crystals suitable for X-ray diffraction studies were obtained via the slow evaporation of a DCM solution of the cyclic byproducts (Figure 5-10).

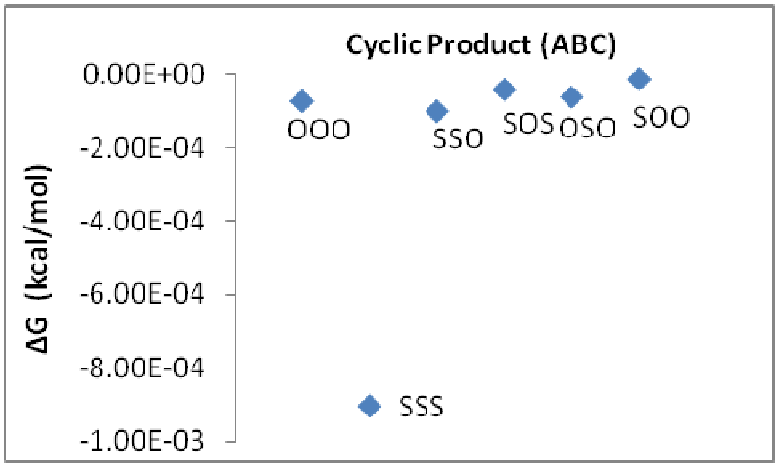

Figure 5- 9. Free energy of formation of cyclic thiocarbonates and carbonate.

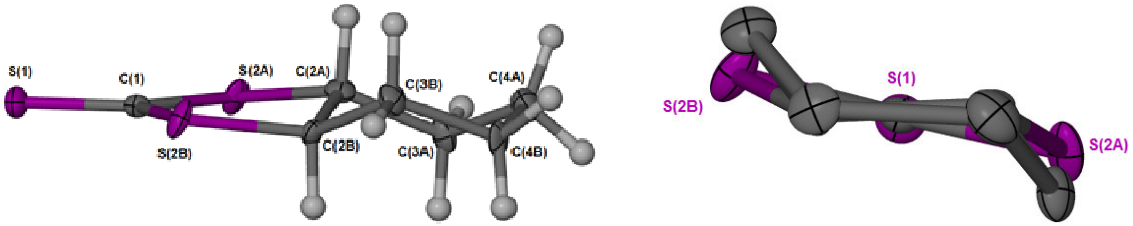

a **b**

Figure 5- 10. Thermal ellipsoid drawing of trithiocarbonate **5-1** at 50% probability (a) side view (b) view down C=S axis with hydrogen atoms removed for clarity.

Cyclohexene oxide is normally chosen in copolymerization experiments for its ease of ring opening and disfavored formation of cyclic carbonate due to the steric demands of the cyclohexane ring.[13] The formation of the five membered cyclic carbonate is disfavored due the high amount of ring strain in the product. The addition of

Table 5- 4. Selected bond distances (Å) and angles (degrees) for compound **5-1**.

S(1)-C(1)	1.637(3)	S(1)-C(1)-S(2B)	123.6(2)
C(1)-S(2B)	1.739(3)	S(1)-C(1)-S(2A)	122.0(2)
C(1)-S(2A)	1.740(3)	S(2B)-C(1)-S(2A)	114.44(16)
S(2A)-C(2A)	1.760(4)	S(2B)-C(2B)-C(2A)	111.4(6)
C(2A)-C(3A)	1.528(4)	S(2A)-C(2A)-C(2B)	112.0(6)
C(3A)-C(4A)	1.528(4)	C(1)-S(2A)-C(2A)	98.3(4)
S(2B)-C(2B)	1.764(3)	C(3A)-C(2A)-S(2A)	118.1(6)
C(2B)-C(3B)	1.528(4)	C(2A)-C(3A)-C(4A)	108.6(8)
C(3B)-C(4B)	1.527(4)	C(1)-S(2B)-C(2B)	98.2(4)
C(2A)-C(2B)	1.529(3)	C(3B)-C(2B)-S(2B)	120.8(6)
		C(4B)-C(3B)-C(2B)	109.4(8)

the larger sulfur atoms to the cyclic ring and longer C-S bond distances serves to reduce the strain and stabilize the cyclic products. A comparison of the bond distances and angles between the cyclic carbonate and trithiocarbonate (Figure 5-11) shows most of the bond distances to be about 0.3 Å longer in the case of the sulfur derivative, with the exception of the C-C bond in the cyclohexane ring at the base of the newly formed carbonate ring. A survey of the bond angles reveals a widening at the base of the five-membered ring by about 10° and contraction of approximately 8° at the sulfur atoms to

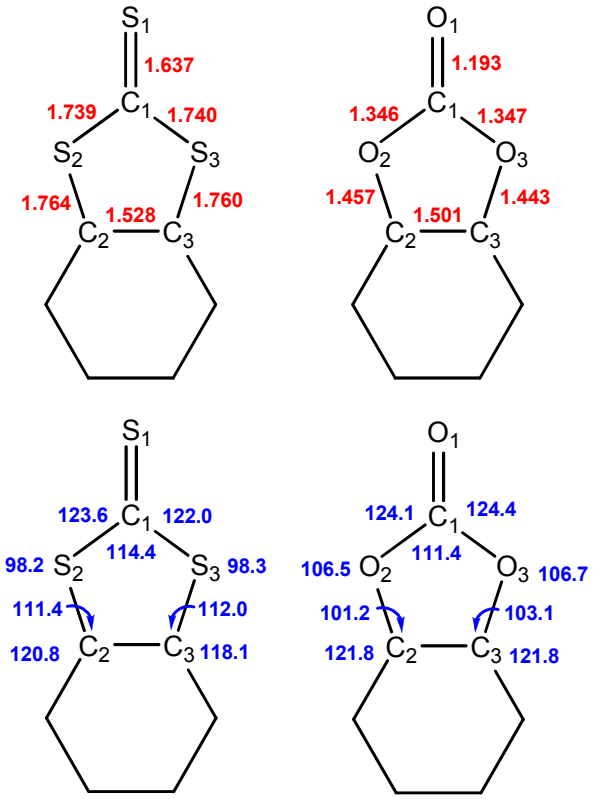

Figure 5- 11. Bond distances (red, Å) and angles (blue, degrees) for trithiocyclohexene carbonate (left) and cyclohexene carbonate (right).

accommodate the chair conformation of the cyclohexane ring. The structure evaluation coupled with the mass spectral and DFT calculations all support the stability of the trithiocarbonate over the other cyclic products.

Thermal Properties of Polymers. Polycarbonates are much sought after for their utility and favorable properties. The addition of sulfur to these products could provide materials with some of the desirable properties of both polycarbonates (heat resistance, high impact strength, clarity) and sulfur rich materials (high refractive index, chemical stability, sulfur-heavy metal interactions). The polymer samples prepared

herein were subjected to TGA and DSC (differential scanning calorimetry) to study their thermal behavior. These polymers all exhibited clean decomposition with a midpoint temperature of approximately 220°C (See Appendix C, Figure C1). It is interesting that in addition to the glass transition temperature (T_g), a crystallization temperature (T_c) was also observed with the sulfur rich polymers that is not observed in the polycarbonates (See Appendix C, Figure C2). Additionally, the sulfur containing polymers do not exhibit any melting phenomena which can be attributed to the irregular structure of the polymers produced in this study. However, other sulfur rich polythiocarbonates exhibit melting temperatures that are higher than the corresponding polycarbonates.[94] The T_g of polythiocarbonates is normally observed lower than or very close to the value of the corresponding poly(carbonates) of similar molecular weight.[94,106] Almost all the polymers obtained from the copolymerization of CS_2 and CHO displayed T_g values lower than the value of 116 °C obtained for poly(cyclohexene carbonate) (Table 5-5). The only sample that does not display this characteristic is sample 6. This could be a result of the higher molecular weight of this sample. Interestingly, as the temperature of the reaction was increased, the T_g value approached that of the pure poly(carbonates) presumably due to a higher oxygen content.

In addition to the glass transition temperature, the sulfur enriched carbonate polymers produced exhibit a crystallization temperature that is not observed in poly(cyclohexene carbonate). The increased crystallinity of the poly(thiocarbonates) can be attributed to the increased ability of the sulfurs to interact and order the polymer chains in the solid state giving rise to the observation T_c values.

Table 5- 5. Thermal data for poly(thiocarbonates).[a]

Sample	Temperature(°C)[b]	Equiv. CS_2	M_w (kg/mol)	PDI	T_g (°C)	T_c (°C)
1	50	0.5	14.7	1.29	101.6	150.4
2	50	1	26.8	1.25	98.4	152.3
3	50	2	17.2	1.19	108.5	148.2
4	50	4	13.3	1.17	106.3	148.2
5	40	1	15.3	1.19	100.3	148.6
6	50	1	34.8	1.31	122.4	151.5
7	60	1	15.2	1.48	115.1	152.4
8	80	1	3.0	1.26	110.2	129.0

[a]DSC routine: 25°C to 150°C at 5°C/min, 140°C to 25°C at -5°C/min, 25°C to 80°C at 2 °C/min. [b]Temperature of polymerization run.

Conclusions

Poly(thiocarbonate) materials have been synthesized *via* the copolymerization of CS_2 and cyclohexene oxide using the well defined (salen)CrCl/[PPN]Cl catalyst system. The reaction proceeds with a high selectivity for copolymer at temperatures equal to or below 50°C. The exchange of sulfur and oxygen is observed at all reaction temperatures as detected in the composition of both polymeric and cyclic products. This oxygen/sulfur scrambling process is summarized in Figure 5-12. Although the mechanistic details of this process are currently poorly defined, it is apparent that the copolymer is enriched in oxygen, whereas the product of polymer degradation, cyclic thiocarbonate, is enriched in sulfur.

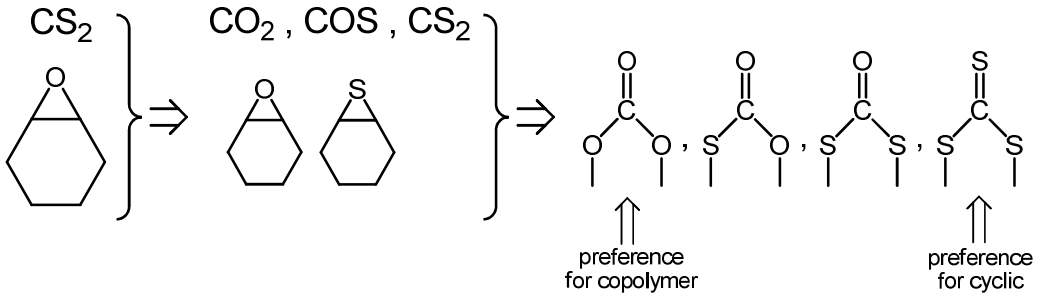

Figure 5- 12. Oxygen/sulfur scrambling process.

Optimal reaction conditions of 1 molar equivalent of CS_2 to CHO and 50°C were found to produce polymers with high molecular weights and relatively narrow molecular weight distributions. Calculations indicate that the trithiocarbonate cyclic byproduct is energetically the most stable of the cyclic materials, providing some insight into the observation of the S/O exchange process. The thermal properties of the polymers were studied by DSC, and the T_gs were found to be lower than the corresponding PCHC in cases of similar molecular weights. The greater electrophilic character of carbon disulfide over that of carbon dioxide should allow activation of other epoxide monomers in the future to produce new materials with useful properties.

CHAPTER VI

CONCLUSION

The design, development, and application of new catalyst systems as well as the modification and utilization of existing catalysts for new processes is immensely important to ensure that the production of medicines, plastics, and other consumer products is achieved with a high degree of efficiency. In order to achieve this goal, every component of the catalytic process from the most fundamental bonding interactions to the ability to recycle the system components must be explored. Additionally, it is important to develop catalyst systems which reduce the environmental footprint of the overall production process. Atom economy, catalyst recyclability, and catalyst efficiency are important factors in reducing the impact that the synthesis of various products has on the planet. Also, the utilization of industrial byproducts, such as carbon dioxide, to make useful goods can serve as a potential avenue to decrease the environmental impact of the waste stream from industrial processes while possibly providing a source of abundant and cheap starting materials.

The work presented here is devoted to the study of several aspects of catalysis and the modification and application of known catalyst systems. Starting with a study of the spatial impact that a ligand has when bonded to metal center, crystallographic data was used to understand a reversal from the expected mechanism for the *cis/trans* isomerization of *cis*-$M(CO)_3[P(OR)_3]_2$ (M = Mo or W, R = Ph or $(OCH_2)_3CC_2H_5$). Also of a fundamental nature, kinetic studies of the displacement of furan and 2,3-

dihydrofuran (DHF) were undertaken to gain insight in to the interaction of aromatic ligands with electron deficient metal centers. The modification of an existing catalyst system and the development of a new system for the separation of a metal based catalyst from the desired polymeric product were investigated. Finally, the utilization of a extensively studied catalyst system to produce new sulfur rich polymeric materials with a variety of potential applications has been investigated.

Ancillary ligands can have a huge impact on the efficacy and selectivity of a transition metal catalyst. For example, phosphines are widely used in catalysis due to the electronic and steric variety available. In the late 1970s, Tolman developed a method to estimate the steric impact of phosphines to aid in the selection of the appropriate ligand for a variety of applications.[2] Although the cone angles Tolman estimated are immensely useful, they must be applied with discretion, especially when the substituents on the phosphorous atom are flexible. For instance, the estimated cone angle for triphenylphosphite ($P(OPh)_3$) is 128°, which would imply that the thermal isomerization of *cis*-$M(CO)_2[P(OPh)_3]$ to the *trans* isomer would take place *via* a intramolecular Bailar twist mechanism.[20-23] However, upon investigation, the isomerization was found to occur *via* the dissociation of the one phosphine ligand followed by a Berry pseudo rotation and re-association of the phosphine ligand to form the *trans*-$M(CO)_2[P(OPh)_3]$ complex. Crystal structures of several phosphite complexes were investigated, and the cone angle was calculated from the data. The cone angle of triphenylphosphite was calculated to be about 140° implying that the intermolecular mechanism would be the expected pathway for isomerization. Additionally, the

orientation of the phenyl groups on the phosphite ligand of metal $P(OPh)_3$ complexes in the Cambridge Crystallographic Database were analyzed. This lead to the conclusion that the most common configuration of the phosphite ligand is the two *down* and one *up* configuration, *vide supra*. From this study, a greater understanding of the true impact that triphenylphosphite has on the reactivity of a transition metal complex has been described, much of which can be be applied to a variety of applications.

In addition to the ligand's steric impact, it is also important to understand the bonding interaction between metals and unsaturated carbon-carbon bonds. Very little quantitative information exists concerning the strength or nature of this very important bonding interaction. The study of the dissociation of DHF and furan from the electron deficient fragments $CpMn(CO)_2$ and $BzCr(CO)_2$ coupled with DFT calculations was able to shed light not only the M-L bond strength, but also provided valuable information regarding the extent of the disruption of the aromaticity that the furan ligand undergoes when bonding with a metal center. In this study, both furan and DHF were found to bind to the Mn center 7-10 kcal mol^{-1} stronger than to the slightly more electron rich Cr center implying a minimal contribution of M-L π-back bonding to the bonding interaction. Also, the aromatic furan was found to bind 7-10 kcal mol^{-1} weaker independent of the identity of the metal center. This is primarily attributed to the interruption of the aromaticity of furan that results from the site isolation of electron density required to bond with the metal center in an η^2 fashion. A resonance stabilization energy of 15.8 kcal mol^{-1} was calculated by E. Brothers implying a ~ 50% loss of aromaticity in the furan ligand upon binding with the metal center.

In addition to fundamental studies, an investigation of the separation of polymer catalyst mixtures was undertaken. Although great improvements in the activity of catalysts for the copolymerization of epoxides and CO_2 have been made in the past 40 years, the separation of the pure polymer product from the catalyst, starting materials, and byproducts has remained relatively unchanged. The traditional method of utilizes acidified methanol (1 M HCl in Methanol) to precipitate the purified polymeric material from a dichloromethane solution. This method creates large volumes of hazardous wasted and does not follow along with the green theme of the polymerization procedure. With all the advancements in catalyst design and the potential for industrial scale production of polycarbonates *via* this methodology, it is important to develop green processes for polymer/catalyst separation. Two approaches were discussed herein. First, the modification of the catalyst to facilitate a highly efficient biphasic separation procedure was studied. A (salen)CrCl catalyst modified by the addition of 1000 Dalton poly(isobutylene) moieties afforded a catalyst with essentially identical activity as the parent complex with the added attribute of solubility in hydrocarbon solvents such as hexane and heptane. This separation process was about 4 times more efficient at removing the undesired Cr catalyst from the polymer after one washing and yielded a catalyst that was recyclable with approximately 20-30% loss of activity.

Contrastingly, a system that did not require any catalyst modification but also utilized CO_2 was studied. The utilization of secondary amines and their reactivity with CO_2 was exploited as a solvent system for polymer purification. Upon completion of the polymerization of cyclohexene oxide and CO_2, the polymer/catalyst mixture was soluble

in the low polarity amine state of EtBuNH. Bubbling CO_2 through the solution resulted in the formation of a high polarity carbamate ionic liquid and the precipitation of the desired polycarbonate product. The advantage of this system is that every component (amine, CO_2, and catalyst) is potentially recyclable. The addition of CO_2 to EtBuNH to form the carabmate ionic liquid is completely reversible and the amine can simply be isolated *via* distillation for reuse. With further studies, the catalyst could also be recycled; however, the current study resulted in a catalyst with little activity towards copolymer formation.

Additionally, the utilization of the well studied (salen)CrCl/PPNCl system was utilized to synthesize sulfur enriched polymers *via* the copolymerization of CS_2 and cyclohexene oxide. The more electrophilic nature of the central carbon of CS_2 when compared to CO_2 facilitated selective formation of poly(cyclohexene thiocarbonate) with high activity at temperatures well below those utilized for the copolymerization using CO_2.[13] Interestingly, the exchange of sulfur and oxygen was observed as evidenced by the presence of several different thiocarbonate functionalities along with carbonate linkages in the polymer. Optimization of the reaction conditions revealed that 50 °C and 1 equivalent of CS_2 were the most favorable conditions for the formation of poly(cyclohexene thiocarbonate). The polymeric products were subjected to thermal analysis by DSC and found to have T_g values less than the analogous poly(cyclohexene carbonate T_g of 116 °C. The polymers also exhibited a crystallization temperature that is not observed for the analogous polycarbonate. This is due to the sulfur atoms ability to increase the ordering, and therefore the crystallinity, of the polymeric material in the

solid state. Future studies in this area will focus on the activation of other monomers such as styrene oxide, trimethylene sulfide, and further studies utilizing propylene oxide to form new and hopefully useful materials.

In summary, it is with great hope that the studies presented here demonstrate the time and effort that has been invested to the study of catalysis from the fundamental level to application towards new products and processes. The further understanding of long standing approximations and the quest for more accurate quantitative information regarding the interaction of transition metals and various ligands and substrates is of the utmost importance. Without these fundamental studies, the development of new catalyst will be stymied. Building on the foundation of such studies, scientist must consider not only how to develop catalysts for green processes, but also address the last step of the production which is the isolation of the product, free from potentially harmful catalyst contamination. Also, the application of known systems to new avenues of utilization must be sought out. Hopefully, this dissertation will serve as an example of the need for fundamental studies as well as application based endeavors, remind others of the rewards of in depth kinetic studies, and encourage future scientists to explore other potential avenues inspired by this work.

REFERENCES

(1) Ragsdale, S. W. *Chem. Rev.* **2006**, *106*, 3317-3337.

(2) Tolman, C. A. *Chem. Rev.* **1977**, *77*, 313-348.

(3) Harman, W. D.; Fairlie, D. P.; Taube, H. *J. Am. Chem. Soc.* **1986**, *108*, 8223-8227.

(4) Harman, W. D. *Chem. Rev.* **1997**, *97*, 1953-1978.

(5) Harman, W. D.; Keane, J. M. *Organometallics* **2005**, *24*, 1786-1798.

(6) Bengali, A. A.; Hall, M. B.; Wu, H. *Organometallics* **2008**, *27*, 5826-5829.

(7) Inoue, S.; Koinuma, H.; Tsuruta, T. *Makromol. Chem.* **1969**, *130*, 210-220.

(8) Darensbourg, D. J.; Rodgers, J. L.; Fang, C. C. *Inorg. Chem.* **2003**, *42*, 4498-4500.

(9) Mang, S.; Cooper, A. I.; Colclough, M. E.; Chauhan, N.; Holmes, A. B. *Macromolecules* **2000**, *33*, 303-308.

(10) S, S.; Min, J. K.; Seong, J. E.; Na, S. J.; Lee, B. Y. *Angew. Chem., Int. Ed.* **2008**, *47*, 7306-7309.

(11) Nakano, K.; Tatsumi, G.; Nozaki, K. *J. Am. Chem. Soc.* **2007**, *129*, 15116-15117.

(12) Zhang, X.-H.; Liu, F.; Sun, X.-K.; Chen, S.; Du, B.-Y.; Qi, G.-R.; Wan, K. M. *Macromolecules* **2008**, *41*, 1587-1590.

(13) Darensbourg, D. J. *Chem. Rev.* **2007**, *107*, 2388-2410.

(14) White, D.; Coville, N. J. *Adv. Organomet. Chem.* **1994**, *36*, 95-158.

(15) Brown, T. L.; Lee, K. J. *Coord. Chem. Rev.* **1993**, *128*, 89-116.

(16) Alyea, E. C.; Dias, S. A.; Ferguson, G.; Restivo, R. J. *Inorg. Chem.* **1977**, *16*, 2329-2334.

(17) Mingos, D. M. P.; Mueller, T. E. *J. Organomet. Chem.* **1995**, *500*, 251-259.

(18) Guzei, I. A.; Wendt, M. *Dalton Trans.* **2006**, 3991-3999.

(19) Tolman, C. A.; Seidel, W. C.; Gosser, L. W. *J. Am. Chem. Soc.* **1974**, *96*, 53-60.

(20) Darensbourg, D. J.; Graves, A. H. *Inorg. Chem.* **1979**, *18*, 1257-1261.

(21) Darensbourg, D. J. *Inorg. Chem.* **1979**, *18*, 14-17.

(22) Cotton, F. A.; Darensbourg, D. J.; Klein, S.; Kolthammer, B. W. S. *Inorg. Chem.* **1982**, *21*, 2661-2666.

(23) Cotton, F. A.; Darensbourg, D. J.; Klein, S.; Kolthammer, B. W. S. *Inorg. Chem.* **1982**, *21*, 294-299.

(24) Darensbourg, D. J.; Kump, R. L. *Inorg. Chem.* **1978**, *17*, 2680-2682.

(25) Bruker; version 6.02 ed. Madison, WI, 1999.

(26) Sheldrick, G. Institut fur Anorganische Chemie der Uniseritat Gottingen: Gottingen, Germany, 1986.

(27) Sheldrick, G. Institut fur Anorganische Chemie der Uniseritat Gottingen: Gottingen, Germany, 1987.

(28) Bruker; version 5.0 ed. Madison, WI, 1999.

(29) Farrugia, L. J. *J. Appl. Crystallogr.* **1999**, *32*, 837-838.

(30) Barbour, L. J. *J. Supramol. Chem.* **2003**, *1*, 189-191.

(31) Alyea, E. C.; Ferguson, G.; Zwikker, M. *Acta Crystallogr., Sect. C: Cryst. Struct. Commun.* **1994**, *C50*, 676-678.

(32) Baker, M. J.; Harrison, K. N.; Orpen, A. G.; Pringle, P. G.; Shaw, G. *J. Chem. Soc., Dalton Trans.* **1992**, 2607-2614.

(33) Atwood, J. L.; Darensbourg, D. J. *Inorg. Chem.* **1977**, *16*, 2314-2317.

(34) Darensbourg, D. J. *Inorg. Chem.* **1979**, *18*, 2821-2825.

(35) Stahl, L.; Ernst, R. D. *J. Am. Chem. Soc.* **1987**, *109*, 5673-5680.

(36) Stahl, L.; Trakarnpruk, W.; Freeman, J. W.; Arif, A. M.; Ernst, R. D. *Inorg. Chem.* **1995**, *34*, 1810-1814.

(37) Smith, J. M.; Coville, N. J.; Cook, L. M.; Boeyens, J. C. A. *Organometallics* **2000**, *19*, 5273-5280.

(38) Smith, J. M.; Coville, N. J. *Organometallics* **2001**, *20*, 1210-1215.

(39) Ghalsasi, P. S.; Yarger, J. In *227th ACS National Meeting*; Abstracts of Papers: Anaheim, CA, 2004.

(40) Mingos, D. M. P.; Muller, T. W. *Transition Met. Chem.* **1995**, *20*, 533-539.

(41) Senker, J.; Ludecke, J. *Z. Naturforsch., B: Chem. Sci.* **2001**, *56*, 1089-1099.

(42) Guss, J. M.; Mason, R. *J. Chem. Soc., Dalton Trans.* **1972**, 2193-2196.

(43) Bengali, A. A. *Organometallics* **2000**, *19*, 4000-4003.

(44) Bengali, A. A.; Grunbeck, A. R. *Organometallics* **2005**, *24*, 5919-5924.

(45) Brooks, B. C.; Gunnoe, T. B.; Harman, W. D. *Coord. Chem. Rev.* **2000**, *206-207*, 3-61.

(46) Brennan, P.; George, M. W.; Jina, O. S.; Long, C.; McKenna, J.; Pryce, M. T.; Sun, X.-Z.; Vuong, K. Q. *Organometallics* **2008**, *27*, 3671-3680.

(47) Bengali, A. A.; Fehnel, R. *Organometallics* **2005**, *24*, 1156-1160.

(48) Tao, J.; Perdew, J. P.; Staroverov, V. N.; Scuseria, G. E. *Phys. Rev. Lett.* **2003**, *91*, 146401/1-146401/4.

(49) Kendall, R. A.; Dunning, T. H., Jr.; Harrison, R. J. *J. Chem. Phys.* **1992**, *96*, 6796-6806.

(50) Couty, M.; Hall, M. B. *J. Comput. Chem.* **1996**, *17*, 1359-1370.

(51) M. Frisch, J.; Truks, G. W.; Schlegel, H. B.; Scuseria, G. E.; Robb, M. A.; Cheeseman, J. R.; Monggomery, J. J. A.; Vreven, T.; Scalmani, G.; Mennucci, B.; Barone, V.; Petersson, G. A.; Caricato, M.; Jakatsuji, H.; Hada, M.; Ehara, M.; Toyota, K.; Fakuda, R.; Hasegawa, J.; Ishida, M.; Nakajima, T.; Honda, Y.; Kitao, O.; Nakai, H.; Li, X.; Hratchian, H. P.; Peralta, J. E.; Izmaylov, A. F.; Kudin, K. N.; Heyd, J. J.; Brothers, E.; Staroverov, V. N.; Zheng, G.; Kobayashi, R.; Normand, J.; Sonnengerg, J. L.; Ogliaro, F.; Bearpark, M.; Parandekar, P. V.; Ferguson, G. A.; Mayhall, N. J.; Iyengar, S. S.; Tomasi, J.; Cossi, M.; Rega, N.; Burant, J. C.; Millam, J. M.; Klene, M.; Knox, J. E.; Cross, J. B.; Bakken, V.; Adamo, C.; Jaramillo, J.; R., G.; Stratmann, R. E.; Yazyeve, O.; Austin, A. J.; Cammi, R.; Pomelli, C.; Ochterski, J. W.; Ayala, P. Y.; Morokuma, K.; Voth, G. A.; Salvador, P.; J., D. J.; Zakrzweski, V. G.; Dapprich, S.; Daniels, A. D.; Strain, M. C.; Farkas, O.; Malick, D. K.; Rabuck, A. D.; Raghhavachari, D.; Foresman, J. B.; Ortiz, J. V.; Cui, Q.; Baboul, A. G.; Clifford, S.; Cioslowski, J.; Stefanov, B. B.; Liu, G.; Liashenko, A.; Piskorz, P.; Komaromi, I.; Martin, R. L.; Fox, D. J.; Keith, T.; Al-Laham, M. A.; Peng, C. Y.; Nanayakara, A.;

Challacombe, M.; Chen, W.; Wong, M. W.; People, J. A. *Gaussian Development Version G.03, Gaussian Inc.* Wallingford, CT **2008**.

(52) Strohmier, W.; Hellmann, H. *Chem. Ber.* **1963**, *96*, 2859-2866.

(53) Cole, S.; Dulaney, K. E.; Bengali, A. A. *J. Organomet. Chem.* **1998**, *560*, 55-61.

(54) Hester, D. M.; Sun, J.; Harper, A. W.; Yang, G. K. *J. Am. Chem. Soc.* **1992**, *114*, 5234-40.

(55) Cowan, A. J.; George, M. W. *Coord. Chem. Rev.* **2008**, *252*, 2504-2511.

(56) Lugovskoy, S.; Lin, J.; Schultz, R. H. *Dalton Trans.* **2003**, 3103-3110.

(57) Epiotis, N. D.; Cherry, W. R.; Bernardi, F.; Hehre, W. J. *J. Am. Chem. Soc.* **1976**, *98*, 4361-4364.

(58) Bean, G. P. *J. Org. Chem.* **1998**, *63*, 2497-2506.

(59) Inoue, S.; Koinuma, H.; Tsuruta, T. *J. Polym. Sci., Part C: Polym. Lett.* **1969**, *7*, 287-292.

(60) Darensbourg, D. J.; Holtcamp, M. W. *Macromolecules* **1995**, *28*, 7577-7579.

(61) Darensbourg, D. J.; Wildeson, J. R.; Yarbrough, J. C.; Reibenspies, J. H. *J. Am. Chem. Soc.* **2000**, *122*, 12387-12396.

(62) Coates, G. W.; Moore, D. R. *Angew. Chem., Int. Ed.* **2004**, *43*, 6618-6639.

(63) Darensbourg, D. J.; Mackiewicz, R. M.; Phelps, A. L.; Billodeaux, D. R. *Acc. Chem. Res.* **2004**, *37*, 836-844.

(64) Qin, Z.; Thomas, C. M.; Lee, S.; Coates, G. W. *Angew. Chem., Int. Ed.* **2003**, *42*, 5484-5487.

(65) Cohen, C. T.; Chu, T.; Coates, G. W. *J. Am. Chem. Soc.* **2005**, *127*, 10869-10878.

(66) Cohen, C. T.; Coates, G. W. *J. Polym. Sci., Part A: Polym. Chem.* **2006**, *44*, 5182-5191.

(67) Noh, E. K.; Na, S. J.; S, S.; Kim, S. W.; Lee, B. Y. *J. Am. Chem. Soc.* **2007**, *129*, 8082-8083.

(68) Demadis, K. D.; Meyer, T. J.; White, P. S. *Inorg. Chem.* **1998**, *37*, 3610-3619.

(69) Darensbourg, D. J.; Mackiewicz, R. M.; Rodgers, J. L.; Fang, C. C.; Billodeaux, D. R.; Reibenspies, J. H. *Inorg. Chem.* **2004**, *43*, 6024-6034.

(70) Hongfa, C.; Tian, J.; Andreatta, J.; Darensbourg, D. J.; Bergbreiter, D. E. *Chem. Comm.* **2008**, 975-977.

(71) Darensbourg, D. J.; Rodgers, J. L.; Mackiewicz, R. M.; Phelps, A. L. *Catalysis Today* **2004**, *98*, 485-492.

(72) Bergbreiter, D. E.; Chen, L. B.; Chandran, R. *Macromolecules* **1985**, *18*, 1055-1057.

(73) Shen, Z.; Chen, Y.; Frey, H.; Stiriba, S.-E. *Macromolecules* **2006**, *39*, 2092-2099.

(74) Bergbreiter, D. E.; Hamilton, P. N.; Koshti, N. M. *J. Amer. Chem. Soc.* **2007**, *129*, 10666-10667.

(75) Liou, S.; Rademacher, J. T.; Malaba, D.; Pallack, M. E.; Brittain, W. J. *Macromolecules* **2000**, *33*, 4295-4296.

(76) Faucher, S.; Zhu, S. *Journal of Polymer Science, Part A Polymer Chemistry* **2007**, *45*, 553-565.

(77) Jessop, P. G.; Heldebrant, D. J.; Xiaowng, L.; Eckert, C. A.; Liotta, C. L. *Nature* **2005**, *436*, 1102.

(78) Schroth, W.; Schaedler, H. D.; Andersch, J. *Z. Chem.* **1989**, *29*, 129-135.

(79) Kreher, U. P.; Rosamilia, A. E.; Raston, C. L.; Scott, J. L.; Strauss, C. R. *Org. Lett.* **2003**, *5*, 3107-3110.

(80) Bhatt, A. I.; Bond, A. M.; MacFarlane, D. R.; Zhang, J.; Scott, J. L.; Strauss, C. R.; Iotov, P. I.; Kalcheva, S. V. *Green Chem.* **2006**, *8*, 161-171.

(81) Nelson, W. T.; (Phillips Petroleum Co.). US 2801151, 1957.

(82) Nelson, W. T.; (Phillips Petroleum Co.). US 2801217, 1957.\

(83) Jessop, P. G.; Hsiao, Y.; Ikariya, T.; Noyori, R. *J. Am. Chem. Soc.* **1994**, *116*, 8851-8852.

(84) Pagni, R. M.; Kabalka, G. W.; Lee, C.; Malladi, R. R.; Collins, B.; Conley, N. *ACS Symp. Ser.* **2002**, *818*, 42-55.

(85) Phan, L.; Andreatta, J. R.; Horvey, L. K.; Edie, C. F.; Luco, A.-L.; Mirchandani, A.; Darensbourg, D. J.; Jessop, P. G. *J. Org. Chem.* **2008**, *73*, 127-132.

(86) 37 mg of PPNC (0.75 eq), based on the origional 0.050 g Cr(salen)Cl, was added to the recovered catalyst, dissolved in DCM, and dried in acordiace with the normal copolymeization routine.

(87) Ochiai, B.; Endo, T. *Prog. Polym. Sci.* **2005**, *30*, 183-215.

(88) Kuran, W. *Prog. Polym. Sci.* **1998**, *23*, 919-992.

(89) Marianucci, E.; Berti, C.; Pilati, F.; Manaresi, P.; Guaita, M.; Chiantore, O. *Polymer* **1994**, *35*, 1564-1566.

(90) Steblyanko, A.; Choi, W.; Sanda, F.; Endo, T. *J. Polym. Sci. Part A: Polym. Chem.* **2001**, *39*, 3967-3980.

(91) Choi, W.; Sanda, F.; Endo, T. *Macromolecules* **1998**, *31*, 2454-2460.

(92) Kricheldorf, H. R.; Damrau, D.-O. *Macromol. Chem. Phys.* **1998**, *199*, 2589-2596.

(93) Berti, C.; Celli, A.; Marianucci, E. *Eur. Polym. J.* **2002**, *38*, 1281-1288.

(94) Berti, C.; Marianucci, E.; Pilati, F. *Makromol. Chem.* **1988**, *189*, 1323-1330.

(95) Soga, K.; Imamura, H.; Ikeda, S. *Makromol. Chem.* **1975**, *176*, 807-811.

(96) Becke, A. D. *J. Chem. Phys.* **1993**, *98*, 5648-5652.

(97) Lee, C.; Yang, W.; Parr, R. G. *Phys. Rev. B: Condens. Matter* **1988**, *37*, 785-789.

(98) Frisch, M. J.; Trucks, G. W.; Schlegel, H. B.; Scuseria, G. E.; Robb, M. A.; Cheeseman, J. R.; Montgomery Jr., J. A.; Vreven, T.; Kudin, K. N.; Burant, J. C.; Millam, J. M.; Iyengar, S. S.; Tomasi, J.; Barone, V.; Mennucci, B.; Cossi, M.; Scalmani, G.; Rega, N.; Petersson, G. A.; Nakatsuji, H.; Hada, M.; Ehara, M.; Toyota, K.; Fukuda, J.; Hasegawa, J.; Ishida, M.; Nakajima, T.; Honda, Y.; Kitao, O.; Nakai, H.; Klene, M.; Li, X.; Knox, J. E.; Hratchian, H. P.; Cross, J. B.; Bakken, V.; Adamo, C.; Jaramillo, J.; Gomperts, R.; Stratmann, R. E.; Yazyev, O.; Austin, A. J.; Cammi, R.; Pomelli, C.; Ochterski, J. W.; Ayala, P. Y.; Morokuma, K.; Voth, G. A.; Salvador, P.; Dannenberg, J. J.; Zakrzweski, V. G.; Dapprich, S.; Daniels, A. D.; Strain, M. C.; Farkas, O.; Malick, D. K.; Rabuck, A. D.; Raghavachari, D.; Foresman, J. B.; Ortiz, C.; Cui, Q.; Baboul, A. G.; Clifford, S.; Cioslowski, J.; Stefanov, B. B.; Liu, G.; Liashenko, A.; Piskorz, P.; Komaromi, I.; Martin, R. L.; Fox, D. J.; Keith, T.; Al-Laham, M. A.; Peng, C. Y.; Nanayakkara, A.; Challacombe, M.; Gill, O. M. W.; Johnson, B.; Chen, W.;

Wong, M. W.; Gonzalez, C.; Pople, J. A. In *Gaussian 03, Rivision C.02; Gaussian, Inc* Wallingford, CT, 2004.

(99) Bruker AXS, I.; version 5.5632 ed. Madison, WI.

(100) Sheldrick, G. SADABS: Program for area detector adsorption correction. Institut fur Anorganische Chemie der Uniseritat Gottingen: Gottingen, Germany, 1996.

(101) Sheldrick, G. SHELXS-97. Institut fur Anorganische Chemie der Uniseritat Gottingen: Gottingen, Germany, 1997.

(102) Sheldrick, G. SHELXL-97. Institut fur Anorganische Chemie der Uniseritat Gottingen: Gottingen, Germany, 1997.

(103) Kuran, W.; Rokicki, A.; Wielgopolan, W. *Makromol. Chem.* **1978**, *179*, 2545-2548.

(104) Darensbourg, D. J.; Phelps, A. L. *Inorg. Chem.* **2005**, *44*, 4622-4629.

(105) Sit, W. N.; Ng, S. M.; Kwong, K. Y.; Lau, C. P. *J. Org. Chem.* **2005**, *70*, 8583-8586.

(106) Rey-Stolle, M. F.; Fernandez-Martin, F.; Tagle, L. H.; Hernandez-Fuentes, I. *Eur. Polym. J.* **1997**, *33*, 295-297.

APPENDIX A

SUPPLEMENTARY MATERIAL FOR CRYSTALLOGRAPHIC STUDIES, BOND ANGLE CALCULATIONS, AND CAMBRIDGE CRYSTALLOGRAPHIC DATABASE SEARCH RESULTS FOR CHAPTER II

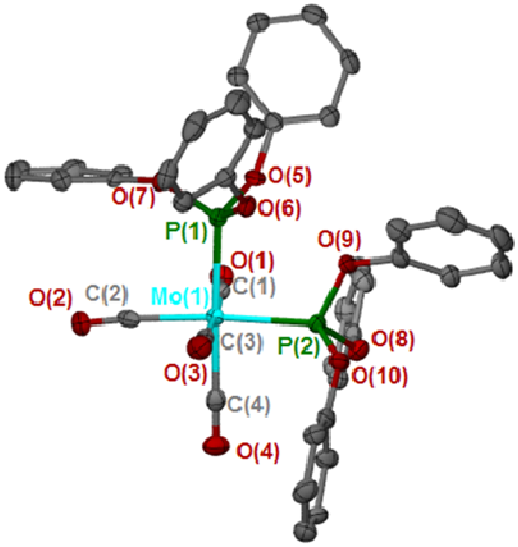

Table A-1. Crystal data and structure refinement for **2-1**		
Identification Code	2-**1**	
Empirical formula	$C_{40}H_{30}MoO_{10}P_2$	
Formula weight	828.52	
Temperature	110(2) K	
Wavelength	0.071073 Å	
Crystal system	Monoclinic	
Space group	P2(1)	
Unit cell dimensions	a = 11.197 Å	α = 90°
	b = 16.033(3) Å	β = 118.030(4)°
	c = 11.737(3) Å	γ = 90°
Volume	1860(1) $Å^3$	
Z	2	
Density (calculated)	1.479 mg/m^3	
Absorption coefficient	0.497mm^{-1}	

F(000)	844	
Crystal Size	0.90 x 0.05 . 0.02 mm	
Theta range for data collection	1.97 to 27.58°	
Index ranges	-14 <= h<= 14, -20<= k <= 20, -15<= l <= 15	
Reflections collected	17547	
Independent reflections	8191	
Completeness to theta = 27.58	98.1%	
Absorption correction	None	
Refinement method	Full-matrix least-squares on F^2	
Data / restraints / parameters	8191 / 1/ 478	
Goodness-of-fit on F^2	1.137	
Final R indices [I>2sigma(I)]	R_1 = 0.0457	R_w = 0.1120
R indices (all data)	R_1 = 0.0490	R_w = 0.1180
Largest diff. peak and hole	2.6545 and -0.0660 e.$Å^{-3}$	

Table A-2. Atomic coordinates (x 10^4) and equivalent isotropic displacement parameters (A^2 x 10^3) for **2.1**. U(eq) is defined as one third of the trace of the orthogonalized Uij tensor.

	x	y	z	U(eq)
C(1)	4722(4)	3193(2)	7227(4)	29(1)
C(2)	6722(4)	2365(3)	6759(4)	30(1)
C(3)	8496(4)	3750(2)	7730(4)	28(1)
C(4)	5751(4)	3934(2)	5597(4)	31(1)
C(5)	7057(4)	3142(3)	11671(4)	30(1)
C(6)	7222(4)	2391(3)	12276(4)	35(1)
C(7)	7620(5)	2381(3)	13587(5)	45(1)
C(8)	7838(5)	3129(3)	14263(5)	43(1)
C(9)	7649(5)	3877(3)	13620(5)	43(1)
C(10)	7267(4)	3892(3)	12316(4)	34(1)
C(11)	10234(4)	3256(2)	11514(4)	29(1)
C(12)	10663(4)	3390(3)	12803(4)	37(1)
C(13)	11992(5)	3172(3)	13673(5)	49(1)
C(14)	12835(5)	2848(3)	13214(5)	51(1)
C(15)	12371(4)	2723(3)	11927(5)	43(1)
C(16)	11042(4)	2934(3)	11048(4)	35(1)
C(17)	7531(4)	1399(2)	9510(4)	27(1)
C(18)	8303(5)	784(3)	9368(4)	38(1)
C(19)	7677(6)	36(3)	8787(5)	52(1)

C(20)	6304(6)	-91(3)	8402(4)	49(1)
C(21)	5591(5)	527(3)	8578(4)	43(1)
C(22)	6168(4)	1284(2)	9119(4)	32(1)
C(23)	3936(4)	5158(2)	7176(4)	30(1)
C(24)	2975(4)	5108(3)	5898(4)	33(1)
C(25)	1704(4)	4822(3)	5600(4)	38(1)
C(26)	1404(4)	4583(3)	6567(5)	41(1)
C(27)	2366(4)	4626(3)	7835(4)	37(1)
C(28)	3657(4)	4921(3)	8160(4)	35(1)
C(29)	7536(4)	5772(2)	10401(4)	30(1)
C(30)	8859(4)	5752(3)	11424(4)	39(1)
C(31)	9326(5)	6466(4)	12209(5)	51(1)
C(32)	8526(6)	7146(3)	11976(5)	51(1)
C(33)	7241(6)	7157(3)	10964(5)	49(1)
C(34)	6729(5)	6469(3)	10171(5)	38(1)
C(35)	7676(4)	5791(2)	6915(4)	31(1)
C(36)	6550(4)	5906(3)	5753(4)	33(1)
C(37)	6697(5)	6144(3)	4684(4)	39(1)
C(38)	7979(5)	6252(3)	4809(5)	45(1)
C(39)	9089(5)	6148(3)	5982(5)	44(1)
C(40)	8966(4)	5911(3)	7054(4)	36(1)
Mo(1)	6601(1)	3510(1)	7447(1)	24(1)
O(1)	3696(3)	2976(2)	7099(3)	34(1)
O(2)	6783(3)	1754(2)	6303(3)	42(1)
O(3)	9581(3)	3880(2)	7941(3)	40(1)
O(4)	5257(3)	4159(2)	4569(3)	43(1)
O(5)	6611(3)	3180(2)	10320(2)	28(1)
O(6)	8934(2)	3554(2)	10653(2)	29(1)
O(7)	8206(2)	2133(2)	10127(3)	27(1)
O(8)	5217(3)	5495(2)	7464(3)	30(1)
O(9)	7066(3)	5040(2)	9674(3)	30(1)
O(10)	7605(3)	5609(2)	8048(3)	29(1)
P(1)	7606(1)	3059(1)	9686(1)	24(1)
P(2)	6585(1)	4935(1)	8156(1)	25(1)

Table A-3. Bond lengths [Å] and angles [deg] for **2-1**.

C(1)-O(1)	1.141(5)	C(3)-O(3)	1.139(4)
C(1)-Mo(1)	2.060(4)	C(3)-Mo(1)	2.025(4)
C(2)-O(2)	1.134(5)	C(4)-O(4)	1.125(5)
C(2)-Mo(1)	2.035(4)	C(4)-Mo(1)	2.034(4)

C(5)-C(6)	1.366(6)	O(5)-P(1)	1.617(3)
C(5)-C(10)	1.381(6)	O(6)-P(1)	1.595(3)
C(5)-O(5)	1.422(5)	O(7)-P(1)	1.611(3)
C(6)-C(7)	1.385(6)	O(8)-P(2)	1.625(3)
C(7)-C(8)	1.395(7)	O(9)-P(2)	1.609(3)
C(8)-C(9)	1.379(7)	O(10)-P(2)	1.620(3)
C(9)-C(10)	1.383(6)		
C(11)-C(16)	1.360(6)	O(1)-C(1)-Mo(1)	176.5(3)
C(11)-C(12)	1.372(6)	O(2)-C(2)-Mo(1)	175.3(3)
C(11)-O(6)	1.409(4)	O(3)-C(3)-Mo(1)	177.2(3)
C(12)-C(13)	1.397(6)	O(4)-C(4)-Mo(1)	178.5(3)
C(13)-C(14)	1.388(8)	C(6)-C(5)-C(10)	122.5(3)
C(14)-C(15)	1.362(8)	C(6)-C(5)-O(5)	120.5(4)
C(15)-C(16)	1.396(6)	C(10)-C(5)-O(5)	117.0(3)
C(17)-C(18)	1.373(6)	C(5)-C(6)-C(7)	118.8(4)
C(17)-C(22)	1.384(6)	C(6)-C(7)-C(8)	120.0(4)
C(17)-O(7)	1.403(4)	C(9)-C(8)-C(7)	119.7(4)
C(18)-C(19)	1.394(7)	C(8)-C(9)-C(10)	120.6(4)
C(19)-C(20)	1.399(8)	C(5)-C(10)-C(9)	118.4(4)
C(20)-C(21)	1.347(7)	C(16)-C(11)-C(12)	123.3(4)
C(21)-C(22)	1.382(6)	C(16)-C(11)-O(6)	119.9(4)
C(23)-C(24)	1.377(5)	C(12)-C(11)-O(6)	116.5(3)
C(23)-C(28)	1.383(6)	C(11)-C(12)-C(13)	117.8(4)
C(23)-O(8)	1.416(5)	C(14)-C(13)-C(12)	119.7(4)
C(24)-C(25)	1.376(6)	C(15)-C(14)-C(13)	120.7(4)
C(25)-C(26)	1.380(6)	C(14)-C(15)-C(16)	120.2(4)
C(26)-C(27)	1.369(7)	C(11)-C(16)-C(15)	118.3(4)
C(27)-C(28)	1.393(6)	C(18)-C(17)-C(22)	121.6(4)
C(29)-C(34)	1.381(6)	C(18)-C(17)-O(7)	116.6(3)
C(29)-O(9)	1.401(4)	C(22)-C(17)-O(7)	121.7(3)
C(29)-C(30)	1.402(6)	C(17)-C(18)-C(19)	118.5(4)
C(30)-C(31)	1.407(7)	C(18)-C(19)-C(20)	120.4(4)
C(31)-C(32)	1.356(8)	C(21)-C(20)-C(19)	119.0(4)
C(32)-C(33)	1.369(8)	C(20)-C(21)-C(22)	122.2(5)
C(33)-C(34)	1.382(7)	C(21)-C(22)-C(17)	118.3(4)
C(35)-C(36)	1.367(6)	C(24)-C(23)-C(28)	121.8(4)
C(35)-C(40)	1.390(6)	C(24)-C(23)-O(8)	117.8(3)
C(35)-O(10)	1.399(5)	C(28)-C(23)-O(8)	120.4(3)
C(36)-C(37)	1.393(6)	C(25)-C(24)-C(23)	118.8(4)
C(37)-C(38)	1.384(7)	C(24)-C(25)-C(26)	120.4(4)
C(38)-C(39)	1.364(7)	C(27)-C(26)-C(25)	120.6(4)
C(39)-C(40)	1.381(6)	C(26)-C(27)-C(28)	120.0(4)
Mo(1)-P(1)	2.4318(10)	C(23)-C(28)-C(27)	118.5(4)
Mo(1)-P(2)	2.4360(10)	C(34)-C(29)-O(9)	122.4(4)

C(34)-C(29)-C(30) 121.1(4)
O(9)-C(29)-C(30) 116.4(4)
C(29)-C(30)-C(31) 117.4(5)
C(32)-C(31)-C(30) 121.1(5)
C(31)-C(32)-C(33) 120.7(4)
C(32)-C(33)-C(34) 120.6(5)
C(33)-C(34)-C(29) 119.2(4)
C(36)-C(35)-C(40) 121.2(4)
C(36)-C(35)-O(10) 122.6(4)
C(40)-C(35)-O(10) 116.0(4)
C(35)-C(36)-C(37) 119.5(4)
C(38)-C(37)-C(36) 119.6(4)
C(39)-C(38)-C(37) 120.0(4)
C(38)-C(39)-C(40) 121.3(4)
C(39)-C(40)-C(35) 118.3(4)
C(3)-Mo(1)-C(4) 92.28(15)
C(3)-Mo(1)-C(2) 88.67(15)
C(4)-Mo(1)-C(2) 87.91(15)
C(3)-Mo(1)-C(1) 176.22(15)
C(4)-Mo(1)-C(1) 90.62(14)
C(2)-Mo(1)-C(1) 89.02(15)
C(3)-Mo(1)-P(1) 87.83(11)
C(4)-Mo(1)-P(1) 177.65(11)
C(2)-Mo(1)-P(1) 94.44(11)
C(1)-Mo(1)-P(1) 89.36(10)
C(3)-Mo(1)-P(2) 86.59(11)
C(4)-Mo(1)-P(2) 88.62(11)
C(2)-Mo(1)-P(2) 174.01(11)
C(1)-Mo(1)-P(2) 95.90(10)
P(1)-Mo(1)-P(2) 89.05(3)
C(5)-O(5)-P(1) 123.5(2)
C(11)-O(6)-P(1) 130.1(3)
C(17)-O(7)-P(1) 124.4(2)
C(23)-O(8)-P(2) 121.3(2)
C(29)-O(9)-P(2) 126.6(2)
C(35)-O(10)-P(2) 124.8(2)
O(6)-P(1)-O(7) 96.97(15)
O(6)-P(1)-O(5) 103.08(14)
O(7)-P(1)-O(5) 103.61(15)
O(6)-P(1)-Mo(1) 115.11(11)
O(7)-P(1)-Mo(1) 122.18(11)
O(5)-P(1)-Mo(1) 113.16(10)
O(9)-P(2)-O(10) 97.80(14)
O(9)-P(2)-O(8) 104.05(15)
O(10)-P(2)-O(8) 97.30(14)
O(9)-P(2)-Mo(1) 115.07(10)
O(10)-P(2)-Mo(1) 118.67(11)
O(8)-P(2)-Mo(1) 120.24(11)

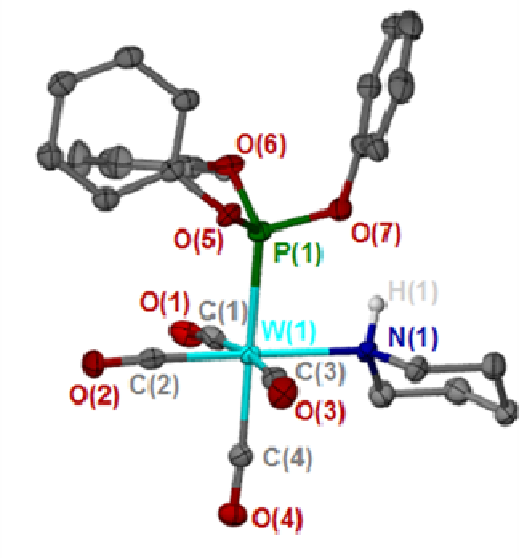

Table A-4. Crystal data and structure refinement for **2-2**		
Identification Code	2-**2**	
Empirical formula	$C_{54}H_{52}N_2O_{14}P_2W_2$	
Formula weight	1382.62	
Temperature	110(2) K	
Wavelength	0.071073 Å	
Crystal system	Orthorhombic	
Space group	Pbca	
Unit cell dimensions	a = 18.3660(18) Å	α = 90°
	b = 14.5829(15) Å	β = 90°
	c = 19.565(2) Å	γ = 90°
Volume	5240.0(9) $Å^3$	
Z	4	
Density (calculated)	1.747 mg/m^3	
Absorption coefficient	4.516 mm^{-1}	
F(000)	2704	
Crystal Size	0.10 x 0.09 . 0.05 mm	
Theta range for data collection	2.62 to 27.54°	
Index ranges	-23 <= h<= 23, -18<= k <= 18, -25<= l <= 25	
Reflections collected	47056	
Independent reflections	5987	
Completeness to theta = 27.54	99.1%	
Absorption correction	None	
Refinement method	Full-matrix least-squares on F^2	
Data / restraints / parameters	5987 / 0 / 337	

Goodness-of-fit on F^2	1.084	
Final R indices [I>2sigma(I)]	$R_1 = 0.0504$	$R_w = 0.1237$
R indices (all data)	$R_1 = 0.0569$	$R_w = 0.1345$
Largest diff. peak and hole	6.430 and -3.174 e.$Å^{-3}$	

Table A-5. Atomic coordinates (x 10^4) and equivalent isotropic displacement parameters (A^2 x 10^3) for **2-2.** U(eq) is defined as one third of the trace of the orthogonalized Uij tensor.

	x	y	z	U(eq)
(1)	2642(3)	9786(3)	652(3)	28(1)
(2)	2475(3)	11322(4)	1465(2)	25(1)
(3)	1271(3)	10709(4)	2126(2)	26(1)
(4)	1356(3)	10732(4)	669(2)	25(1)
(5)	3342(2)	10579(4)	3291(2)	24(1)
(6)	3573(3)	11424(4)	3063(2)	28(1)
(7)	4188(3)	11814(4)	3350(2)	30(1)
(8)	4578(3)	11331(4)	3851(2)	30(1)
(9)	4336(3)	10483(4)	4063(2)	29(1)
(10)	3715(3)	10089(4)	3783(3)	28(1)
(11)	3907(3)	9148(4)	1785(2)	26(1)
(12)	4410(3)	9833(4)	1721(3)	36(1)
(13)	4903(4)	9820(5)	1175(4)	46(2)
(14)	4868(3)	9110(5)	706(3)	40(1)
(15)	4359(3)	8420(4)	778(3)	34(1)
(16)	3874(3)	8436(4)	1329(2)	27(1)
(17)	2404(3)	8299(4)	3357(2)	25(1)
(18)	2899(3)	7601(5)	3373(3)	35(1)
(19)	3047(3)	7175(6)	3998(4)	43(2)
(20)	2711(4)	7477(5)	4587(3)	47(2)
(21)	2219(4)	8192(5)	4558(3)	43(2)
(22)	2054(3)	8617(4)	3939(3)	33(1)
(23)	1093(3)	8534(4)	663(2)	31(1)
(24)	677(3)	7627(4)	620(3)	35(1)
(25)	-8(3)	7656(5)	1048(3)	38(1)
(26)	198(3)	7901(4)	1781(3)	36(1)
(27)	622(3)	8800(4)	1813(2)	29(1)
(1)	1284(2)	8804(3)	1377(2)	23(1)
(1)	3039(2)	9685(3)	198(2)	36(1)
(2)	2763(2)	12038(3)	1488(2)	33(1)

(3)	912(2)	11079(3)	2524(2)	36(1)
(4)	1041(2)	11100(3)	237(2)	31(1)
(5)	2694(2)	10220(2)	3022(2)	25(1)
(6)	3449(2)	9158(3)	2355(2)	28(1)
(7)	2204(2)	8691(3)	2724(2)	27(1)
(1)	2626(1)	9533(1)	2381(1)	22(1)
(1)	1947(1)	10166(1)	1414(1)	19(1)

Table A-6. Bond lengths [A] and angles [deg] for **2-2.**

C(1)-O(1)	1.159(7)	C(24)-C(25)	1.512(8)
C(1)-W(1)	2.039(5)	C(25)-C(26)	1.526(7)
C(2)-O(2)	1.171(7)	C(26)-C(27)	1.526(7)
C(2)-W(1)	1.947(6)	C(27)-N(1)	1.485(6)
C(3)-O(3)	1.155(6)	N(1)-W(1)	2.332(5)
C(3)-W(1)	2.027(5)	O(5)-P(1)	1.610(4)
C(4)-O(4)	1.157(6)	O(6)-P(1)	1.608(3)
C(4)-W(1)	1.995(5)	O(7)-P(1)	1.600(4)
C(5)-C(6)	1.377(7)	P(1)-W(1)	2.4465(12)
C(5)-C(10)	1.380(7)		
C(5)-O(5)	1.403(5)	O(1)-C(1)-W(1)	171.5(5)
C(6)-C(7)	1.384(7)	O(2)-C(2)-W(1)	176.9(4)
C(7)-C(8)	1.404(7)	O(3)-C(3)-W(1)	174.9(5)
C(8)-C(9)	1.377(8)	O(4)-C(4)-W(1)	176.1(5)
C(9)-C(10)	1.391(7)	C(6)-C(5)-C(10)	122.4(5)
C(11)-C(12)	1.367(8)	C(6)-C(5)-O(5)	118.3(4)
C(11)-C(16)	1.368(7)	C(10)-C(5)-O(5)	119.3(5)
C(11)-O(6)	1.398(5)	C(5)-C(6)-C(7)	119.3(5)
C(12)-C(13)	1.400(8)	C(6)-C(7)-C(8)	119.5(5)
C(13)-C(14)	1.385(10)	C(9)-C(8)-C(7)	119.7(5)
C(14)-C(15)	1.380(9)	C(8)-C(9)-C(10)	121.2(5)
C(15)-C(16)	1.399(7)	C(5)-C(10)-C(9)	117.9(5)
C(17)-C(18)	1.365(8)	C(12)-C(11)-C(16)	121.7(5)
C(17)-C(22)	1.388(7)	C(12)-C(11)-O(6)	118.1(5)
C(17)-O(7)	1.413(5)	C(16)-C(11)-O(6)	120.1(5)
C(18)-C(19)	1.398(9)	C(11)-C(12)-C(13)	119.8(5)
C(19)-C(20)	1.379(10)	C(14)-C(13)-C(12)	119.0(6)
C(20)-C(21)	1.381(10)	C(15)-C(14)-C(13)	120.6(5)
C(21)-C(22)	1.394(8)	C(14)-C(15)-C(16)	119.9(5)
C(23)-N(1)	1.493(6)	C(11)-C(16)-C(15)	119.1(5)
C(23)-C(24)	1.529(8)	C(18)-C(17)-C(22)	122.6(5)

C(18)-C(17)-O(7)	119.7(5)	O(6)-P(1)-O(5)	99.40(18)
C(22)-C(17)-O(7)	117.6(5)	O(7)-P(1)-W(1)	111.51(13)
C(17)-C(18)-C(19)	118.7(6)	O(6)-P(1)-W(1)	125.72(12)
C(20)-C(19)-C(18)	120.1(7)	O(5)-P(1)-W(1)	114.02(14)
C(19)-C(20)-C(21)	120.0(5)	C(2)-W(1)-C(4)	87.2(2)
C(20)-C(21)-C(22)	120.9(6)	C(2)-W(1)-C(3)	86.1(2)
C(17)-C(22)-C(21)	117.7(6)	C(4)-W(1)-C(3)	90.4(2)
N(1)-C(23)-C(24)	113.4(4)	C(2)-W(1)-C(1)	87.8(2)
C(25)-C(24)-C(23)	111.2(5)	C(4)-W(1)-C(1)	85.4(2)
C(24)-C(25)-C(26)	108.7(4)	C(3)-W(1)-C(1)	172.7(2)
C(27)-C(26)-C(25)	111.5(5)	C(2)-W(1)-N(1)	178.00(17)
N(1)-C(27)-C(26)	113.3(4)	C(4)-W(1)-N(1)	92.58(18)
C(27)-N(1)-C(23)	110.2(4)	C(3)-W(1)-N(1)	91.96(19)
C(27)-N(1)-W(1)	114.4(3)	C(1)-W(1)-N(1)	94.16(18)
C(23)-N(1)-W(1)	112.1(3)	C(2)-W(1)-P(1)	91.88(14)
C(5)-O(5)-P(1)	126.2(3)	C(4)-W(1)-P(1)	176.23(14)
C(11)-O(6)-P(1)	126.4(3)	C(3)-W(1)-P(1)	85.90(14)
C(17)-O(7)-P(1)	123.6(3)	C(1)-W(1)-P(1)	98.23(15)
O(7)-P(1)-O(6)	102.0(2)	N(1)-W(1)-P(1)	88.23(10)
O(7)-P(1)-O(5)	100.78(18)		

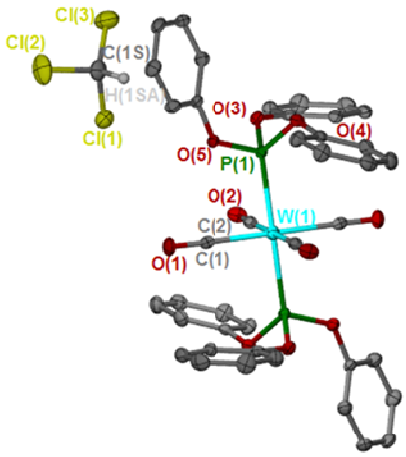

Table A-7. Crystal data and structure refinement for **2-4**	
Identification Code	2-**4**
Empirical formula	$C_{20.5}H_{5.5}O_5PW_{0.5}$
Formula weight	517.90

Temperature	110(2) K	
Wavelength	0.071073 Å	
Crystal system	Triclinic	
Space group	Pbca	
Unit cell dimensions	a = 9.170(1) Å	α = 69.755(1)°
	b = 11.151(1) Å	β = 89.766(1)°
	c = 11.375(1) Å	γ = 68.296(1)°
Volume	1000.37(3) $Å^3$	
Z	2	
Density (calculated)	1.714 mg/m^3	
Absorption coefficient	3.215 mm^{-1}	
F(000)	512	
Crystal Size	0.20 x 0.10 . 0.10 mm	
Theta range for data collection	2.87 to 25.00°	
Index ranges	-10 <= h<= 10, -13<= k <= 13, -13<= l <= 13	
Reflections collected	7889	
Independent reflections	3453	
Completeness to theta = 25.00	97.6%	
Absorption correction	None	
Refinement method	Full-matrix least-squares on F^2	
Data / restraints / parameters	3453 / 6 / 277	
Goodness-of-fit on F^2	1.069	
Final R indices [I>2sigma(I)]	R_1 = 0.0200	R_w = 0.0490
R indices (all data)	R_1 = 0.0200	R_w = 0.0490
Largest diff. peak and hole	0.558 and -0.402 e.$Å^{-3}$	

Table A-8. Atomic coordinates (x 10^4) and equivalent isotropic displacement parameters (A^2 x 10^3) for **2-4**.
U(eq) is defined as one third of the trace of the orthogonalized Uij tensor.

	x	y	z	U(eq)
C(1)	9973(3)	-1401(3)	9242(2)	21(1)
C(2)	11765(3)	247(3)	8958(3)	22(1)
C(3)	9599(3)	3576(3)	7283(2)	20(1)
C(4)	10781(4)	3672(3)	6540(3)	27(1)
C(5)	11602(4)	4464(4)	6648(3)	36(1)
C(6)	11246(4)	5144(3)	7488(3)	34(1)

C(7)	10066(4)	5042(3)	8220(3)	29(1)
C(8)	9231(3)	4252(3)	8127(3)	23(1)
C(9)	5672(3)	2770(3)	9274(3)	20(1)
C(10)	5791(4)	3244(3)	10223(3)	27(1)
C(11)	4824(4)	3095(3)	11165(3)	31(1)
C(12)	3784(4)	2465(3)	11146(3)	29(1)
C(13)	3705(4)	1975(3)	10193(3)	31(1)
C(14)	4653(3)	2128(3)	9242(3)	26(1)
C(15)	6282(3)	1819(3)	6322(2)	19(1)
C(16)	5343(3)	1094(3)	6323(3)	26(1)
C(17)	4115(4)	1642(3)	5337(3)	30(1)
C(18)	3824(4)	2907(3)	4374(3)	30(1)
C(19)	4778(4)	3615(3)	4387(3)	30(1)
C(20)	6022(4)	3076(3)	5363(3)	27(1)
C(1S)	170(5)	9948(4)	5532(4)	35(2)
Cl(1)	2071(2)	8973(2)	6445(2)	37(1)
Cl(2)	-304(3)	8950(3)	4794(3)	60(1)
Cl(3)	125(3)	11512(2)	4379(2)	53(1)
O(1)	9961(3)	-2165(2)	8786(2)	29(1)
O(2)	12706(2)	414(2)	8333(2)	30(1)
O(3)	8784(2)	2805(2)	7087(2)	20(1)
O(4)	6589(2)	3007(2)	8287(2)	20(1)
O(5)	7530(2)	1163(2)	7327(2)	20(1)
P(1)	8177(1)	1792(1)	8180(1)	16(1)
W(1)	10000	0	10000	21(1)

Table A-9. Bond lengths [A] and angles [deg] for **2-4**.

C(1)-O(1)	1.144(3)	C(6)-H(6)	0.9500
C(1)-W(1)	2.036(3)	C(7)-C(8)	1.392(4)
C(2)-O(2)	1.143(3)	C(7)-H(7)	0.9500
C(2)-W(1)	2.047(3)	C(8)-H(8)	0.9500
C(3)-C(8)	1.383(4)	C(9)-C(10)	1.377(4)
C(3)-C(4)	1.384(4)	C(9)-C(14)	1.378(4)
C(3)-O(3)	1.398(3)	C(9)-O(4)	1.409(3)
C(4)-C(5)	1.389(4)	C(10)-C(11)	1.393(4)
C(4)-H(4)	0.9500	C(10)-H(10)	0.9500
C(5)-C(6)	1.383(5)	C(11)-C(12)	1.382(4)
C(5)-H(5)	0.9500	C(11)-H(11)	0.9500
C(6)-C(7)	1.376(4)	C(12)-C(13)	1.385(4)

C(12)-H(12)	0.9500
C(13)-C(14)	1.390(4)
C(13)-H(13)	0.9500
C(14)-H(14)	0.9500
C(15)-C(20)	1.381(4)
C(15)-C(16)	1.382(4)
C(15)-O(5)	1.402(3)
C(16)-C(17)	1.388(4)
C(16)-H(16)	0.9500
C(17)-C(18)	1.384(4)
C(17)-H(17)	0.9500
C(18)-C(19)	1.382(4)
C(18)-H(18)	0.9500
C(19)-C(20)	1.391(4)
C(19)-H(19)	0.9500
C(20)-H(20)	0.9500
C(1S)-Cl(3)	1.769(4)
C(1S)-Cl(1)	1.770(4)
C(1S)-Cl(2)	1.772(4)
C(1S)-H(1SA)	0.9600
O(3)-P(1)	1.6190(18)
O(4)-P(1)	1.6197(19)
O(5)-P(1)	1.6034(18)
P(1)-W(1)	2.4017(7)
W(1)-C(1)#1	2.036(3)
W(1)-C(2)#1	2.047(3)
W(1)-P(1)#1	2.4017(7)

O(1)-C(1)-W(1)	178.2(2)
O(2)-C(2)-W(1)	177.2(2)
C(8)-C(3)-C(4)	121.0(3)
C(8)-C(3)-O(3)	123.2(2)
C(4)-C(3)-O(3)	115.8(2)
C(3)-C(4)-C(5)	119.1(3)
C(3)-C(4)-H(4)	120.4
C(5)-C(4)-H(4)	120.4
C(6)-C(5)-C(4)	120.4(3)
C(6)-C(5)-H(5)	119.8
C(4)-C(5)-H(5)	119.8
C(7)-C(6)-C(5)	119.9(3)
C(7)-C(6)-H(6)	120.1
C(5)-C(6)-H(6)	120.1
C(6)-C(7)-C(8)	120.5(3)
C(6)-C(7)-H(7)	119.7
C(8)-C(7)-H(7)	119.7
C(3)-C(8)-C(7)	119.0(3)
C(3)-C(8)-H(8)	120.5
C(7)-C(8)-H(8)	120.5
C(10)-C(9)-C(14)	122.1(3)
C(10)-C(9)-O(4)	117.9(2)
C(14)-C(9)-O(4)	119.9(2)
C(9)-C(10)-C(11)	118.8(3)
C(9)-C(10)-H(10)	120.6
C(11)-C(10)-H(10)	120.6
C(12)-C(11)-C(10)	120.1(3)
C(12)-C(11)-H(11)	119.9
C(10)-C(11)-H(11)	119.9
C(11)-C(12)-C(13)	120.1(3)
C(11)-C(12)-H(12)	120.0
C(13)-C(12)-H(12)	120.0
C(12)-C(13)-C(14)	120.4(3)
C(12)-C(13)-H(13)	119.8
C(14)-C(13)-H(13)	119.8
C(9)-C(14)-C(13)	118.6(3)
C(9)-C(14)-H(14)	120.7
C(13)-C(14)-H(14)	120.7
C(20)-C(15)-C(16)	121.4(3)
C(20)-C(15)-O(5)	123.3(2)
C(16)-C(15)-O(5)	115.2(2)
C(15)-C(16)-C(17)	119.1(3)
C(15)-C(16)-H(16)	120.4
C(17)-C(16)-H(16)	120.4
C(18)-C(17)-C(16)	120.4(3)
C(18)-C(17)-H(17)	119.8
C(16)-C(17)-H(17)	119.8
C(19)-C(18)-C(17)	119.7(3)
C(19)-C(18)-H(18)	120.2
C(17)-C(18)-H(18)	120.2
C(18)-C(19)-C(20)	120.7(3)
C(18)-C(19)-H(19)	119.6
C(20)-C(19)-H(19)	119.6
C(15)-C(20)-C(19)	118.7(3)
C(15)-C(20)-H(20)	120.7
C(19)-C(20)-H(20)	120.7
Cl(3)-C(1S)-Cl(1)	110.2(2)
Cl(3)-C(1S)-Cl(2)	110.3(3)
Cl(1)-C(1S)-Cl(2)	109.6(3)
Cl(3)-C(1S)-H(1SA)	114.6

Cl(1)-C(1S)-H(1SA)	93.5	C(1)-W(1)-C(2)	87.71(10)
Cl(2)-C(1S)-H(1SA)	117.3	C(1)#1-W(1)-C(2)#1	87.71(10)
C(3)-O(3)-P(1)	125.42(16)	C(1)-W(1)-C(2)#1	92.29(10)
C(9)-O(4)-P(1)	122.66(16)	C(2)-W(1)-C(2)#1	180.0
C(15)-O(5)-P(1)	130.21(17)	C(1)#1-W(1)-P(1)	92.14(8)
O(5)-P(1)-O(3)	98.53(10)	C(1)-W(1)-P(1)	87.86(8)
O(5)-P(1)-O(4)	103.43(10)	C(2)-W(1)-P(1)	86.50(8)
O(3)-P(1)-O(4)	96.32(10)	C(2)#1-W(1)-P(1)	93.50(8)
O(5)-P(1)-W(1)	111.93(7)	C(1)#1-W(1)-P(1)#1	87.87(8)
O(3)-P(1)-W(1)	120.08(7)	C(1)-W(1)-P(1)#1	92.14(8)
O(4)-P(1)-W(1)	122.69(7)	C(2)-W(1)-P(1)#1	93.50(8)
C(1)#1-W(1)-C(1)	180.0	C(2)#1-W(1)-P(1)#1	86.50(8)
C(1)#1-W(1)-C(2)	92.29(10)	P(1)-W(1)-P(1)#1	180.0

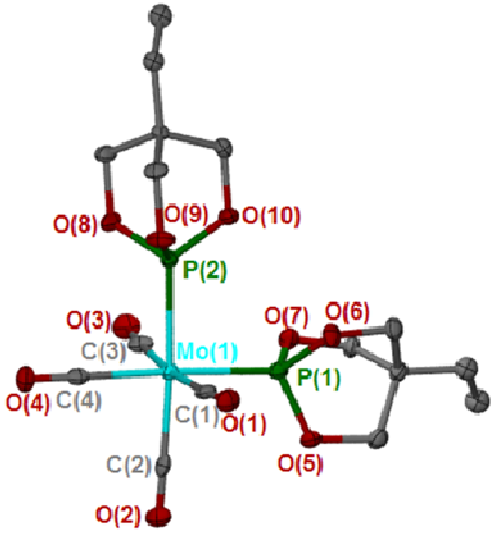

Table A-10. Crystal data and structure refinement for **2-5**		
Identification Code	**2-5**	
Empirical formula	$C_{16}H_{22}MoO_{10}P_2$	
Formula weight	532.22	
Temperature	110(2) K	
Wavelength	0.071073 Å	
Crystal system	Monoclinic	
Space group	P2(1)/n	
Unit cell dimensions	a = 13.017(4) Å	α = 90°
	b = 19.538(6) Å	β = 99.544(5)°
	c = 16.406(5) Å	γ = 90°
Volume	4115(2) $Å^3$	

Z	4	
Density (calculated)	0.859 mg/m^3	
Absorption coefficient	0.422 mm^{-1}	
F(000)	1080	
Crystal Size	0.22 x 0.20. 0.16 mm	
Theta range for data collection	1.63 to 27.56°	
Index ranges	-15 <= h<= 16, -25<= k <=25, -21<= l <= 17	
Reflections collected	38363	
Independent reflections	9318	
Completeness to theta = 27.56	98.0%	
Absorption correction	None	
Refinement method	Full-matrix least-squares on F^2	
Data / restraints / parameters	9318 / 0 / 507	
Goodness-of-fit on F^2	1.015	
Final R indices [I>2sigma(I)]	R_1 = 0.0778	R_w = 0.1675
R indices (all data)	R_1 = 0.0992	R_w = 0.1924
Largest diff. peak and hole	6.049 and -1.171 e.Å^{-3}	

Table A-11. Atomic coordinates (x 10^4) and equivalent isotropic displacement parameters (A^2 x 10^3) for **2-5**. U(eq) is defined as one third of the trace of the orthogonalized Uij tensor.

	x	y	z	U(eq)
C(1)	1878(3)	1811(2)	7174(3)	23(1)
C(2)	151(4)	1923(2)	8124(3)	23(1)
C(3)	91(3)	419(2)	8169(3)	21(1)
C(4)	-88(4)	1211(2)	6576(3)	21(1)
C(5)	2599(4)	1598(3)	10450(3)	35(1)
C(6)	3983(4)	1650(2)	9594(3)	27(1)
C(7)	3420(4)	531(2)	10078(3)	33(1)
C(8)	3618(3)	1279(2)	10314(3)	19(1)
C(9)	4465(4)	1300(2)	11086(3)	24(1)
C(10)	4839(4)	2015(2)	11375(3)	30(1)
C(11)	1506(4)	-819(2)	6044(3)	28(1)
C(12)	3200(4)	-206(2)	6263(3)	26(1)
C(13)	2726(4)	-964(2)	7356(3)	27(1)
C(14)	2656(4)	-875(2)	6424(3)	22(1)
C(15)	3174(4)	-1498(2)	6083(3)	30(1)

C(16)	3317(4)	-1457(3)	5184(3)	38(1)
C(17)	6877(4)	1927(2)	7161(3)	25(1)
C(18)	5070(3)	2121(2)	7957(3)	23(1)
C(19)	4896(3)	610(2)	8072(3)	21(1)
C(20)	4833(4)	1341(2)	6490(3)	21(1)
C(21)	8225(4)	2158(2)	9871(3)	25(1)
C(22)	8735(4)	936(2)	9804(3)	25(1)
C(23)	7250(4)	1272(2)	10500(3)	25(1)
C(24)	8333(3)	1481(2)	10345(3)	17(1)
C(25)	9049(3)	1570(2)	11183(3)	23(1)
C(26)	10176(3)	1736(2)	11140(3)	30(1)
C(27)	6525(4)	-663(2)	6008(3)	25(1)
C(28)	8224(4)	-64(2)	6367(3)	23(1)
C(29)	7610(4)	-840(2)	7382(3)	26(1)
C(30)	7650(4)	-734(2)	6461(3)	22(1)
C(31)	8235(4)	-1336(2)	6153(3)	30(1)
C(32)	8473(4)	-1267(2)	5279(3)	34(1)
Mo(1)	919(1)	1149(1)	7656(1)	19(1)
Mo(2)	5824(1)	1300(1)	7589(1)	18(1)
O(1)	2416(3)	2170(2)	6898(2)	35(1)
O(2)	-285(3)	2352(2)	8383(2)	34(1)
O(3)	-319(3)	-2(2)	8469(2)	30(1)
O(4)	-631(3)	1286(2)	5962(2)	30(1)
O(5)	1835(2)	1596(2)	9685(2)	31(1)
O(6)	3246(2)	1546(2)	8831(2)	24(1)
O(7)	2575(3)	471(2)	9372(2)	31(1)
O(8)	1038(2)	-205(2)	6340(2)	26(1)
O(9)	2778(2)	360(1)	6679(2)	24(1)
O(10)	2156(3)	-423(2)	7696(2)	27(1)
O(11)	7492(3)	2256(2)	6944(2)	35(1)
O(12)	4660(3)	2598(2)	8158(2)	31(1)
O(13)	4431(3)	215(2)	8352(2)	29(1)
O(14)	4295(3)	1382(2)	5875(2)	32(1)
O(15)	7523(3)	2081(1)	9088(2)	32(1)
O(16)	8005(2)	852(2)	9030(2)	29(1)
O(17)	6524(2)	1195(2)	9717(2)	29(1)
O(18)	6052(2)	-43(2)	6270(2)	27(1)
O(19)	7777(2)	488(1)	6795(2)	23(1)
O(20)	6961(3)	-317(2)	7682(2)	26(1)
P(1)	2177(1)	1176(1)	8924(1)	19(1)
P(2)	1760(1)	200(1)	7082(1)	19(1)
P(3)	7012(1)	1338(1)	8892(1)	18(1)
P(4)	6684(1)	331(1)	7078(1)	19(1)

Table A-12. Bond lengths [A] and angles [deg] for **2-5**.

C(1)-O(1)	1.138(5)	C(25)-C(26)	1.516(6)
C(1)-Mo(1)	2.044(5)	C(27)-O(18)	1.457(5)
C(2)-O(2)	1.133(5)	C(27)-C(30)	1.533(6)
C(2)-Mo(1)	2.032(5)	C(28)-O(19)	1.459(5)
C(3)-O(3)	1.136(5)	C(28)-C(30)	1.528(6)
C(3)-Mo(1)	2.051(5)	C(29)-O(20)	1.461(5)
C(4)-O(4)	1.140(6)	C(29)-C(30)	1.536(6)
C(4)-Mo(1)	2.026(5)	C(30)-C(31)	1.532(6)
C(5)-O(5)	1.466(5)	C(31)-C(32)	1.523(7)
C(5)-C(8)	1.515(6)	Mo(1)-P(2)	2.4218(13)
C(6)-O(6)	1.461(5)	Mo(1)-P(1)	2.4247(14)
C(6)-C(8)	1.526(6)	Mo(2)-P(4)	2.4184(13)
C(7)-O(7)	1.464(5)	Mo(2)-P(3)	2.4229(13)
C(7)-C(8)	1.524(6)	O(5)-P(1)	1.617(3)
C(8)-C(9)	1.536(6)	O(6)-P(1)	1.597(3)
C(9)-C(10)	1.527(6)	O(7)-P(1)	1.607(3)
C(11)-O(8)	1.465(5)	O(8)-P(2)	1.617(3)
C(11)-C(14)	1.527(6)	O(9)-P(2)	1.606(3)
C(12)-O(9)	1.453(5)	O(10)-P(2)	1.609(3)
C(12)-C(14)	1.531(6)	O(15)-P(3)	1.608(3)
C(13)-O(10)	1.455(5)	O(16)-P(3)	1.589(3)
C(13)-C(14)	1.527(6)	O(17)-P(3)	1.612(3)
C(14)-C(15)	1.540(6)	O(18)-P(4)	1.614(3)
C(15)-C(16)	1.519(7)	O(19)-P(4)	1.598(3)
C(17)-O(11)	1.130(5)	O(20)-P(4)	1.612(3)
C(17)-Mo(2)	2.047(5)		
C(18)-O(12)	1.149(5)	O(1)-C(1)-Mo(1)	178.8(4)
C(18)-Mo(2)	2.025(5)	O(2)-C(2)-Mo(1)	179.4(4)
C(19)-O(13)	1.125(5)	O(3)-C(3)-Mo(1)	176.3(4)
C(19)-Mo(2)	2.054(5)	O(4)-C(4)-Mo(1)	175.7(4)
C(20)-O(14)	1.131(6)	O(5)-C(5)-C(8)	111.0(4)
C(20)-Mo(2)	2.037(5)	O(6)-C(6)-C(8)	110.7(3)
C(21)-O(15)	1.456(5)	O(7)-C(7)-C(8)	110.5(3)
C(21)-C(24)	1.528(5)	C(5)-C(8)-C(7)	108.4(4)
C(22)-O(16)	1.464(5)	C(5)-C(8)-C(6)	108.2(4)
C(22)-C(24)	1.532(6)	C(7)-C(8)-C(6)	108.6(4)
C(23)-O(17)	1.470(5)	C(5)-C(8)-C(9)	113.2(4)
C(23)-C(24)	1.529(6)	C(7)-C(8)-C(9)	107.6(3)
C(24)-C(25)	1.537(6)	C(6)-C(8)-C(9)	110.6(4)

C(10)-C(9)-C(8)	115.4(4)
O(8)-C(11)-C(14)	110.9(3)
O(9)-C(12)-C(14)	110.3(3)
O(10)-C(13)-C(14)	110.6(3)
C(13)-C(14)-C(11)	108.0(4)
C(13)-C(14)-C(12)	108.5(4)
C(11)-C(14)-C(12)	108.6(4)
C(13)-C(14)-C(15)	108.5(4)
C(11)-C(14)-C(15)	111.5(4)
C(12)-C(14)-C(15)	111.6(4)
C(16)-C(15)-C(14)	116.3(4)
O(11)-C(17)-Mo(2)	176.9(4)
O(12)-C(18)-Mo(2)	178.2(4)
O(13)-C(19)-Mo(2)	176.5(4)
O(14)-C(20)-Mo(2)	177.9(4)
O(15)-C(21)-C(24)	110.6(3)
O(16)-C(22)-C(24)	110.2(3)
O(17)-C(23)-C(24)	111.0(3)
C(21)-C(24)-C(23)	107.9(4)
C(21)-C(24)-C(22)	108.5(4)
C(23)-C(24)-C(22)	108.9(3)
C(21)-C(24)-C(25)	110.4(3)
C(23)-C(24)-C(25)	108.7(3)
C(22)-C(24)-C(25)	112.4(3)
C(26)-C(25)-C(24)	\ 115.6(4)
O(18)-C(27)-C(30)	110.4(3)
O(19)-C(28)-C(30)	110.1(4)
O(20)-C(29)-C(30)	110.7(3)
C(28)-C(30)-C(31)	110.3(4)
C(28)-C(30)-C(27)	108.6(3)
C(31)-C(30)-C(27)	113.3(4)
C(28)-C(30)-C(29)	108.1(4)
C(31)-C(30)-C(29)	108.7(4)
C(27)-C(30)-C(29)	107.7(4)
C(32)-C(31)-C(30)	115.6(4)
C(4)-Mo(1)-C(2)	89.92(17)
C(4)-Mo(1)-C(1)	88.39(17)
C(2)-Mo(1)-C(1)	92.64(18)
C(4)-Mo(1)-C(3)	95.29(17)
C(2)-Mo(1)-C(3)	92.15(17)
C(1)-Mo(1)-C(3)	173.97(17)
C(4)-Mo(1)-P(2)	88.51(12)
C(2)-Mo(1)-P(2)	177.40(13)
C(1)-Mo(1)-P(2)	89.40(13)
C(3)-Mo(1)-P(2)	85.93(12)
C(4)-Mo(1)-P(1)	174.93(12)
C(2)-Mo(1)-P(1)	87.97(13)
C(1)-Mo(1)-P(1)	87.10(13)
C(3)-Mo(1)-P(1)	89.40(12)
P(2)-Mo(1)-P(1)	93.76(4)
C(18)-Mo(2)-C(20)	88.00(17)
C(18)-Mo(2)-C(17)	90.75(18)
C(20)-Mo(2)-C(17)	91.96(17)
C(18)-Mo(2)-C(19)	93.40(17)
C(20)-Mo(2)-C(19)	92.32(17)
C(17)-Mo(2)-C(19)	174.14(18)
C(18)-Mo(2)-P(4)	177.08(13)
C(20)-Mo(2)-P(4)	89.17(12)
C(17)-Mo(2)-P(4)	88.60(14)
C(19)-Mo(2)-P(4)	87.46(12)
C(18)-Mo(2)-P(3)	89.00(13)
C(20)-Mo(2)-P(3)	175.96(11)
C(17)-Mo(2)-P(3)	85.37(13)
C(19)-Mo(2)-P(3)	90.56(12)
P(4)-Mo(2)-P(3)	93.79(4)
C(5)-O(5)-P(1)	115.3(3)
C(6)-O(6)-P(1)	116.1(3)
C(7)-O(7)-P(1)	115.9(3)
C(11)-O(8)-P(2)	115.4(3)
C(12)-O(9)-P(2)	116.6(3)
C(13)-O(10)-P(2)	116.1(3)
C(21)-O(15)-P(3)	116.6(2)
C(22)-O(16)-P(3)	116.9(3)
C(23)-O(17)-P(3)	115.5(3)
C(27)-O(18)-P(4)	115.8(3)
C(28)-O(19)-P(4)	116.3(3)
C(29)-O(20)-P(4)	115.1(3)
O(6)-P(1)-O(7)	102.20(17)
O(6)-P(1)-O(5)	101.60(17)
O(7)-P(1)-O(5)	100.96(18)
O(6)-P(1)-Mo(1)	113.75(12)
O(7)-P(1)-Mo(1)	119.64(12)
O(5)-P(1)-Mo(1)	116.12(13)
O(9)-P(2)-O(10)	101.81(17)
O(9)-P(2)-O(8)	101.54(17)
O(10)-P(2)-O(8)	100.77(17)
O(9)-P(2)-Mo(1)	117.95(12)
O(10)-P(2)-Mo(1)	117.01(12)

O(8)-P(2)-Mo(1)	115.10(12)	O(19)-P(4)-O(20)	102.13(17)
O(16)-P(3)-O(15)	102.20(18)	O(19)-P(4)-O(18)	101.85(17)
O(16)-P(3)-O(17)	101.60(18)	O(20)-P(4)-O(18)	100.49(17)
O(15)-P(3)-O(17)	101.31(18)	O(19)-P(4)-Mo(2)	115.83(12)
O(16)-P(3)-Mo(2)	119.48(13)	O(20)-P(4)-Mo(2)	118.08(12)
O(15)-P(3)-Mo(2)	112.73(12)	O(18)-P(4)-Mo(2)	115.89(12)
O(17)-P(3)-Mo(2)	116.96(13)		

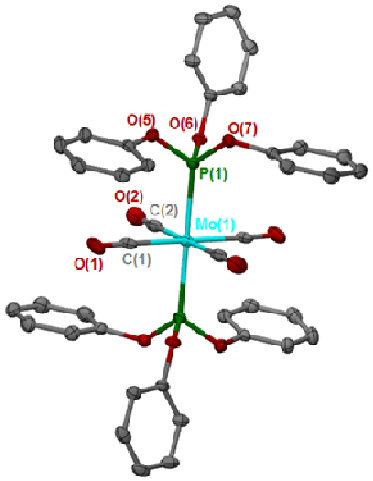

Table A-13. Crystal data and structure refinement for **2-6**		
Identification Code	**2-6**	
Empirical formula	$C_{20}H_{15}Mo_{0.5}O_5P$	
Formula weight	414.26	
Temperature	110(2) K	
Wavelength	0.071073 Å	
Crystal system	Triclinic	
Space group	P-1	
Unit cell dimensions	a = 8.483(7)Å	α = 74,834(5)°
	b = 9.623(4) Å	β = 75.001(2)°
	c = 12.110(5) Å	γ = 76.930(5)°
Volume	909(1) $Å^3$	
Z	2	
Density (calculated)	1.515 mg/m^3	
Absorption coefficient	0.509 mm^{-1}	
F(000)	422	

Crystal Size	0.14 x 0.08 x 0.06 mm	
Theta range for data collection	1.78 to 27.55°	
Index ranges	-11 <= h<= 10, -12<= k <=11, -15<= l <= 15	
Reflections collected	8549	
Independent reflections	3966	
Completeness to theta = 27.55	94.5%	
Absorption correction	None	
Refinement method	Full-matrix least-squares on F^2	
Data / restraints / parameters	3966 / 0 / 241	
Goodness-of-fit on F^2	1.131	
Final R indices [I>2sigma(I)]	R_1 = 0.0475	R_w = 0.1160
R indices (all data)	R_1 = 0.0554	R_w = 0.1199
Largest diff. peak and hole	2.475 and -0.534 e.$Å^{-3}$	

Table A-14. Atomic coordinates (x 10^4) and equivalent isotropic displacement parameters (A^2 x 10^3) for **2-6**. U(eq) is defined as one third of the trace of the orthogonalizedUij tensor.

	x	y	z	U(eq)
C(1)	9755(3)	1472(3)	-1532(3)	26(1)
C(2)	12102(4)	714(3)	-30(3)	28(1)
C(3)	7367(3)	4006(3)	-382(2)	22(1)
C(4)	6166(3)	3349(3)	-535(3)	24(1)
C(5)	5462(3)	3944(3)	-1513(3)	27(1)
C(6)	5939(4)	5177(3)	-2294(3)	31(1)
C(7)	7103(4)	5835(3)	-2107(3)	33(1)
C(8)	7835(3)	5245(3)	-1151(3)	27(1)
C(9)	9216(3)	2607(3)	2958(2)	21(1)
C(10)	8291(3)	3987(3)	2897(3)	26(1)
C(11)	8010(4)	4656(3)	3839(3)	32(1)
C(12)	8640(4)	3939(4)	4827(3)	32(1)
C(13)	9562(4)	2558(4)	4864(3)	31(1)
C(14)	9855(3)	1888(3)	3938(3)	25(1)
C(15)	6186(3)	414(3)	2743(2)	23(1)
C(16)	6891(3)	-339(3)	3683(3)	26(1)
C(17)	6218(4)	-1522(3)	4436(3)	30(1)
C(18)	4859(4)	-1932(3)	4245(3)	32(1)

C(19)	4179(4)	-1159(4)	3296(3)	35(1)
C(20)	4832(4)	21(3)	2542(3)	31(1)
Mo(1)	10000	0	0	20(1)
O(1)	9638(3)	2267(3)	-2401(2)	43(1)
O(2)	13260(3)	1141(3)	-35(2)	39(1)
O(5)	8151(2)	3469(2)	568(2)	23(1)
O(6)	9662(2)	1875(2)	2032(2)	21(1)
O(7)	6742(2)	1677(2)	2022(2)	23(1)
P(1)	8552(1)	1756(1)	1171(1)	19(1)

Table A-15. Bond lengths [A] and angles [deg] for **2-5**.

C(1)-O(1)	1.140(4)	O(6)-P(1)	1.6140(18)
C(1)-Mo(1)	2.045(3)	O(7)-P(1)	1.617(2)
C(2)-O(2)	1.146(4)		
C(2)-Mo(1)	2.040(3)	O(1)-C(1)-Mo(1)	178.3(2)
C(3)-C(8)	1.375(4)	O(2)-C(2)-Mo(1)	178.4(3)
C(3)-C(4)	1.386(4)	C(8)-C(3)-C(4)	121.5(3)
C(3)-O(5)	1.402(3)	C(8)-C(3)-O(5)	116.1(2)
C(4)-C(5)	1.394(4)	C(4)-C(3)-O(5)	122.4(2)
C(5)-C(6)	1.377(4)	C(3)-C(4)-C(5)	118.7(3)
C(6)-C(7)	1.379(4)	C(6)-C(5)-C(4)	120.1(3)
C(7)-C(8)	1.385(4)	C(5)-C(6)-C(7)	120.2(3)
C(9)-C(10)	1.376(4)	C(6)-C(7)-C(8)	120.5(3)
C(9)-C(14)	1.384(4)	C(3)-C(8)-C(7)	119.0(3)
C(9)-O(6)	1.404(3)	C(10)-C(9)-C(14)	120.7(3)
C(10)-C(11)	1.396(4)	C(10)-C(9)-O(6)	123.5(2)
C(11)-C(12)	1.387(4)	C(14)-C(9)-O(6)	115.7(2)
C(12)-C(13)	1.377(4)	C(9)-C(10)-C(11)	118.9(3)
C(13)-C(14)	1.377(4)	C(12)-C(11)-C(10)	120.7(3)
C(15)-C(16)	1.380(4)	C(13)-C(12)-C(11)	119.1(3)
C(15)-C(20)	1.382(4)	C(14)-C(13)-C(12)	120.8(3)
C(15)-O(7)	1.398(3)	C(13)-C(14)-C(9)	119.8(3)
C(16)-C(17)	1.391(4)	C(16)-C(15)-C(20)	121.4(3)
C(17)-C(18)	1.389(4)	C(16)-C(15)-O(7)	120.4(2)
C(18)-C(19)	1.382(5)	C(20)-C(15)-O(7)	118.0(2)
C(19)-C(20)	1.382(4)	C(15)-C(16)-C(17)	118.7(3)
Mo(1)-C(2)#1	2.040(3)	C(18)-C(17)-C(16)	120.5(3)
Mo(1)-C(1)#1	2.045(3)	C(19)-C(18)-C(17)	119.5(3)
Mo(1)-P(1)	2.4063(7)	C(18)-C(19)-C(20)	120.6(3)
Mo(1)-P(1)#1	2.4063(7)	C(15)-C(20)-C(19)	119.2(3)
O(5)-P(1)	1.6162(18)	C(2)-Mo(1)-C(2)#1	180.0

C(2)-Mo(1)-C(1)#1 90.13(12)	C(1)-Mo(1)-P(1)#1 87.26(8)
C(2)#1-Mo(1)-C(1)#1 89.87(12)	P(1)-Mo(1)-P(1)#1 180.0
C(2)-Mo(1)-C(1) 89.87(12)	C(3)-O(5)-P(1) 123.87(17)
C(2)#1-Mo(1)-C(1) 90.13(12)	C(9)-O(6)-P(1) 129.15(16)
C(1)#1-Mo(1)-C(1) 180.0	C(15)-O(7)-P(1) 125.99(16)
C(2)-Mo(1)-P(1) 86.35(8)	O(6)-P(1)-O(5) 98.65(10)
C(2)#1-Mo(1)-P(1) 93.66(8)	O(6)-P(1)-O(7) 103.08(10)
C(1)#1-Mo(1)-P(1) 87.26(8)	O(5)-P(1)-O(7) 95.79(10)
C(1)-Mo(1)-P(1) 92.74(8)	O(6)-P(1)-Mo(1) 110.49(7)
C(2)-Mo(1)-P(1)#1 93.65(8)	O(5)-P(1)-Mo(1) 120.52(8)
C(2)#1-Mo(1)-P(1)#1 86.34(8)	O(7)-P(1)-Mo(1) 124.24(8)
C(1)#1-Mo(1)-P(1)#1 92.74(8)	

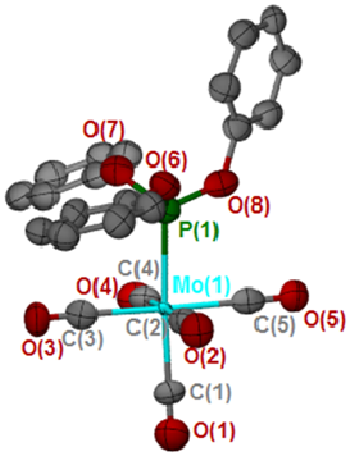

Table A-16. Crystal data and structure refinement for **2-7**		
Identification Code	**2-7**	
Empirical formula	$C_{23}H_{15}MoO_8P$	
Formula weight	546.26	
Temperature	110(2) K	
Wavelength	0.071073 Å	
Crystal system	Triclinic	
Space group	P1	
Unit cell dimensions	a = 9.505(54) Å	α = 105.927(6)°
	b = 11.103(4) Å	β = 95.806(6)°
	c = 11.161(4) Å	γ = 98.846(6)°
Volume	1109.3(7) $Å^3$	
Z	2	
Density (calculated)	1.635 mg/m^3	
Absorption coefficient	0.711 mm^{-1}	

F(000)	548	
Crystal Size	0.15 x 0.12 x 0.08 mm	
Theta range for data collection	3.24 to 25.00°	
Index ranges	-11 <= h<= 11, -13<= k <=13, -13<= l <= 13	
Reflections collected	7624	
Independent reflections	3634	
Completeness to theta = 25.00	88.5%	
Absorption correction	None	
Refinement method	Full-matrix least-squares on F^2	
Data / restraints / parameters	3634 / 0 / 299	
Goodness-of-fit on F^2	1.069	
Final R indices [I>2sigma(I)]	R_1 = 0.0488	R_w = 0.1230
R indices (all data)	R_1 = 0.0503	R_w = 0.1250
Largest diff. peak and hole	2.037 and -0.799 e.$Å^{-3}$	

Table A-17. Atomic coordinates (x 10^4) and equivalent isotropic displacement parameters (A^2 x 10^3) for **2-7**. U(eq) is defined as one third of the trace of the orthogonalized Uij tensor.

	x	y	z	U(eq)
Mo(1)	2207(1)	8514(1)	3855(1)	18(1)
P(1)	1874(2)	6455(2)	2242(2)	59(1)
O(1)	2757(7)	11066(7)	5989(7)	84(2)
O(2)	4676(6)	9662(6)	2512(6)	76(1)
O(3)	-170(6)	9467(6)	2376(6)	75(1)
O(4)	-193(6)	7575(6)	5395(5)	74(1)
O(5)	4621(7)	7516(6)	5291(6)	70(1)
O(6)	2552(5)	6351(5)	949(5)	67(1)
O(7)	278(6)	5664(5)	1654(5)	71(1)
O(8)	2688(6)	5519(5)	2740(5)	70(1)
C(1)	2575(8)	10221(7)	5269(6)	57(2)
C(2)	3786(9)	9238(7)	2957(7)	63(2)
C(3)	651(9)	9116(7)	2865(7)	63(2)
C(4)	635(8)	7847(7)	4810(7)	61(2)
C(5)	3761(9)	7879(7)	4779(7)	63(2)
C(6)	2411(8)	7165(7)	204(7)	64(2)
C(7)	1205(7)	7591(8)	-28(6)	65(2)
C(8)	1160(9)	8390(7)	-802(7)	68(2)

C(9)	2369(9)	8714(8)	-1344(7)	69(2)
C(10)	3588(9)	8236(9)	-1126(8)	74(2)
C(11)	3605(8)	7495(8)	-341(7)	67(2)
C(12)	-840(8)	5503(7)	2337(6)	63(2)
C(13)	-1977(8)	6136(7)	2247(7)	66(2)
C(14)	-3148(8)	5889(8)	2812(7)	69(2)
C(15)	-3195(8)	5036(7)	3513(7)	70(2)
C(16)	-2084(9)	4451(8)	3639(8)	69(2)
C(17)	-891(9)	4649(8)	3024(8)	69(2)
C(18)	2652(7)	4192(6)	2216(7)	60(2)
C(19)	2687(8)	3649(7)	936(7)	66(2)
C(20)	2674(8)	2348(8)	519(7)	71(2)
C(21)	2653(8)	1617(7)	1310(7)	62(2)
C(22)	2606(8)	2179(7)	2582(7)	69(2)
C(23)	2626(8)	3466(7)	3039(7)	66(2)

Table A-18. Bond lengths [Å] and angles [deg] for **2-7**.

Mo(1)-C(5)	2.051(9)	C(9)-C(10)	1.378(12)
Mo(1)-C(2)	2.056(8)	C(9)-H(9)	0.9500
Mo(1)-C(1)	2.066(7)	C(10)-C(11)	1.357(11)
Mo(1)-C(4)	2.068(8)	C(10)-H(10)	0.9500
Mo(1)-C(3)	2.071(9)	C(11)-H(11)	0.9500
Mo(1)-P(1)	2.448(2)	C(12)-C(17)	1.372(11)
P(1)-O(8)	1.574(6)	C(12)-C(13)	1.387(11)
P(1)-O(6)	1.612(5)	C(13)-C(14)	1.353(11)
P(1)-O(7)	1.616(6)	C(13)-H(13)	0.9500
O(1)-C(1)	1.034(9)	C(14)-C(15)	1.381(11)
O(2)-C(2)	1.121(9)	C(14)-H(14)	0.9500
O(3)-C(3)	1.094(10)	C(15)-C(16)	1.340(12)
O(4)-C(4)	1.122(9)	C(15)-H(15)	0.9500
O(5)-C(5)	1.144(10)	C(16)-C(17)	1.393(12)
O(6)-C(6)	1.399(9)	C(16)-H(16)	0.9500
O(7)-C(12)	1.376(9)	C(17)-H(17)	0.9500
O(8)-C(18)	1.423(9)	C(18)-C(23)	1.377(10)
C(6)-C(7)	1.337(11)	C(18)-C(19)	1.396(11)
C(6)-C(11)	1.380(11)	C(19)-C(20)	1.388(11)
C(7)-C(8)	1.400(11)	C(19)-H(19)	0.9500
C(7)-H(7)	0.9500	C(20)-C(21)	1.352(11)
C(8)-C(9)	1.387(11)	C(20)-H(20)	0.9500
C(8)-H(8)	0.9500	C(21)-C(22)	1.393(11)

C(21)-H(21)	0.9500
C(22)-C(23)	1.376(11)
C(22)-H(22)	0.9500
C(23)-H(23)	0.9500
C(5)-Mo(1)-C(2)	87.7(3)
C(5)-Mo(1)-C(1)	90.5(3)
C(2)-Mo(1)-C(1)	90.2(3)
C(5)-Mo(1)-C(4)	92.2(3)
C(2)-Mo(1)-C(4)	177.9(2)
C(1)-Mo(1)-C(4)	87.8(3)
C(5)-Mo(1)-C(3)	178.1(2)
C(2)-Mo(1)-C(3)	91.4(3)
C(1)-Mo(1)-C(3)	91.2(3)
C(4)-Mo(1)-C(3)	88.7(3)
C(5)-Mo(1)-P(1)	86.3(2)
C(2)-Mo(1)-P(1)	89.7(2)
C(1)-Mo(1)-P(1)	176.9(2)
C(4)-Mo(1)-P(1)	92.4(2)
C(3)-Mo(1)-P(1)	92.0(2)
O(8)-P(1)-O(6)	99.0(3)
O(8)-P(1)-O(7)	106.1(3)
O(6)-P(1)-O(7)	98.5(3)
O(8)-P(1)-Mo(1)	110.0(2)
O(6)-P(1)-Mo(1)	120.1(2)
O(7)-P(1)-Mo(1)	120.4(2)
C(6)-O(6)-P(1)	124.4(4)
C(12)-O(7)-P(1)	125.0(4)
C(18)-O(8)-P(1)	130.3(5)
O(1)-C(1)-Mo(1)	179.0(7)
O(2)-C(2)-Mo(1)	177.3(7)
O(3)-C(3)-Mo(1)	177.7(7)
O(4)-C(4)-Mo(1)	174.7(6)
O(5)-C(5)-Mo(1)	179.5(7)
C(7)-C(6)-C(11)	119.7(7)
C(7)-C(6)-O(6)	124.4(7)
C(11)-C(6)-O(6)	115.8(6)
C(6)-C(7)-C(8)	120.3(7)
C(6)-C(7)-H(7)	119.9
C(8)-C(7)-H(7)	119.9
C(9)-C(8)-C(7)	119.3(7)
C(9)-C(8)-H(8)	120.3
C(7)-C(8)-H(8)	120.3
C(10)-C(9)-C(8)	119.7(8)
C(10)-C(9)-H(9)	120.2
C(8)-C(9)-H(9)	120.2
C(11)-C(10)-C(9)	119.2(7)
C(11)-C(10)-H(10)	120.4
C(9)-C(10)-H(10)	120.4
C(10)-C(11)-C(6)	121.7(7)
C(10)-C(11)-H(11)	119.2
C(6)-C(11)-H(11)	119.2
C(17)-C(12)-O(7)	120.5(7)
C(17)-C(12)-C(13)	119.9(7)
O(7)-C(12)-C(13)	119.5(6)
C(14)-C(13)-C(12)	120.0(7)
C(14)-C(13)-H(13)	120.0
C(12)-C(13)-H(13)	120.0
C(13)-C(14)-C(15)	120.1(7)
C(13)-C(14)-H(14)	119.9
C(15)-C(14)-H(14)	119.9
C(16)-C(15)-C(14)	120.3(7)
C(16)-C(15)-H(15)	119.9
C(14)-C(15)-H(15)	119.9
C(15)-C(16)-C(17)	120.7(8)
C(15)-C(16)-H(16)	119.7
C(17)-C(16)-H(16)	119.7
C(12)-C(17)-C(16)	118.9(8)
C(12)-C(17)-H(17)	120.6
C(16)-C(17)-H(17)	120.6
C(23)-C(18)-C(19)	121.2(7)
C(23)-C(18)-O(8)	116.9(6)
C(19)-C(18)-O(8)	121.9(6)
C(20)-C(19)-C(18)	117.6(7)
C(20)-C(19)-H(19)	121.2
C(18)-C(19)-H(19)	121.2
C(21)-C(20)-C(19)	122.3(7)
C(21)-C(20)-H(20)	118.8
C(19)-C(20)-H(20)	118.8
C(20)-C(21)-C(22)	119.0(7)
C(20)-C(21)-H(21)	120.5
C(22)-C(21)-H(21)	120.5
C(23)-C(22)-C(21)	120.7(7)
C(23)-C(22)-H(22)	119.6
C(21)-C(22)-H(22)	119.6
C(22)-C(23)-C(18)	119.2(7)
C(22)-C(23)-H(23)	120.4
C(18)-C(23)-H(23)	120.4

APPENDIX B

SUPPLEMENTARY MATERIAL FOR CRYSTALLOGRAPHIC STUDIES FOR CHAPTER III

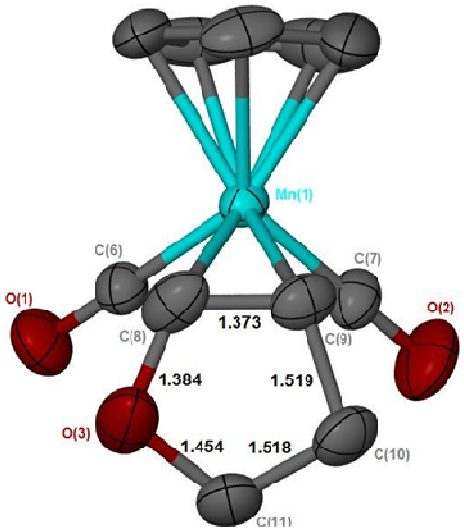

Table B-1. Crystal data and structure refinement for $CpMn(CO)_2(\eta^2\text{-DHF})$		
Identification Code	$CpMn(CO)_2(\eta^2\text{-DHF})$	
Empirical formula	$C_{11}H_{11}MnO$	
Formula weight	246.14	
Temperature	213(2) K	
Wavelength	0.071073 Å	
Crystal system	Monoclinic	
Space group	C 2/c	
Unit cell dimensions	a = 11.8494(15) Å	α = 90°
	b = 13.2037(17) Å	β = 107.760(7)°
	c = 14.3448(18) Å	γ = 90°
Volume	2137.4(5) $Å^3$	
Z	8	
Density (calculated)	1.530 mg/m^3	
Absorption coefficient	1.217 mm^{-1}	
F(000)	1008	
Crystal Size	0.22 x 0.16 . 0.08 mm	

Theta range for data collection	2.37 to 32.79°	
Index ranges	-17 <= h<= 17, -20<= k <= 19, -21<= l <= 21	
Reflections collected	21968	
Independent reflections	3925	
Completeness to theta = 32.79°	99.4%	
Absorption correction	None	
Refinement method	Full-matrix least-squares on F^2	
Data / restraints / parameters	3935 / 0/ 136	
Goodness-of-fit on F^2	1.050	
Final R indices [I>2sigma(I)]	R_1 = 0.0362	R_w = 0.0990
R indices (all data)	R_1 = 0.0484	R_w = 0.1071
Largest diff. peak and hole	0.442 and -0.378 e.$Å^{-3}$	

Table C-2. Atomic coordinates (x 10^4) and equivalent isotropic displacement parameters ($Å^2$x 10^3)for $CpMn(CO)_2(\eta^2$-DHF). U(eq) is defined as one third of the trace of the orthogonalized U^{ij} tensor.

	x	y	z	U(eq)
C(1)	1358(3)	2290(2)	6226(2)	85(1)
C(2)	2462(3)	2347(2)	6910(3)	94(1)
C(3)	2547(2)	1609(3)	7579(2)	80(1)
C(4)	1499(2)	1072(2)	7328(2)	63(1)
C(5)	739(2)	1481(2)	6478(2)	61(1)
C(6)	1651(2)	837(1)	4894(1)	41(1)
C(7)	3724(2)	1109(2)	6029(1)	48(1)
C(8)	1896(2)	-693(1)	6069(2)	55(1)
C(9)	2996(2)	-538(2)	6731(1)	50(1)
C(10)	3884(2)	-1101(2)	6351(2)	59(1)
C(11)	3183(2)	-1239(2)	5280(2)	62(1)
Mn(1)	2302(1)	938(1)	6175(1)	34(1)
O(1)	1213(2)	788(1)	4057(1)	63(1)
O(2)	4649(1)	1239(2)	5930(1)	77(1)
O(3)	1947(1)	-1237(1)	5257(1)	68(1)

Table C-3. Bond lengths [Å] and angles [°] for $CpMn(CO)_2(\eta^2$-DHF).

C(1)-C(2)	1.377(5)	C(3)-C(4)-C(5)	108.8(2)
C(1)-C(5)	1.405(4)	C(3)-C(4)-Mn(1)	70.68(12)
C(1)-Mn(1)	2.119(2)	C(5)-C(4)-Mn(1)	71.12(11)
C(2)-C(3)	1.351(4)	C(4)-C(5)-C(1)	105.8(2)
C(2)-Mn(1)	2.118(2)	C(4)-C(5)-Mn(1)	71.29(11)
C(3)-C(4)	1.378(4)	C(1)-C(5)-Mn(1)	69.61(12)
C(3)-Mn(1)	2.137(2)	O(1)-C(6)-Mn(1)	178.61(17)
C(4)-C(5)	1.386(3)	O(2)-C(7)-Mn(1)	178.7(2)
C(4)-Mn(1)	2.1519(19)	C(9)-C(8)-O(3)	112.54(18)
C(5)-Mn(1)	2.1496(18)	C(9)-C(8)-Mn(1)	70.46(11)
C(6)-O(1)	1.155(2)	O(3)-C(8)-Mn(1)	120.04(15)
C(6)-Mn(1)	1.7681(17)	C(8)-C(9)-C(10)	107.10(18)
C(7)-O(2)	1.160(2)	C(8)-C(9)-Mn(1)	72.96(11)
C(7)-Mn(1)	1.7752(19)	C(10)-C(9)-Mn(1)	122.30(14)
C(8)-C(9)	1.373(3)	C(11)-C(10)-C(9)	101.32(16)
C(8)-O(3)	1.384(3)	O(3)-C(11)-C(10)	104.98(19)
C(8)-Mn(1)	2.203(2)	C(6)-Mn(1)-C(7)	90.89(8)
C(9)-C(10)	1.519(3)	C(6)-Mn(1)-C(2)	121.92(13)
C(9)-Mn(1)	2.1712(18)	C(7)-Mn(1)-C(2)	90.19(11)
C(10)-C(11)	1.518(3)	C(6)-Mn(1)-C(1)	91.87(10)
C(11)-O(3)	1.454(3)	C(7)-Mn(1)-C(1)	115.30(12)
		C(2)-Mn(1)-C(1)	37.92(13)
C(2)-C(1)-C(5)	108.4(2)	C(6)-Mn(1)-C(3)	154.43(10)
C(2)-C(1)-Mn(1)	71.00(15)	C(7)-Mn(1)-C(3)	101.41(10)
C(5)-C(1)-Mn(1)	71.98(11)	C(2)-Mn(1)-C(3)	37.01(12)
C(3)-C(2)-C(1)	108.4(2)	C(1)-Mn(1)-C(3)	62.63(11)
C(3)-C(2)-Mn(1)	72.27(15)	C(6)-Mn(1)-C(5)	96.09(8)
C(1)-C(2)-Mn(1)	71.08(13)	C(7)-Mn(1)-C(5)	152.77(10)
C(2)-C(3)-C(4)	108.6(2)	C(2)-Mn(1)-C(5)	63.82(11)
C(2)-C(3)-Mn(1)	70.72(14)	C(1)-Mn(1)-C(5)	38.41(11)
C(4)-C(3)-Mn(1)	71.84(12)	C(3)-Mn(1)-C(5)	63.22(8)

C(6)-Mn(1)-C(4)	130.59(10)	C(5)-Mn(1)-C(9)	118.57(9)
C(7)-Mn(1)-C(4)	137.59(10)	C(4)-Mn(1)-C(9)	89.90(8)
C(2)-Mn(1)-C(4)	62.53(10)	C(6)-Mn(1)-C(8)	80.62(8)
C(1)-Mn(1)-C(4)	62.80(8)	C(7)-Mn(1)-C(8)	108.09(9)
C(3)-Mn(1)-C(4)	37.48(10)	C(2)-Mn(1)-C(8)	151.42(11)
C(5)-Mn(1)-C(4)	37.59(9)	C(1)-Mn(1)-C(8)	136.07(12)
C(6)-Mn(1)-C(9)	108.03(8)	C(3)-Mn(1)-C(8)	115.74(12)
C(7)-Mn(1)-C(9)	83.69(8)	C(5)-Mn(1)-C(8)	99.02(9)
C(2)-Mn(1)-C(9)	129.77(13)	C(4)-Mn(1)-C(8)	89.74(9)
C(1)-Mn(1)-C(9)	152.69(8)	C(9)-Mn(1)-C(8)	36.58(8)
C(3)-Mn(1)-C(9)	95.65(10)	C(8)-O(3)-C(11)	106.50(16)

APPENDIX C

SUPPLEMENTARY MATERIAL FOR CRYSTALLOGRAPHIC STUDIES FOR CHAPTER V

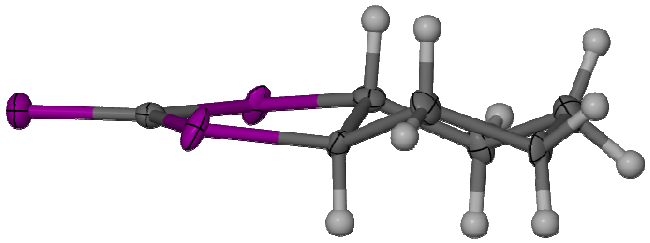

Table C-1. Crystal data and structure refinement for **5-1**		
Identification Code	**5-1**	
Empirical formula	$C_{28}H_{40}S12$	
Formula weight	76121	
Temperature	110(2) K	
Wavelength	0.071073 Å	
Crystal system	Orthorhombic	
Space group	Pnma	
Unit cell dimensions	a = 12.6594(14 Å	α = 90°
	b = 10.0870(11) Å	β = 90 °
	c = 6.6497(7) Å	γ = 90°
Volume	851.5(5) $Å^3$	
Z	2	
Density (calculated)	1.485 mg/m^3	
Absorption coefficient	7.302 mm^{-1}	
F(000)	400	
Crystal Size	0.2 x 0.2 . 0.1 mm	

Theta range for data collection	3.49 to 31.49°	
Index ranges	-14 <= h<= 13, -11<= k <= 11, -7<= l <= 7	
Reflections collected	17547	
Independent reflections	718	
Completeness to theta = 31.49	98.4%	
Absorption correction	None	
Refinement method	Full-matrix least-squares on F^2	
Data / restraints / parameters	718 / 85/ 34	
Goodness-of-fit on F^2	1.009	
Final R indices [I>2sigma(I)]	R_1 = 0.0376	R_w = 0.829
R indices (all data)	R_1 = 0.0333	R_w = 0.0811
Largest diff. peak and hole		

Table C-2. Atomic coordinates (x 10^4) and equivalent isotropic displacement parameters (A^2 x 10^3) for **5-1**. U(eq) is defined as one third of the trace of the orthogonalized Uij tensor.

	x	y	z	U(eq)
S(1)	17556(8)	2500	1029(3)	19(1)
C(1)	2551(2)	2500	2969(4)	15(1)
S(2A)	2896(5)	1046(5)	4214(11)	20(1)
C(2A)	3595(5)	1760(7)	6226(10)	18(1)
C(3A)	4505(7)	972(10)	7141(12)	19(1)
C(4A)	4867(8)	1672(12)	9057(13)	24(1)
S(2B)	3111(5)	1071(4)	3970(11)	20(1)
C(2B)	3956(5)	1830(7)	5732(10)	14(1)
C(3B)	4274(7)	1110(11)	7661(11)	22(1)
C(4B)	5158(7)	1876(11)	8695(14)	19(1)

Table C-3. Bond lengths [Å] and angles [°] for **5-1**.

S(1)-C(1) 1.637(3)
C(1)- S(2B) 1.739(3)
C(1)- S(2A) 1.740(3)
S(2B)- C(1)- S(2A) 10.5(5)
S(2A)- C(1)- S(2A) 114.9(5)
C(1)-S(2A)- C(2A) 98.3(4)
C(3A)- C(2A)- C(2B) 110.1(7)
C(3A)- C(2A)- S(2A) 118.1(6)
C(2B)- C(2A)- S(2A) 111.6(6)
C(4A)- C(3A) -C(2A) 108.6(8)
C(3A)- C(4A)- C(4B 112.6(11)
C(1)- S(2B)- C(2B) 98.2(4)
C(3B)- C(2B)- C(2A 109.9(7)
S(2A)-C(2A) 1.760(4)
C(2A) -C(3A) 1.528(4)
C(2A) -C(2B) 1.529(3)
C(3A) -C(4A) 1.528(4)
C(4A)- C(4B) 1.529(4)

S(2B)- C(2B)	1.764(3)
C(2B)- C(3B)	1.528(4)
C(2B)- C(2A)	1.529(3)
C(3B)- C(4B)	1.527(4)
C(4B)- C(4A)	1.529(4)

S(1)- C(1)- (2B)	123.6(2)
S(2B)- C(1)- S(2B)	111.9(5)
S(1) -C(1)- S(2A)	122.0(2
S(2B)- C(1)- S(2A)	10.5(5)
S(2B)- C(1)- S(2A)	114.44(16)
S(1)- C(1)- S(2A)	122.0(2)
S(2B)- C(1)- S(2A)	114.44(16)
C(3B0- C(2B)- S(2B)	120.8(6)
C(2A)- C(2B)- S(2B)	111.4(6)
C(4B)- C(3B)- C(2B)	109.4(8)
C(3B)- C(4B)- C(4A)	112.2(12)

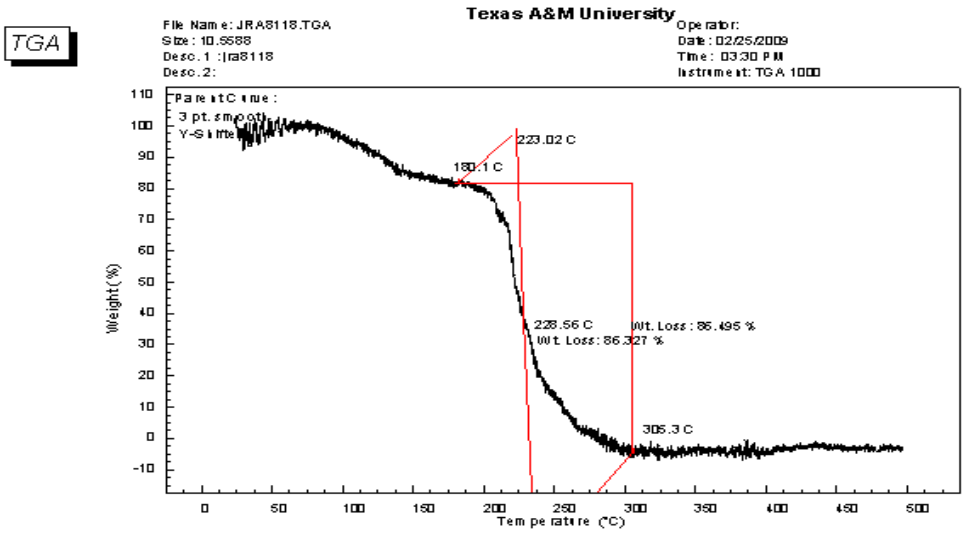

Figure C- 1 TGA of polythiocarbonate from the copolymerization of CS_2 and CHO at 50 °C

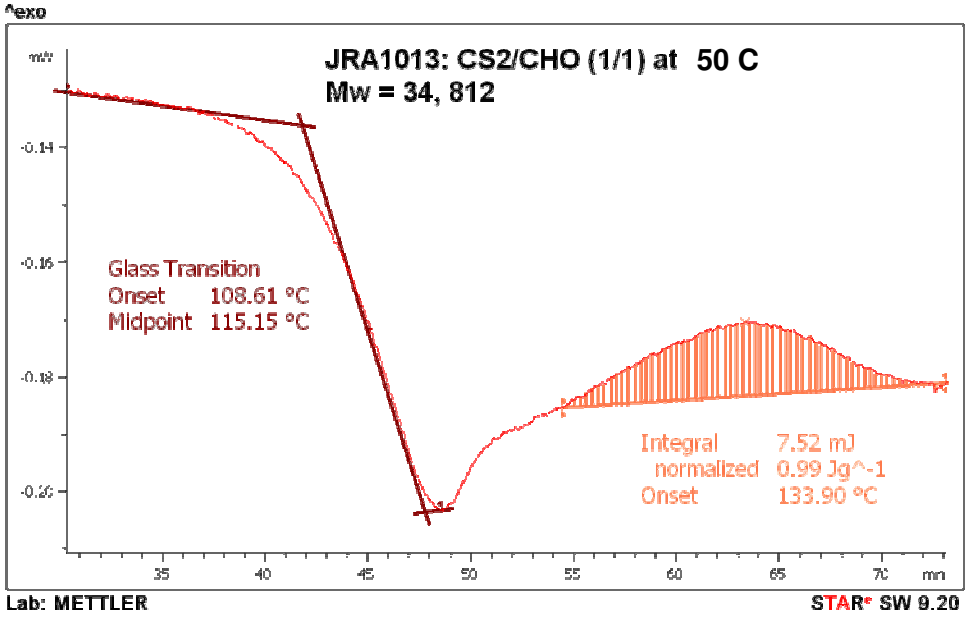

Figure C- 2. DSC of polythiocarbonate obtained from the copolymerization of CS_2 and CHO at 50 °C

VITA

Jeremy Rex Andreatta was born in Mineral Wells to Jimmy and Donna Andreatta. He grew up just outside the small town of Santo, Texas where he graduated from Santo High School in the Fall of 1999. He received his Bachelor of Science in chemistry and mathematics from Tarleton State University in May 2004. He began his graduate studies in June of that same year under the supervision of Professor Donald J. Darensbourg and graduated with his Ph.D. in December 2009. His research interests include organometallic chemistry, polymerization catalysis, and utilization of carbon dioxide and carbon disulfide towards the production of useful materials. He may be reached at: Texas A&M University, Department of Chemistry, P.O. Box 3002, College Station, Texas 77842-3255. His e-mail is: jandreatta@gmail.com.